Minnesota Department of Transportation

RESEARCH SERVICES & LIBRARY

Office of Transportation System Management

Optimal Timing of Preventive Maintenance for Addressing Environmental Aging in Hot-Mix Asphalt Pavements

R. Michael Anderson, Principal Investigator
Asphalt Institute, Inc.
Lexington, KY

December 2014

Research Project
Final Report 2014-45

LRRB
LOCAL ROAD RESEARCH BOARD

To request this document in an alternative format call 651-366-4718 or 1-800-657-3774 (Greater Minnesota) or email your request to ADArequest.dot@state.mn.us. Please request at least one week in advance.

Technical Report Documentation Page

1. Report No.	2.	3. Recipients Accession No.
MN/RC 2014-45		

4. Title and Subtitle	5. Report Date
Optimal Timing of Preventive Maintenance for Addressing Environmental Aging in Hot-Mix Asphalt Pavements	December 2014 6.

7. Author(s)	8. Performing Organization Report No.
R. Michael Anderson, Phillip B. Blankenship, Alireza Zeinali, Gayle N. King, and Douglas I. Hanson	

9. Performing Organization Name and Address	10. Project/Task/Work Unit No. 11. Contract (C) or Grant (G) No.
Asphalt Institute 2696 Research Park Dr. Lexington, KY 40511-8480	(C) 95099

12. Sponsoring Organization Name and Address	13. Type of Report and Period Covered 14. Sponsoring Agency Code
Minnesota Department of Transportation Research Services & Library 395 John Ireland Boulevard, MS 330 St. Paul, Minnesota 55155-1899	Final Report

15. Supplementary Notes
http://www.lrrb.org/pdf/201445.pdf

16. Abstract (Limit: 250 words)

The main goal of this research was to help users determine the proper timing of preventive maintenance by identifying how environmental aging affects asphalt material properties (binder and/or mixture) in the pavement and how the application of pavement preservation treatments impact the aging process. Two main test sections were studied: (1) a designed experiment on the Low Volume Road portion of MnROAD to look at aging through the application of treatments on an annual basis over a five-year period; and (2) a 10-year-old pavement on TH 56 in southern Minnesota, also a designed experiment, with seals applied on an annual basis over a four-year period.

Mix testing on TH 56 cores indicated that subsections with chip seals applied more than two years after construction had essentially the same fracture energy properties as the unsealed control subsection – implying that the initial treatment from a preservation standpoint should occur within the first two years of the pavement's life to mitigate damage from environmental aging. The MnROAD sections did not show the same response.

Based on the testing conducted during the study and the associated findings, it appears that rheological tests can be conducted on the asphalt binder recovered from a pavement core to assess the effects of oxidative aging. When possible, it appears prudent to use a mixture fracture energy test, such as the DC(T), in conjunction with asphalt binder rheological testing to quantify the effects of aging within a pavement and suggest appropriate timing for the application of preservation treatments.

17. Document Analysis/Descriptors	18. Availability Statement
Aging, Asphalt pavements, Preventive maintenance, Binder content, Rheology	No restrictions. Document available from: National Technical Information Services, Alexandria, Virginia 22312

19. Security Class (this report)	20. Security Class (this page)	21. No. of Pages	22. Price
Unclassified	Unclassified	140	

Optimal Timing of Preventive Maintenance for Addressing Environmental Aging in Hot-Mix Asphalt Pavements

Final Report

Prepared by:
R. Michael Anderson
Phillip B. Blankenship
Asphalt Institute, Inc.
Lexington, KY

Alireza Zeinali
InstroTek, Inc.
Raleigh, NC

Gayle N. King
GHK, Inc.
Houston, TX

Douglas I. Hanson
Retired (formerly AMEC Earth and Environmental, Inc.)
Phoenix, AZ

December 2014

Published by:
Minnesota Department of Transportation
Research Services & Library
395 John Ireland Boulevard MS 330
St. Paul, MN 55155

Acknowledgments

The information in this report is the outcome of research conducted as part of a pooled fund research program, TPF (153), *Optimal Timing of Preventive Maintenance for Addressing Environmental Aging in Hot-Mix Asphalt Pavements*. The authors would like to thank the following participating agencies for their financial and technical support:

Minnesota Department of Transportation
Maryland State Highway Administration
Ohio Department of Transportation
Texas Department of Transportation
Wisconsin Department of Transportation
Minnesota Local Road Research Board

The authors also thank the following individuals from the Minnesota Department of Transportation for their input during the project:

Thomas Wood
Bruce Holdhusen
Jerry Geib
Jim McGraw

No research project is ever accomplished without the assistance of many other individuals who execute the quality testing that makes the analysis and reporting possible. Thanks to all the current and former Asphalt Institute Laboratory staff – Wes Cooper, Jason Lamb, Zachary McKay, Madison Pohl, Jonathan Oepping, Gary Wooldridge, and Nick Beavin – for providing consistently quality data in a timely manner.

Last, but not least, the support of the Asphalt Institute is gratefully acknowledged. Without the support of the Asphalt Institute, none of the work presented herein could have been accomplished.

Table of Contents

List of Figures

List of Tables

\

Executive Summary

Effective pavement preservation programs consist of applying surface treatments at the right time in the pavement's life to mitigate deterioration due to either load-related or environmentally induced damage. Oxidative aging of asphalt pavements can ultimately lead to environmentally induced damage by increasing the stiffness and reducing the flexibility of the asphalt binder in the pavement. Strategies to counter the effects of oxidative aging will vary with pavement condition and the physical state of the aged binder. Aging mitigation strategies may include:

- Seals (chip, fog) to reduce surface permeability so that the supply of oxygen to the underlying pavement is restricted;
- Thin surface layers, such as microsurfacing or thin overlays, to add a layer to the pavement structure and shift the point of maximum stress away from the location where the asphalt binder is likely to have become most brittle and thereby susceptible to top-down cracking; and/or
- Rejuvenators, applied through fog seals or in-place recycling techniques, to improve the mechanical properties of the aged asphalt binder.

Systematic, successive preservation treatments should allow the user to extend the time needed before the application of more expensive rehabilitation and reconstruction, resulting in a reduced user cost on a life-cycle basis.

The need for pavement preservation is widely recognized by many as being critical to extending the life of their pavements, yet a related need recognized by those same users is establishing the proper timing when treatments should be applied to maximize benefits and minimize costs.

As part of that proper timing, the user would need to apply some treatments before any visible distress could be observed. For an individual pavement the proper timing of a treatment would have to be determined based on a predictable rate of pavement deterioration over time, using material properties that can quantify accumulated damage from aging with time and depth in the pavement structure. Using these properties in combination with a projection of the rate of aging can allow the user to identify a critical point for intervention in the form of an appropriate pavement preservation treatment. This would then suggest that the timing would be optimal to provide the highest benefit-to-cost ratio to the user.

The main goal of this research study was to help users determine the proper timing of preventive maintenance by first identifying how environmental aging affects asphalt material properties (binder and/or mixture) in the pavement and how the application of pavement preservation treatments impact the aging process. Toward this end, two main test sections were studied: (1) a designed experiment on the Low Volume Road portion of MnROAD (Cell 24) to look at aging through the application of treatments on an annual basis over a five-year period; and (2) a 10-year-old pavement on TH 56 in southern Minnesota, also a designed experiment, with seals applied on an annual basis over a four-year period. Cores were taken from the pavement of both test sections representing various aging times and subdivided into layers so that the effect of depth on aging could be examined.

The findings from the research showed that for both test sections the aging of the asphalt pavement, as measured using several asphalt binder properties, was shown to be significantly higher near the surface – within the top one-half inch (12.5 millimeters) – than farther down in the pavement structure. Near the surface, the asphalt binder shows an increase in stiffness and a decrease in phase angle, indicating a loss of relaxation properties as the binder ages.

The time between the initial construction and treatment application was expected to be an important factor in the measured properties related to aging. The hypothesis of the study was that the control portion of each test section studied would have experienced the most environmental aging at the time of coring compared to the subsections that had been treated with a seal. It was also expected that the aging would be the least in the subsections where the treatment was applied early in the pavement life and would eventually reach a plateau where treatment after "x" number of years would be approximately the same as the control subsection. In other words, if treatment was not applied early enough in the pavement's life the damage from environmental aging may have already occurred such that the treatment application, from an aging perspective, would not be effective.

The TH 56 test section confirmed the hypothesis, with mixture testing indicating that the subsections with chip seals applied more than two years after construction had essentially the same fracture energy properties as the unsealed control subsection. The findings from this test section imply that to mitigate damage from environmental aging, the initial treatment from a preservation standpoint should occur within the first two years of the pavement's life. After that, while some benefits may still be obtained from treatment, it appears that the damage from environmental aging may have already substantially occurred.

Conversely, the MnROAD Cell 24 test section could not confirm the hypothesis as all sealing times appeared to be somewhat equal in most of the properties used to assess aging. In evaluating why one test section confirmed the hypothesis and one did not, it is worthwhile considering that the TH56 test section was 12 years old at the time of coring and had experienced measurable distress in all subsections. The MnROAD Cell 24 test section at the time of the last coring was only five years old and had experienced no distress in any of the subsections at that time. Allowing the MnROAD Cell 24 test section to remain in-place and continue aging would provide the opportunity for future testing to see if the initial findings change after 10 years in service instead of just five.

Based on the testing conducted during the study and the associated findings, it appears that rheological tests can be conducted on the asphalt binder recovered from a pavement core to assess the effects of oxidative aging. Asphalt binder tests have the advantage of requiring less material and generally having less variability than asphalt mixture tests, allowing them to be used to quantify aging with time. Because of the small quantities required, testing can be conducted on the pavement layers closest to the surface where aging is expected to be the worst. Mixture tests do offer the opportunity to examine fracture energy of the specimen through the use of the Disk-Shaped Compact Tension, DC(T), test. When possible, it appears prudent to use this test in conjunction with asphalt binder rheological testing to quantify the effects of aging within a pavement.

Chapter 1 - Introduction

An effective pavement preservation program can consist of applying surface treatments at the right time to delay or prevent deterioration of the pavement due to either load-related or environmentally-induced damage. Strategies to counter the effects of oxidative aging (illustrated in Figure 1.1) will vary with pavement condition and the physical state of the aged binder. Seals may be applied to reduce permeability so that the supply of oxygen is restricted. Thin surface layers may be used to shift the point of maximum tire stress away from the most brittle aged binders susceptible to top-down cracking. Rejuvenators can be applied through fog seals or in-place recycling techniques to improve the mechanical properties of the aged binder. The cumulative impact of systematic, successive preservation treatments should be to postpone costly rehabilitation and reconstruction. On a life-cycle cost basis, this cumulative series of pavement preservation treatments is substantially less expensive than extensive reconstruction and major rehabilitation strategies.

Figure 1.1 Pavement Showing Block Cracking Distress

Unfortunately, users recognize that currently there are no quantitative techniques available for establishing when these treatments should be applied, nor are their benefits fully understood. The concept of preventive maintenance implies that some treatments should be applied before any visible distress can be observed. Hence, a timing strategy must be developed from a predictable rate of pavement deterioration over time, or by applying tools which measure accumulated damage with depth and identify critical points for intervention (conceptually shown in Figure 1.2).

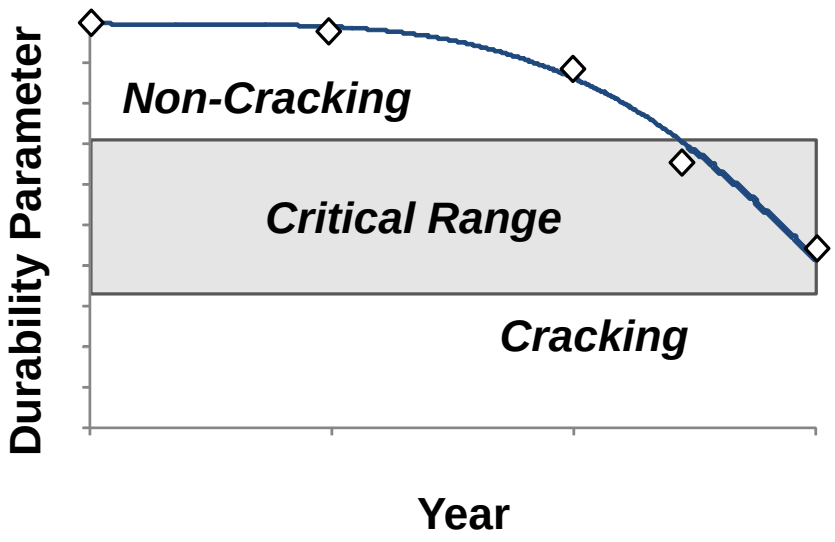

Figure 1.2 Conceptual Approach to Identifying Proper Timing of Preventive Maintenance

There are four principal options to generate the conceptual durability curve shown in Figure 1.2:

- Use conventional construction data (e.g. binder properties, density, etc.) with climatic data together in an aging/cracking model to project time to remediation;
- Perform a mixture test (or tests) on cores at construction to get a cracking property and fit data within an aging/cracking model to project time to remediation;
- Perform a binder test (or tests) on sample recovered from cores at construction to get a cracking property and fit data within an aging/cracking model to project time to remediation; or
- Perform a binder and/or mix test at construction to get cracking property and continue to pull cores from pavement at periodic intervals to check progression of cracking property.

The overall goal of the research study discussed herein is to determine the proper timing of preventive maintenance treatments in order to optimize life cycle costs and pavement performance. To accomplish this overall goal it is necessary to better understand the mechanism of environmental aging of the asphalt binder in the pavement and how it can be reduced through pavement preservation.

To assist this study, the Minnesota Department of Transportation (MnDOT) established a test section on the Low Volume Road of MnROAD (Cell 24) with the intent of sealing 100-foot test sections each year from the time of construction through five years after construction. The test sections could then be cored at periodic intervals and tested using asphalt binder and/or mixture tests to assess the effect of the timing of treatment on the aging of the underlying asphalt pavement. Although the principal focus of the study was on the controlled MnROAD Cell 24 experiment, other test sections could be considered if resources were available and the project was considered suitable.

The first part of the study was intended to evaluate asphalt binder and/or mixture tests and properties that could be used as indicators of aging. This would be accomplished through initial

coring and materials evaluation. The second part of the study was intended to use the information gathered in the initial evaluation to focus in on a limited set of asphalt binder and mixture tests related to aging and to use those tests to monitor the progression of aging of the Cell 24 test sections with time.

This research was limited, by design, to the evaluation of two test sections: the MnROAD Cell 24 test section (which was constructed specifically for this project) and a 1999-2003 project on Minnesota TH 56 that was included as part of MnDOT's Aging/Optimization Study. These two test sections represented controlled sections with surface treatments applied at one-year intervals so that the effect of treatment time on aging of the underlying asphalt pavement could be studied.

The principal deliverables expected to result from the conduct of this research are as follows:

- Identification of asphalt binder and/or mixture tests and associated parameters that could be determined from the testing of pavement cores and would be related to environmental aging and durability;
- Identification/validation of appropriate criteria that could indicate the imminent onset of cracking and serve as a trigger for preventive maintenance; and
- Economic considerations of the cost effectiveness of applying surface treatments at various times in the life of an asphalt pavement.

The report is divided into six chapters, with the majority of the information presented in Chapter 3 – representing the initial evaluation of the MnROAD Cell 24 test section and other MnROAD test sections to identify appropriate tests and parameters related to aging/durability – and Chapter 4 – representing the field evaluation of the MnROAD Cell 24 test section as a function of time and the MN TH 56 test sections. Chapter 2 provides a review of literature related to the study. Chapter 5 briefly discusses economic considerations in timing of treatments. Chapter 6 provides a summary of the results of the testing program, presents some relevant conclusions, and offers recommendations based on the research efforts.

Chapter 2 - Literature Review

In 1991, the Intermodal Surface Transportation Efficiency Act (ISTEA) opened new avenues for highway maintenance by making pavement preservation activities eligible for matching funds on Federal highways [1]. In combination with strong ongoing support from the Federal Highway Administration (FHWA) Office of Construction and Preservation, this funding created a profound interest in extending pavement life through preservation activities, rather than waiting for damage to occur and then rebuilding the badly damaged roads. The impact of this legislation was greatest for high volume roads, because previous federal funding allocations had inhibited development and use of preservation techniques on the Federal Highway System. As new and better technologies became available to meet these needs, it became apparent that significant research was needed to optimize the selection, timing and construction of preservation treatments. In 1998, a document entitled "Pavement Preservation: A Road Map for the Future" [2] was created as a product from a national forum organized to define "ideas, strategies, and techniques" that could better clarify a path forward for pavement preservation in the United States. As a by-product of that effort, FHWA partnered with the American Association of State Highway and Transportation Officials (AASHTO) to host three regional workshops in 2007, from which came the Transportation System Preservation (TSP) Research Roadmap [3]. A primary product of this latter document was a list of forty research-needs statements for pavement preservation, divided into six preservation sectors, coming with an estimated price tag of $28.3 million. One research need stands out in this document with a high-assigned priority, an eight to ten-year time frame for study, and a ten million dollar price tag – more than one third of estimated total expenditures. This materials-related project was entitled "Triggers for the Timing of Surface Treatments." The reason for the scope and importance of this effort is clear. Sessions in 2005 and 2009 at the Transportation Research Board (TRB) Annual Meeting specifically targeted agency prioritization and timing strategies for preservation treatments. Virtually all presentations focused on the use of historical data from pavement management systems for budget allocations and timing of preventive maintenance treatments. When the question was asked, "Have you used any measure of the materials properties of the in-place pavement as part of preservation timing strategies?" - the answer was a universal "NO". In responding, authors were quick to point out that they would prefer to use materials-based measures to predict critical damage, but no reliable methods to do so were available.

It is recognized that environmental damage near the pavement surface is caused by some combination of asphalt oxidative aging and moisture damage. To satisfy the unmet need for a materials-based trigger for timing preservation strategies, a predictive material parameter for surface raveling or cracking must objectively quantify critical changes in binder and/or mixture properties as damage progresses.

2.1 Moisture Damage

Moisture damage testing is a required component of many asphalt mix design procedures, including the Superpave mix design process. Static immersion tests (e.g. AASHTO T-283) or

submerged wheel tracking tests (e.g. Hamburg Wheel-Tracking Device) are included in agency specifications to prevent the construction of highly moisture-sensitive pavements. However, moisture-induced damage can still occur in mixes that pass design requirements, because critical variables such as traffic-loading, temperature and in-place air voids can be difficult to simulate in the laboratory.

2.2 Oxidation

Oxidation is the dominant cause of asphalt embrittlement that results in raveling or block cracking near the pavement surface. Laboratory and field research studies report high correlations between rising carbonyl content and rheological measures of embrittlement in the asphalt binder [4]. In the past, asphalt specifications frequently used aging ratios that tracked relative changes in absolute viscosity as the asphalt was aged in simulated laboratory aging equipment such as the Thin Film Oven Test (TFOT) or the Rolling Thin Film Oven (RTFO). Both of these tests simulated aging that occurs as the asphalt is mixed at hot mix plant temperatures (135°C), but neither adequately captured the relative damage caused by environmental aging in the pavement. Superpave binder specifications introduced the Pressure Aging Vessel (PAV) procedure, which is designed to simulate binder aging in the pavement. Although material rankings appear to be correct, it seems clear that after 20 hours, PAV-aged materials have not yet reached the advanced state of deterioration that would require remediation in the form of surface treatments. Very likely, longer PAV aging times or more stringent aging conditions will be needed if pavement damage is to be predicted using only laboratory methods, as might be needed for environmental effects models in the pavement design guide.

Although traditional research refers to the oxidation process as asphalt age-hardening, a recent study for the Federal Aviation Administration (FAA) by Anderson and co-workers [5] showed that oxidation not only increases binder modulus, but also has a dramatic negative impact on binder phase angle (or its surrogate, the BBR m-value). Lower phase angles result in less binder fluidity, lack of healing, and more rapid accumulation of damage. To demonstrate the evolution of damage, the researchers evaluated long-term PAV-aged binders from three different crude sources using the Dynamic Shear Rheometer (DSR) and the Bending Beam Rheometer (BBR) [6]. Age-induced rheological changes were then compared on Black Space Diagrams plotting log G* vs phase angle [7]. A number of potential predictive parameters for binder age-induced damage were evaluated on these same Black Space Diagrams, including:

- Superpave specification parameter $G^*\sin\delta$
- R-value from the Christensen-Anderson Model [8]
- $\tan\delta$ as proposed by Goodrich & Reese [9]
- Glover-Rowe (G-R) Parameter [10]: Rowe's mathematical rearrangement of a Maxwell direct tension model originally developed by Glover and co-workers [4].

The Glover-Rowe approach requires only a single measurement of G* and phase angle at one temperature and one frequency, and appeared to reasonably predict damage for a very limited set of four field samples. This parameter was recommended for further evaluation in field studies to validate its predictive value and determine two separate failure limits:

- onset of micro-damage, as noted by loss in modulus; and
- appearance of visible cracks.

Figure 2.1 shows how three conventional binders would change their relative position in Black Space as each is RTFO-aged and then placed in a PAV for 0, 20, 40, and 80 hours at standard conditions. It further shows how the G-R parameter could be used to define a damage envelope that might identify both the onset of micro-damage and a more advanced stage where damage in the form of raveling and/or cracking can be detected visually. Because Glover's original binder fatigue parameter was purposely modeled to be a rheological prediction of failure strain, it was found to correlate very well with ductility as measured at 15°C and 1 cm/min. Kandhal [11] had previously conducted a broad-ranging field study evaluating surface damage on aged pavements. He reported that surfaces began to show the first signs of visible damage, in the form of fine aggregate raveling, when the ductility of the binder at the surface dropped to five centimeters. When further aging caused the ductility to drop to three centimeters, visible cracking was apparent. Glover used the high correlations with ductility to predict damage limits for his parameter reflecting the same conditions noted by Kandhal.

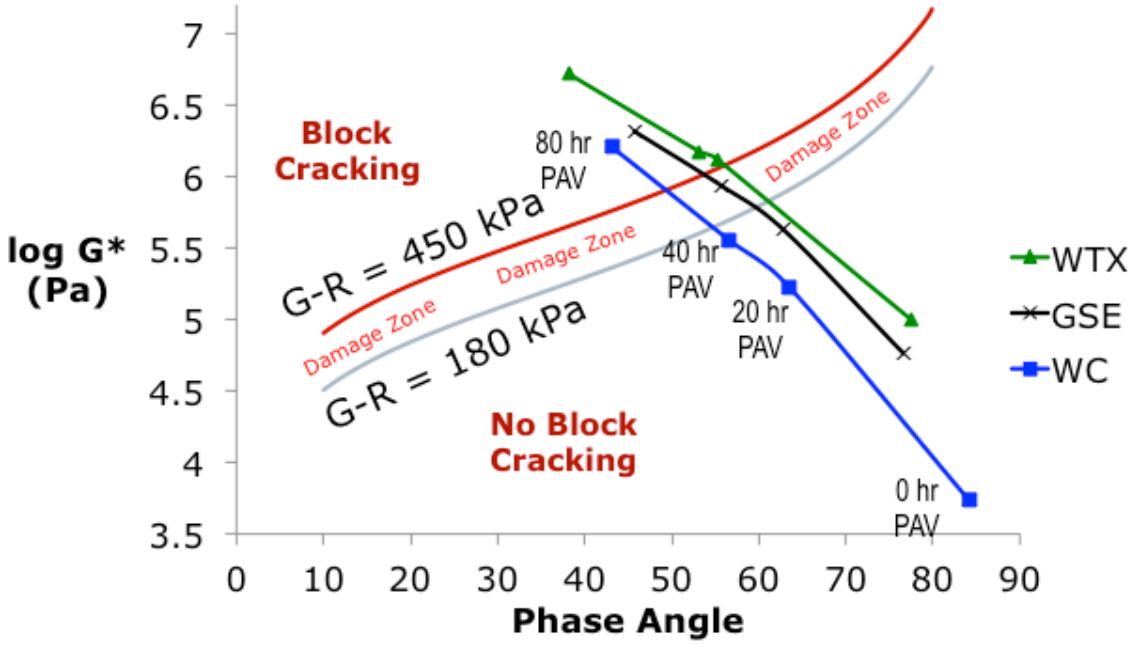

Figure 2.1 Asphalt Aging & Glover-Rowe Damage Zone in Black Space

Figure 2.1 also contains some very important implications for past and future binder specifications that deal with aged materials. As mentioned earlier, aging ratios were commonly used in viscosity specifications to limit binders that change viscosity too quickly upon laboratory aging. Of the three asphalts shown, note that the Western Canadian (WC) asphalt shows the largest change in modulus on a log scale after PAV aging, which would give this material the highest aging ratio using G* as the control test. However, after 40 hours of PAV aging, this asphalt has not yet reached the damage zone, whereas the other two asphalts have reached or

passed through it. The key observation here is that there are two equally important criteria when evaluating the potential for aged materials to crack:

- the initial quality of the asphalt, as determined by its starting point in Black Space; and
- the change in quality during aging, as determined by the length of the line between initial and aged properties (aging index).

Asphalt specifications should define aging and limit the use of poor materials using Black Space locations, not aging ratios. Furthermore, these same Black Space criteria are potential predictors of performance in a manner that can be easily applied to "time" preservation strategies.

In the second phase of the same FAA study described above, the experimental design was extended to better understand the cause and form of micro-damage as materials age through the damage zone. Loose mixes made with the same three binders were subjected to long-term oven aging for 0, 4, 24, and 48 hours @ 135° C. Specimens were then compacted in the Superpave Gyratory Compactor (SGC), and evaluated for mixture properties using the BBR Sliver Test [12] and the Disk-Shaped Compact Tension Test, DC(T). Results from the Sliver Test [7] were totally unexpected, so much so that these findings force changes in the basic assumptions used to develop fundamental cracking models for asphalt mixes. As expected, BBR tests on aged binder specimens consistently showed that binder modulus increases and the phase angle drops when the binder is cooled to lower temperatures, or when the PAV aging time is increased. However, the same expected result was not true for the BBR mixture specimens. For all three mixes using different binders in the same mix design, the modulus increased and phase angle decreased until each reached a limit common to all three mixes, and then unexpectedly reversed direction toward lower modulus and higher phase angle with additional aging or cooling. These results suggest that micro-damage occurs when a highly aged mixture specimen is cooled to a temperature approaching the BBR-predicted T_{low}, even though the small BBR mix specimen is not confined as it cools. Accepted transverse thermal cracking theories predict that tensile stresses build up as a confined mix shrinks on cooling. Thermal Stress Restrained Specimen tests (TSRST) confirm those predictions quite well. However, with no external confinement, such theories are not applicable to the damage observed when cooling unconfined BBR-sized specimens in a manner thought to be more relevant for block cracking. The authors of the Federal Aviation Administration (FAA) study [7] propose that a different kind of confinement controls age-induced damage. If aggregate particles are interlocked, the asphalt within the interstices creates an internal tensile stress by shrinking much faster than its aggregate surroundings. Either an adhesive failure at the aggregate interface or a cohesive failure within the asphalt itself can occur if the binder has a very low failure strain. When the sample is reheated, the asphalt should swell back to its original position, and any previous contact points broken during cooling should be reestablished. However, if the binder phase angle is too low, reestablishing contact across a micro-crack does not recreate the strength of the original bond, because molecules cannot flow sufficiently to re-establish the original molecular network within the binder. Hence, no problems are observed during early stages of pavement life, but damage accumulates rapidly as the phase angle of the aged asphalt drops to the point it can no longer self-heal during the pavements normal wintertime thermal cycles. This theory forms the basis for the use of Black Space Diagrams, as both phase angle and modulus are postulated to be critical binder properties for crack prediction. Although G* and δ are independent variables in a rheological study, the Glover-Rowe parameter suggests that the onset of block cracking is a function of both, such that

neither can independently predict damage. This is an important observation for other pavement cracking mechanisms as well. Although the G-R parameter seems to predict damage in unconfined aged mixtures, it is probably not an appropriate predictor for transverse thermal cracking, where external confinement of the mixture creates the critical cracking stresses and there is little time for healing. However, some function of G* and delta (or S and m-value) should predict thermal cracking better than current Superpave binder specifications which place individual limits on each variable.

As shown by Buttlar [13], the onset of micro-damage can also be detected by using Acoustic Emission Spectroscopy to listen to the sound waves emitted as micro-cracks begin to form within cooling mixtures.

Although moisture damage can only be evaluated by monitoring damage using mixture modulus and phase angle, evolving binder properties are responsible for the damage caused by oxidation. However, stresses responsible for the failure mechanism can only come from differential cooling of asphalt and aggregate, so damage can only be directly measured when the asphalt is present in a mix. This is similar to the problem with rutting, where the binder modulus at high pavement temperatures is relevant and specified, but the final prediction for rutting is not made from the binder alone.

Although the rate of oxidation is dominated by asphalt chemistry and temperature, the availability of oxygen also plays an important role. Kemp [14] reported that chemical changes deleterious to asphalt performance can be slowed by reducing in-place air voids, and thereby restricting the supply of oxygen within the asphalt mix. With regard to pavement preservation, this finding raises an important question, “Can the rate of oxidative damage be slowed significantly by placing an oxygen-impermeable surface treatment on a newer HMA pavement.”

2.3 Preservation Surface Treatments

The Pavement Preservation Toolbox contains numerous surface treatments, some of which can fully seal the pavement from intrusion by moisture and oxygen from above. The method of choice will depend upon many factors, including:

- pavement condition, structure and grade;
- traffic loads and volume;
- cost and life-cycle considerations;
- availability of materials and construction equipment;
- managing traffic during construction;
- climate;
- vehicle damage; and
- public perception or local preference.

Although pavement preservation includes a broad spectrum of treatments covering preventive maintenance, minor rehabilitation and routine maintenance [15], the most significant cost savings result when pavement surfaces are kept at high ride quality standards. This is usually

accomplished by applying thin treatments to protect the aging pavement surface before damage is visible. Surface treatments include fog seals, sand seals, chip seals, cape seals, slurry seals, micro-surfacing, thin HMA layers, hybrid HMA/emulsion applications using spray pavers, such as ultra-thin bonded wearing courses, and proprietary systems such as Novachip® and FiberMat®. For details regarding the selection, construction and anticipated performance of the various treatments, consult FHWA's Pavement Preservation Toolbox [16].

2.4 Field Studies Evaluating Timing Strategies for Pavement Preservation

Many pavement research studies have been conducted around the world to determine the effectiveness of various surface treatments in extending pavement service life while reducing overall life-cycle costs. Unfortunately, relatively few field studies have included an objective to optimize the timing of the various applications to maximize value. A few field research trials that are relevant to this study include:

2.4.1 LTPP SPS-3

The SPS-3 test sections from the Long Term Pavement Performance (LTPP) program have received much attention, but those field projects were not particularly designed to answer the "Right Time" question. More recent efforts to make the LTPP historical records available to other researches through a new database library (LTPP InfoPave [17]) and a TSP competitive research competition to analyze local LTPP data [18] may prove more fruitful, as will a newly funded LTPP program extension targeting pavement preservation [19]. A request for proposals [20] to design the field experiments for this program is expected soon.

2.4.2 FHWA/FP^2 Spray-Applied Polymer Sealer Study

One nationwide field study of note was funded by FHWA's Office of Construction and Preservation, and managed by the Foundation for Pavement Preservation (FP^2). Called the "Spray Applied Polymer Sealer Study" [21,22,23], this project constructed numerous test sections at each of five locations around the country, with different types of surface seal applications scheduled to be applied over a series of four years. Most of the test sections on these projects evaluated different fog seal emulsions and rejuvenators for use on mainline pavements, shoulders, and new chip seals. Identical test sections were sealed at different times, and some sections received multiple treatments. It was noted that mainline pavements became slick if fogged too heavily, so it is not practical to fully seal the surface in this manner to prevent intrusion of moisture or oxygen. However, the Minnesota Department of Transportation (MnDOT) applies heavy applications of fog seal emulsion to pavement shoulders with very good results. Rejuvenator seals can soften the aged asphalt near the surface of an aged pavement if

they are formulated properly, and if the pavement surface is permeable enough for the emulsion to carry the rejuvenator oil down into the mix about 0.375 to 0.5 inches (9.5-12.5 millimeters) deep. Fog seals are also very effective in preventing chip loss, especially from snow plow abrasion, when applied very early in the life of chip seals. Based in part on this study, a number of agencies, including the Bureau of Federal Lands, now fog seal all chip seals soon after placement. One important part of this study was the search for testing devices that could measure physical properties of binders and mixes within the top 0.5-inch (12.5 millimeters) of the pavement surface. The Portable Seismic Pavement Analyzer (PSPA) developed by Noureldin has been used to analyze the in-place modulus of the mix. Unfortunately, due to theoretical limitations, the PSPA could only be tuned to a thickness greater than two times the nominal maximum aggregate size – which was too thick to be helpful for all but the finest asphalt surface mixes. The Dynamic Shear Rheometer (DSR) Torsion Test (Reinke) and BBR Sliver Test (Marasteanu) have value in testing mixes in layers as thin as 0.5-inch (12.5 millimeters). However, testing such thin mixes creates size effects which make these tools good index tests for comparing results in the same mix, but less useful for comparing mixes with different aggregate configurations [24]. When evaluating the effectiveness of different fog seal treatments on the same pavement, these tools proved invaluable, because binder extraction could not help researchers determine whether the rejuvenator emulsions had effectively penetrated into and restored physical properties of the aged asphalt.

2.4.3 MnDOT Aging/Optimization Study

The MnDOT research team designed a field study to optimize their use of three surface treatment applications:

- Seal Coats over HMA;
- Seal Coats over HMA shoulders; and
- Fog Seals and rejuvenators on HMA pavements.

Cochran [25] described the experimental design, construction and testing of these sections in a 2005 report prepared soon after the projects were built.

A chip seal study was designed for highway TH 56. Initial one-mile long test sections were laid out on two different pavement sections, one built in 1995 and a second built in 1999. The first chip seal sections were placed in 2000, with additional sections added in 2001, 2002 and 2003. Hence, chip seals were placed for the first time over pavements ranging in age from one to eight years. This study is particularly important for answering a question posed earlier, “Can oxidation be slowed by placing chip seals soon after construction?”

A study evaluating both chip seals and rejuvenator fog seals on asphalt shoulders was begun at the same time on I-35 northbound. The shoulders were constructed in 1998. Chip seals were placed in 2000 and 2001, and a rejuvenator fog seal was placed in 2002.

A third MnDOT study on I-90 westbound shoulders evaluated several fog seal applications. The shoulder mix was placed in 1999, and then fogged fairly heavily with CSS-1h one year later. A

portion of the original fog-sealed section was retreated with a diluted CRS-2P emulsion in 2003, and a new one-mile section was also treated with the CRS-2P at the same time. All of the fog-sealed sections were performing well in 2005, and the report concluded that the various fog seal treatments had enhanced the performance of the shoulder mix. Project costs, pictures and early performance reviews are included in the report.

These field projects will continue to be monitored for performance, and a more detailed life-cycle analysis will be undertaken at the end of each project's service life.

Chapter 3 - MnROAD Low Volume Road Initial Testing For Aging/Durability

As noted in Chapter 1, the ultimate goal of this study is to determine the proper timing of preventive maintenance treatments in order to optimize life cycle costs and pavement performance. While this is the overall goal, it is important to better understand how environmental aging of the asphalt binder in the underlying pavement occurs and how it can be affected by pavement preservation treatments.

Earlier research conducted for the Airfield Asphalt Pavement Technology Program indicated that two related parameters – $G'/(\eta'/G')$ at 15°C and 0.005 rad/s (determined from Dynamic Shear Rheometer testing) and the difference between $T_{c,m}$ and $T_{c,S}$ (determined from Bending Beam Rheometer testing), termed ΔTc – both appear to provide an indication of a loss of relaxation properties as the asphalt binder ages [5,6]. Using one or both of these parameters as a part of routine pavement evaluation testing could provide an indication when the asphalt is reaching a critical state of loss of flexibility that would lead to an increased risk of block cracking in the pavement.

Initial testing for this project was desired to identify one or more asphalt binder and/or mixture parameters that could be determined from testing of pavement cores that appear to be related to durability as a result of environmental aging. Subsequent testing to determine the durability parameter(s) would need to be done to validate the failure limits that could be used as objective triggers for various pavement preservation strategies

3.1 MnROAD Low Volume Road

The MnROAD Low Volume Road is a two-lane, 2.5-mile closed loop containing defined test cells. Traffic was restricted to a MnROAD-operated vehicle – an 18-wheel, 5-axle, tractor/trailer with a gross vehicle weight of 80 kips (80K configuration) – travelling on the inside lane of the Low Volume Road loop five days per week. The outside lane was designed to have no traffic so that the environmental effects on pavement performance could be studied [26].

Cell 24 of the MnROAD Low Volume Road (Figure 3.1) was established as a test section to study the effects of aging on asphalt pavements, with the goal of identifying the best timing for preventive maintenance treatments. This test section was constructed using three inches (75 millimeters) of hot mix asphalt (HMA) placed on top of four inches (100 millimeters) of a Class 6 aggregate base and seven feet (approximately 2.1 meters) of sand subgrade. The HMA was a Superpave Level 4 (3-10 million ESAL design) mixture using a PG 58-34 asphalt binder and 20% RAP. Cell 24 also served as the control section for the warm-mix asphalt (WMA) study. It had the same gradation as the WMA mixture cells, but was produced as an HMA. Average in-place density was 91.4% (8.6% air voids) [26]. Built in October 2008, Cell 24 was subdivided into five 100-foot test sections with a control section. A fog seal using CSS-1 emulsion, diluted

1:1, was applied at a rate of 0.03 gallons per square yard to the first section immediately after construction. Subsequent 100-foot sections were sealed each year thereafter using undiluted CRS-2P emulsion at an application rate of 0.15-0.18 gallons per square yard with the final seal scheduled for 2012. To represent these different subsections, Cell 24 was divided as indicated in Figure 3.2.

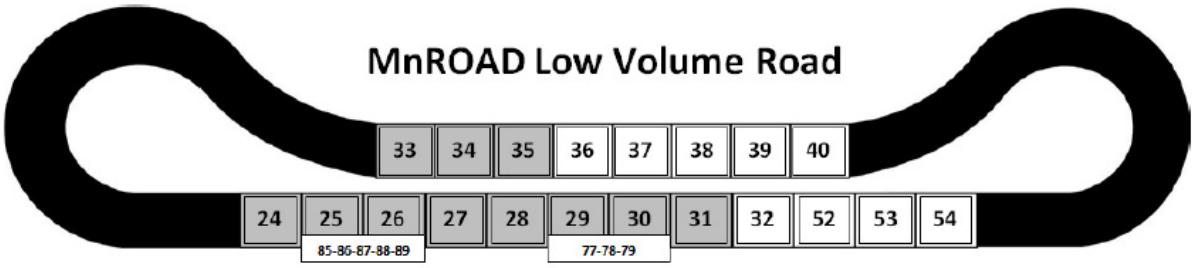

Figure 3.1 MnROAD Low Volume Road Sections

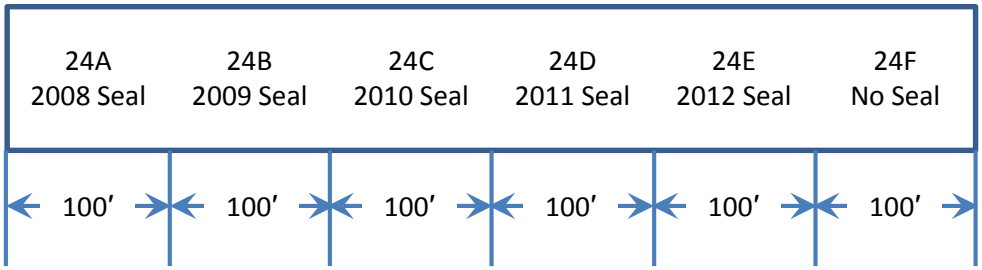

Figure 3.2 Cell 24 Test Sections

Cell 24A represents the test section that was sealed immediately after construction (2008). Cells 24B, 24C, 24D, and 24E represent the test sections that were sealed in 2009, 2010, 2011, and 2012 respectively. Cell 24F will remain unsealed throughout the life of the project.

In late 2010, cores (150-mm diameter) were taken from several test sections of the Low Volume Road including the Travel and Non-Travel lanes of Cell 24 in each of the 100-foot sections that had been sealed (Cells 24A, 24B, and 24C) as well as the last 100-foot section that had not been sealed and would remain unsealed throughout the project (Cell 24F). Table 3.1 shows the test sections and number of cores taken.

Table 3.1 2010 MnROAD Low Volume Road Cores

Cell	Designation	Non-Travel	Travel
24	Aging Study (2008)		
24A	Sealed in 2008	6	6
24B	Sealed in 2009	6	6
24C	Sealed in 2010	6	6
24F	Unsealed	6	6
27	Geocomposite Barrier Drain 2006 (Chip Seal in 2009)	6	
28	Geocomposite Barrier Drain 2006 (No Chip Seal)	6	
33	Acid Modification Study (2007) 0.75% PPA	6	
34	Acid Modification Study (2007) 0.3% PPA + 1% SBS	6	
35	Acid Modification Study (2007) 2% SBS	6	

Cores from Cells 27 and 28 were retained, but were not tested for this study. The team elected to focus on cores from Cell 24 – the section designated to be used in the aging study – and Cells 33, 34, and 35 from the Acid Modification Study. Cells from the Acid Modification Study were selected since they represented asphalt mixtures without RAP, using a modified PG 58-34 asphalt binder. Additionally, these cells were not sealed – allowing for an evaluation of aging effects on unsealed pavement sections.

Cores from Cell 24C were retained, but were not tested. Since this pavement section was sealed less than three months prior to the cores being cut, it was felt that any data from Cell 24C would be most similar to Cell 24F.

For Cells 24A (Travel and Non-Travel), 24B (Travel and Non-Travel), 24F (Travel and Non-Travel), 33, 34, and 35, two cores were selected and each core was cut into four layers starting at the top of the core. From the top of the core, a line was marked on the side of the core representing a layer thickness of approximately 12.5 millimeters. This layer was identified as “Top”. After cutting the top layer, another line was marked on the side of the core representing a layer thickness of approximately 12.5 millimeters. This layer was identified as “Mid”. After cutting the middle layer, another line was marked on the side of the core representing a layer thickness of approximately 12.5 millimeters. This layer was identified as “Bottom”. The remainder of the core was discarded. This cutting pattern is illustrated in Figure 3.3.

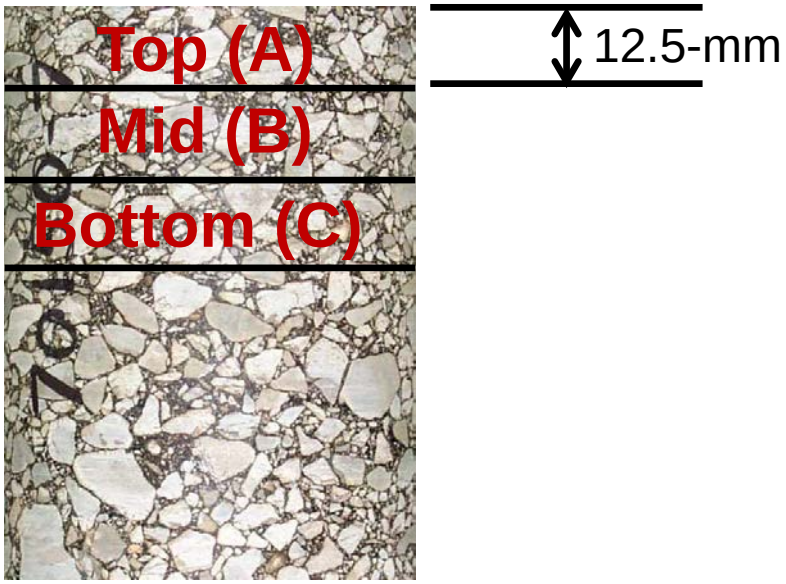

Figure 3.3 Preparation (Cutting) of Cores Used for Extraction/Recovery of Asphalt Binder

The thickness of the saw blade used for cutting specimens was approximately five millimeters. This means that the Top layer of each core represents material from the surface to a depth of 12.5 millimeters. The Mid layer of each core represents material from a depth of 17.5 millimeters (12.5 millimeters to the bottom of the Top layer plus five millimeters for the thickness of the saw blade) to a depth of 30 millimeters. The Bottom layer of each core represents material from a depth of 35 millimeters (30 millimeters to the bottom of the Mid layer plus five millimeters for the thickness of the saw blade) to a depth of 47.5 millimeters.

By cutting cores into layers, the effect of aging could be studied as a function of depth in addition to time. Witczak and Mirza in the development of a global aging model for asphalt binders found that the modulus changed significantly with depth from the pavement surface due to aging and temperature effects – both of which are reduced further into the pavement layer [27]. This is illustrated in Figure 3.4 from their paper published in 1995. As can be seen in the figure, the mixture modulus at a depth of 50 millimeters, or two inches, is less than half of the modulus at the pavement surface. It is expected that much of the change in modulus is a result of oxidative aging that occurs more near the pavement surface.

3.2 Initial Test Plan

After cutting, the layers from two cores were combined to use for solvent extraction and recovery testing. With each layer having approximate dimensions of 150-mm diameter and 12.5-mm thickness, the volume of the core could be estimated to be approximately 220 cm^3. Assuming that the average bulk specific gravity of the core (G_{mb}) was 2.300, the mass of the core layer could be estimated to be approximately 500 grams. Finally, assuming an average asphalt binder content of 5.5%, the estimated recovered asphalt binder mass for each layer would be

approximately 28 grams. To conduct binder testing using both the Dynamic Shear Rheometer (DSR) and Bending Beam Rheometer (BBR), it was determined that at least 50 grams of recovered asphalt binder should be obtained, thereby leading to the decision to combine like layers of two cores before conducting solvent extraction and recovery procedures.

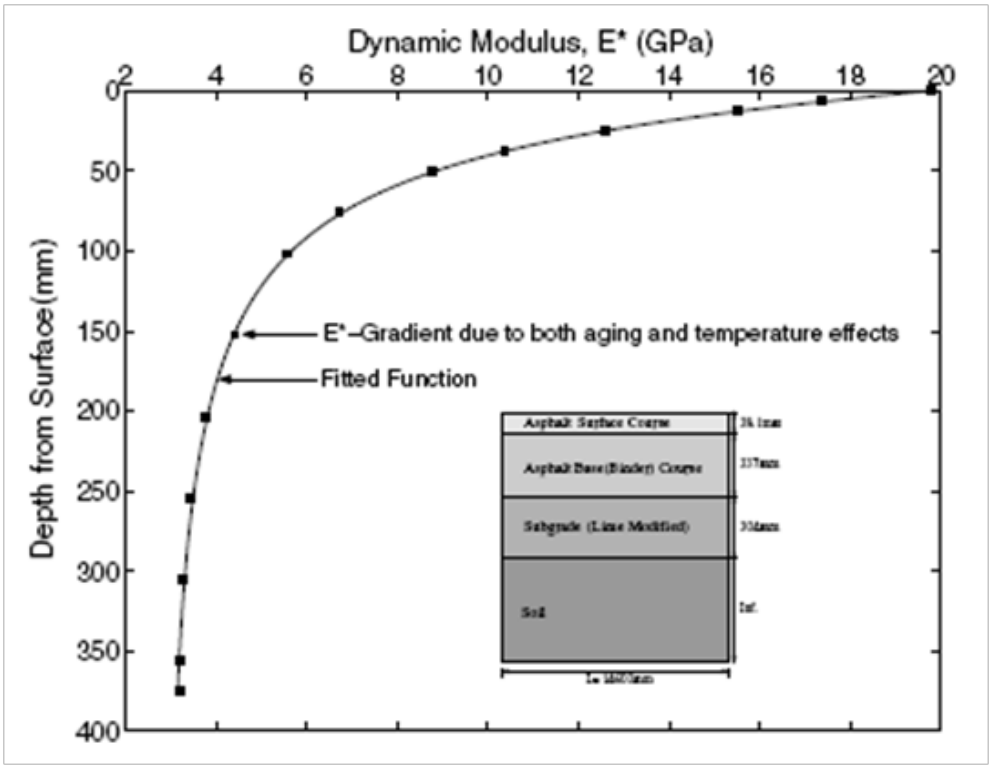

Figure 3.4 Effect of Layer Depth on Mixture Modulus (Witczak and Mirza, 1995)

Although not conducted on all the cores, layers from Cells 24A and 24B were tested to determine the G_{mb} of the core after cutting. The data, shown in Table 3.2, generally confirms the assumptions used.

Table 3.2 Bulk Specific Gravity of Cut Layers for Cells 24A and 24B

Cell	Lane	Layer	Replicate	Dry Weight, g	Volume, cm^3	G_{mb}
24A	Non-Travel	Top	1	496.4	213.2	2.328
			2	451.7	195.3	2.313
		Mid	1	526.6	222.9	2.362
			2	493.5	210.2	2.348
		Bottom	1	563.2	238.2	2.364
			2	507.4	217.1	2.337
24B	Non-Travel	Top	1	495.3	213.3	2.322
			2	571.4	246.1	2.322
		Mid	1	570.1	241.6	2.360
			2	462.7	197.0	2.349
		Bottom	1	539.5	232.7	2.318
			2	508.8	221.5	2.297

Solvent extraction and recovery testing was conducted on the combined layers from two cores of a particular cell. For instance, the Top layers from two cores of the Cell 24A Non-Travel section were combined to perform one extraction/recovery procedure. Solvent extraction was conducted following AASHTO T 164, *Quantitative Extraction of Asphalt Binder from Hot-Mix Asphalt (HMA)*, except that toluene was used as the solvent. Toluene was selected since it was believed to perform better with the recovery of modified asphalt binders and was not considered as hazardous a solvent as trichloroethylene. Recovery of the asphalt binder from solution was accomplished using the recovery procedure described in AASHTO T 319, *Quantitative Extraction and Recovery of Asphalt Binder from Asphalt Mixtures*. The procedures in AASHTO T 319 were originally developed during the Strategic Highway Research Program (SHRP) to recover asphalt binder from a mixture without inducing additional "aging" as a result of solvent hardening and excess recovery temperatures. During the conduct of a project for the National Cooperative Highway Research Program (NCHRP), the procedure was refined for the recovery of recycled asphalt pavement (RAP) materials, and is described in NCHRP Web Document 30, Recommended Use of Reclaimed Asphalt Pavement in the Superpave Mix Design Method [28]. At the completion of the recovery procedure, the recovered asphalt binder was poured into a container and identified by pavement section and layer.

Testing that was planned for the recovered asphalt binder samples is shown below:

- **Bending Beam Rheometer (BBR)** – testing to determine Stiffness and m-value at multiple temperatures. Data can then be used to determine the continuous grade temperature based on S(60) = 300 MPa and m(60) = 0.300. Research conducted as part of the AAPTP 06-01 project indicated that the difference between the continuous grade temperature where m(60) = 0.300, designated as $T_c(m)$, and the continuous grade temperature where S(60) = 300 MPa, designated as $T_c(S)$, may be related to aging [5,6]. This parameter is identified as ΔT_c.
- **Dynamic Shear Rheometer (DSR) Frequency Sweep** – testing to determine the temperature-frequency response of the recovered asphalt binder using intermediate temperatures of 5, 15, and 25°C and loading frequency from 0.1 to 100 rad/s. Data from the temperature-frequency sweep testing can be combined into a mastercurve at a reference temperature. Research conducted as part of the AAPTP 06-01 project validated findings from earlier research at Texas A&M University [4] that a durability parameter, $G'/(\eta'/G')$ at 15°C and 0.005 rad/s was related to asphalt binder ductility, which, in turn, was related to durability.
- **Dynamic Shear Rheometer (DSR) Single Point Test** – testing conducted at 45°C and 10 rad/s to determine complex shear modulus (G*) and phase angle (δ). Research conducted at Texas A&M University indicated that the durability parameter, $G'/(\eta'/G')$, could be determined directly at 44.7°C and 10 rad/s and would provide equivalent results as $G'/(\eta'/G')$ determined at 15°C and 0.005 rad/s [4]. The advantage of this approach is that it uses a direct measurement and does not rely on temperature-frequency sweep testing and determination of a mastercurve to derive the durability parameter. The disadvantage of this approach is that it assumes that time-temperature superposition principles apply for all asphalt binders. Findings during the AAPTP 06-01 research indicated that the single point test did not work as well for determining the durability parameter as the mastercurve approach [5]. An alternative method would be to directly measure $G'/(\eta'/G')$ at 15°C and 0.005 rad/s. The disadvantage is that the slow loading

means that each cycle would take approximately 20 minutes. To collect 10 cycles would require nearly 3.5 hours per test. Temperature-frequency sweep testing as described above can be accomplished in less than two hours (with some additional time required to generate the mastercurve and derive the durability parameter).

- **Double Edge Notched Tension (DENT) Test** – testing conducted at 15°C using duplicate tests at three ligament lengths. This test has been proposed by Professor Simon Hesp and is intended to examine ductile failure and provide an indication of the crack tip opening displacement and essential work of fracture. The disadvantage of the test is that the test specimens are modified ductility specimens. Each test specimen requires a considerably greater amount of asphalt binder than required by a DSR test. To get the six test specimens needed for the DENT analysis would require additional recovery procedures.
- **Linear Amplitude Sweep (LAS) Test** – testing conducted at an intermediate temperature (such as 15°C). This test has been proposed by Dr. Hussain Bahia as a possible intermediate temperature test related to asphalt binder fatigue. The test is conducted by first performing a frequency sweep at small strain (0.1%) and a range of loading frequencies to determine the parameter α, which is related to the slope of the log storage modulus (G′) versus log frequency. The second part of the test involves testing at a fixed loading frequency of 10 Hz and a linearly increasing strain from 1% to a maximum of 30%. At each strain level, the average data is collected for each 10 cycles (1 second) until 10 data points (10 seconds) are completed. The resulting dissipated energy is calculated per data point and used in a viscoelastic continuum damage (VECD) analysis. VECD analysis has been used for asphalt mixtures to relate to fatigue cracking.

As discussed, the DENT test requires the most amount of material, approximately 180 grams (30 grams per specimen x 2 specimens per ligament length x 3 ligament lengths). By testing 12.5-mm layers, it takes two cores to generate approximately 50-60 grams of recovered asphalt binder. With only six cores taken from each site, there was insufficient mixture to be recovered to produce enough asphalt binder for a complete DENT test evaluation. Therefore the DENT test was not explored in this study.

3.3 Asphalt Binder Testing

Table 3.3 indicates the testing matrix for the 2010 MnROAD Cores. Completed tests are indicated as noted in the table. Table 3.4 provides information on testing of the materials used in the pavement sections. Asphalt binders were tested after being subjected to Rolling Thin Film Oven (RTFO) aging and after additional aging following the Pressure Aging Vessel (PAV) procedure. The RTFO procedure is described in AASHTO T 240, *Effect of Heat and Air on a Moving Film of Asphalt Binder (Rolling Thin Film Oven Test)*. The PAV procedure is described as AASHTO R 28, *Accelerated Aging of Asphalt Binder Using a Pressurized Aging Vessel (PAV).*

Table 3.3 Recovered Asphalt Binder Testing - 2010 MnROAD Low Volume Road Cores

				DSR		
Cell	**Lane**	**Layer**	**BBR T_c**	**Freq. Sweep 5, 15, 25°C 0.1-100 rad/s**	**Single Pt. 45°C 10 rad/s**	**LAS 16°C**
24A	Non-Travel	Top	X	X	X	X
		Mid	X	X	X	X
		Bot	X	X	X	X
	Travel	Top	X	X	X	X
		Mid	X	X	X	X
		Bot	X	X	X	X
24B	Non-Travel	Top	X	X	X	X
		Mid	X	X	X	X
		Bot	X	X	X	X
	Travel	Top	X	X	X	X
		Mid	X	X	X	X
		Bot	X	X	X	X
24F	Non-Travel	Top	X	X	X	X
		Mid	X	X	X	X
		Bot	X	X	X	X
	Travel	Top	X	X	X	X
		Mid	X	X	X	X
		Bot	X	X	X	X
33	Non-Travel	Top	X	X	X	X
		Mid	X	X	X	X
		Bot	X	X	X	X
34	Non-Travel	Top	X	X	X	X
		Mid	X	X	X	X
		Bot	X	X	X	X
35	Non-Travel	Top	X	X	X	X
		Mid	X	X	X	X
		Bot	X	X	X	X

Completed testing indicated by "x" in appropriate cell.
BBR testing conducted at two temperatures to determine T_c(S) and T_c(m).

Table 3.4 Binder Testing - MnROAD Materials

				DSR		
Cell	**Material**	**Cond.**	**BBR T_c**	**Freq. Sweep 5, 15, 25°C 0.1-100 rad/s**	**Single Pt. 45°C 10 rad/s**	**LAS 16°C**
27	PG 52-34 Binder	RTFO	n/a	X	X	X
		PAV	X	X	X	X
		PAV 90°C	X	X	X	X
33	PG 58-34 Binder 0.75% PPA	RTFO	n/a	X	X	X
		PAV	X	X	X	X
34	PG 58-34 Binder 0.3% PPA + 1% SBS	RTFO	n/a	X	X	X
		PAV	X	X	X	X
35	PG 58-34 Binder 2% SBS	RTFO	n/a	X	X	X
		PAV	X	X	X	X

Completed testing indicated by "x" in appropriate cell.
An entry of "n/a" is used to indicate that testing is not anticipated to be conducted.
PAV aging conducted at 100°C, except as noted.
BBR testing conducted at two temperatures to determine T_c(S) and T_c(m).

As indicated in Tables 3.3 and 3.4, BBR testing to determine ΔT_c was completed for all recovered asphalt binder sections/layers from the 2010 MnROAD cores and for all PAV-aged asphalt binder materials (no RTFO-aged material was tested). All DSR testing – Frequency Sweep, Single Point, and LAS – was completed for all recovered asphalt binder sections/layers from the 2010 MnROAD cores and for all asphalt binder materials (RTFO and PAV-aged material).

3.3.1 BBR Results

BBR test results are shown in Tables 3.5 and 3.6 for the cores and asphalt binders, respectively.

Table 3.5 BBR Test Results - 2010 MnROAD Recovered Asphalt Binder

			-18°C		-24°C		-30°C				
Cell	**Lane**	**Layer**	**S(60)**	**m(60)**	**S(60)**	**m(60)**	**S(60)**	**m(60)**	**T_c(S)**	**T_c(m)**	**ΔT_c**
24A	Non-Travel	Top	140	0.364	313	0.299			-33.7	-33.9	-0.2
		Mid			274	0.326	566	0.254	-34.7	-36.2	-1.4
		Bot			261	0.332	530	0.253	-35.2	-36.4	-1.3
	Travel	Top	156	0.347	342	0.290			-33.0	-32.9	0.1
		Mid			278	0.319	576	0.252	-34.6	-35.7	-1.1
		Bot	125	0.384	302	0.318			-34.0	-35.6	-1.7
24B	Non-Travel	Top			271	0.317	539	0.258	-34.9	-35.7	-0.8
		Mid			292	0.320	615	0.244	-34.2	-35.6	-1.4
		Bot			266	0.335	578	0.258	-34.9	-36.7	-1.8
	Travel	Top	146	0.356	335	0.296			-33.2	-33.6	-0.4
		Mid			280	0.327	605	0.252	-34.5	-36.1	-1.6
		Bot			281	0.327	600	0.254	-34.5	-36.2	-1.7
24F	Non-Travel	Top			264	0.316	549	0.254	-35.0	-35.5	-0.5
		Mid			258	0.336	544	0.262	-35.2	-36.9	-1.7
		Bot			253	0.340	537	0.264	-35.4	-37.2	-1.8
	Travel	Top	130	0.370	300	0.312			-34.0	-35.2	-1.2
		Mid			265	0.334	535	0.252	-35.1	-36.5	-1.4
		Bot			260	0.342	566	0.260	-35.1	-37.0	-1.9
33	Non-Travel	Top	140	0.346	312	0.296			-33.7	-33.5	0.3
		Mid			266	0.316	536	0.252	-35.0	-35.5	-0.4
		Bot			284	0.300	532	0.250	-34.5	-34.0	0.5
34	Non-Travel	Top	137	0.352	296	0.294			-34.1	-33.3	0.8
		Mid			252	0.328	527	0.264	-35.4	-36.6	-1.2
		Bot			224	0.347	518	0.273	-36.1	-37.8	-1.7
35	Non-Travel	Top			290	0.302	559	0.244	-34.3	-34.2	0.2
		Mid			221	0.334	505	0.267	-36.2	-37.0	0.8
		Bot			218	0.337	498	0.275	-36.3	-37.6	-1.3

Shaded cells indicate that testing is not needed or will not be conducted.
The Stiffness in MPa determined at 60 seconds is designated as S(60). Values shown are in MPa.
The m-value determined at 60 seconds is designated as m(60). Values are unitless.
T_c(S) is the temperature at which S(60) is equal to the specification limit (300 MPa). Values shown are in °C.
T_c(m) is the temperature at which m(60) is equal to the specification limit (0.300). Values shown are in °C.
ΔT_c is the difference between T_c(m) and T_c(S). Values shown are in °C.

Table 3.6 BBR Test Results - MnROAD Asphalt Binders

			-18°C		-24°C		-30°C				
Cell	**Material**	**Cond.**	**S(60)**	**m(60)**	**S(60)**	**m(60)**	**S(60)**	**m(60)**	**T_c(S)**	**T_c(m)**	**ΔT_c**
27	PG 52-34 Binder	RTFO									
		PAV			272	0.338	571	0.268	-34.8	-37.3	-2.5
		PAV 90°C			240	0.355	542	0.280	-35.6	-38.4	-2.7
33	PG 58-34 Binder 0.75% PPA	RTFO									
		PAV			218	0.319	484	0.269	-36.4	-36.3	0.1
34	PG 58-34 Binder 0.3% PPA + 1% SBS	RTFO									
		PAV			214	0.330	471	0.274	-36.6	-37.2	-0.7
35	PG 58-34 Binder 2% SBS	RTFO									
		PAV			244	0.323	516	0.266	-35.7	-36.4	-0.7

Shaded cells indicate that testing is not needed or will not be conducted.
The Stiffness in MPa determined at 60 seconds is designated as S(60). Values shown are in MPa.
The m-value determined at 60 seconds is designated as m(60). Values are unitless.
T_c(S) is the temperature at which S(60) is equal to the specification limit (300 MPa). Values shown are in °C.
T_c(m) is the temperature at which m(60) is equal to the specification limit (0.300). Values shown are in °C.
ΔT_c is the difference between T_c(m) and T_c(S). Values shown are in °C.

The data in Table 3.5 can also be illustrated to show the effect of pavement section and average layer depth on the BBR parameter, ΔT_c. In the following figures, the average layer depth is calculated by determining the midpoint of the depth from the top to the bottom of each cut layer. With 12.5-mm thick layers (and allowing for the thickness of the saw blade cut), the average layer depth for the Top, Mid, and Bot layers is 6.25, 23.75, and 41.25 mm, respectively.

Figure 3.5 illustrates the ΔT_c values for the Cell 24 cores taken from the Non-Travel lane of the MnROAD Low Volume loop. Figure 3.6 illustrates the ΔT_c values for the Cell 24 cores taken from the Travel lane of the MnROAD Low Volume loop. In both Figures, the plot is arranged so that pavement depth is illustrated by moving down the y-axis from the origin in the top left corner. Pavement aging is represented by increasing ΔT_c values, progressing from left to right on the x-axis.

Looking at the data as a whole, it can be seen that the figures generally match the shape of the curve shown in Figure 3.4. That is, the asphalt stiffness, or the aging effect, is less the further the layer is from the pavement surface. This is a rational response.

The expectation in Figures 3.5 and 3.6 is that the section that was sealed in 2008 immediately after construction (Cell 24A) would show less aging compared to the section sealed in 2009 (Cell 24B) and the unsealed section (Cell 24F). This is not the case as indicated in either figure. In Figures 3.5 and 3.6, Cell 24A has the highest value of ΔT_c at each layer depth. By contrast, the recovered binder from Cell 24F has generally the lowest value of ΔT_c at each layer depth.

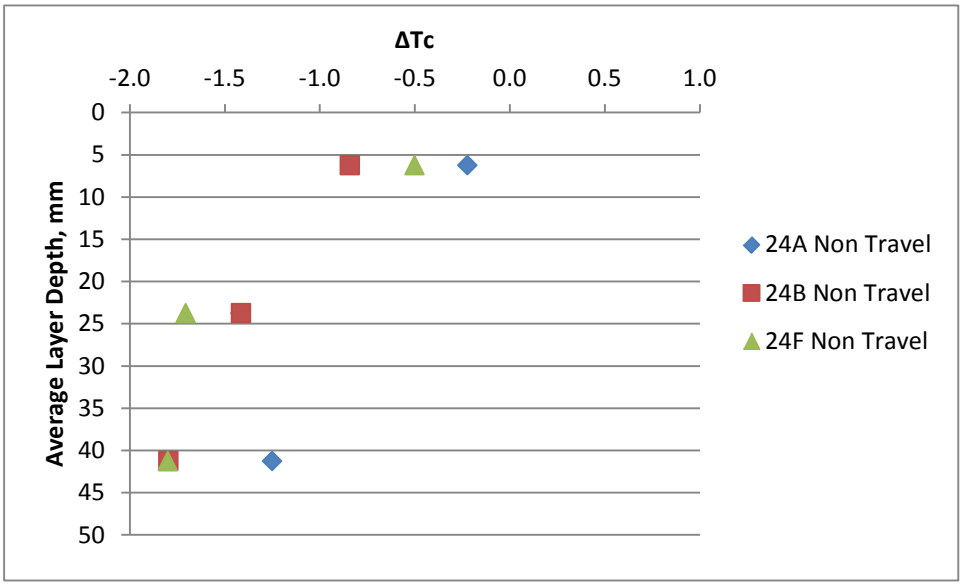

Figure 3.5 BBR ΔTc as a Function of Layer Depth - Cell 24 Non-Travel Lane

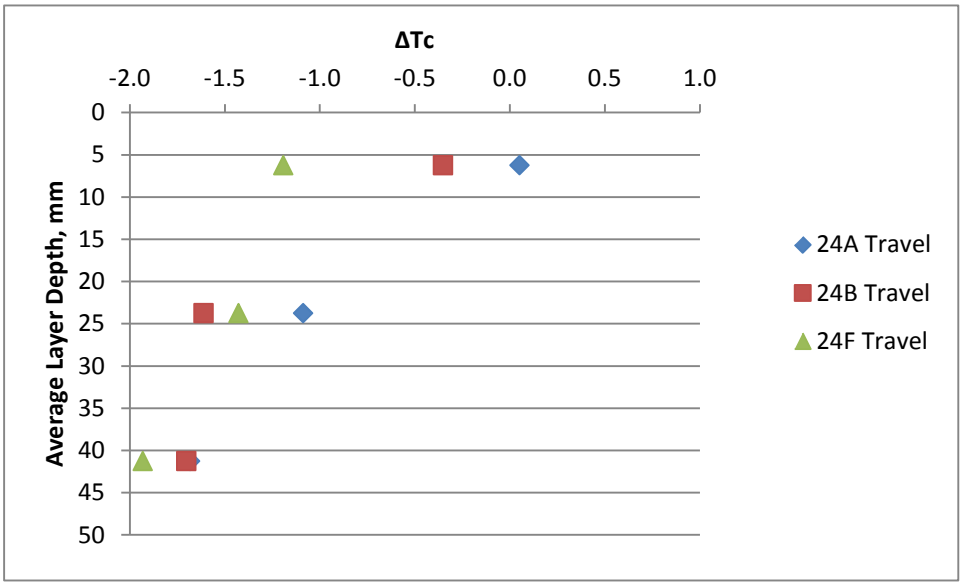

Figure 3.6 BBR ΔTc as a Function of Layer Depth - Cell 24 Travel Lane

Several possibilities exist to explain the data in Figures 3.5 and 3.6. These are explored as follows (in no particular order):

- The ΔT_c parameter may not be indicative of aging as previously thought.

- After only two years of in-service aging, the data is still far enough below the expected cracking warning limit (ΔT_c = 2.5 from previous research), that the ΔT_c parameter is not indicating significant aging.
- Material or construction variability (pavement density, percentage of RAP used, and stiffness of RAP) may be affecting results.
- Testing variability (single operator variability of BBR Stiffness and m-value)

Figure 3.7 illustrates the change in BBR ΔT_c value as a function of layer depth for the mixtures used in the MnROAD Acid Modification Study (Cells 33-35). Only cores from the Non-Travel lane were obtained and recovered.

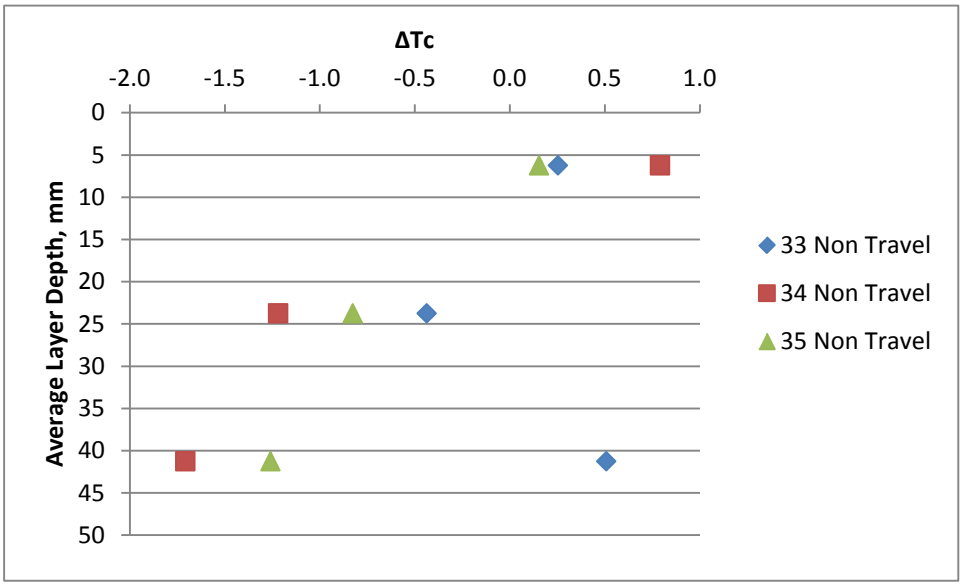

Figure 3.7 BBR ΔTc as a Function of Layer Depth - Acid Modification Study Cells

One key observation from Figure 3.7 is that the ΔT_c value generally decreases with increasing depth, as expected. The exception to this is the recovered asphalt binder from the Bottom layer of Cell 33. In this case, the ΔT_c value is actually higher than the value of the recovered asphalt binder from the Top layer of Cell 33. This value may be in error.

The data in Figure 3.7 is also shown in Figure 3.8, with the ΔT_c values for the PAV-aged asphalt binders shown as dashed vertical lines.

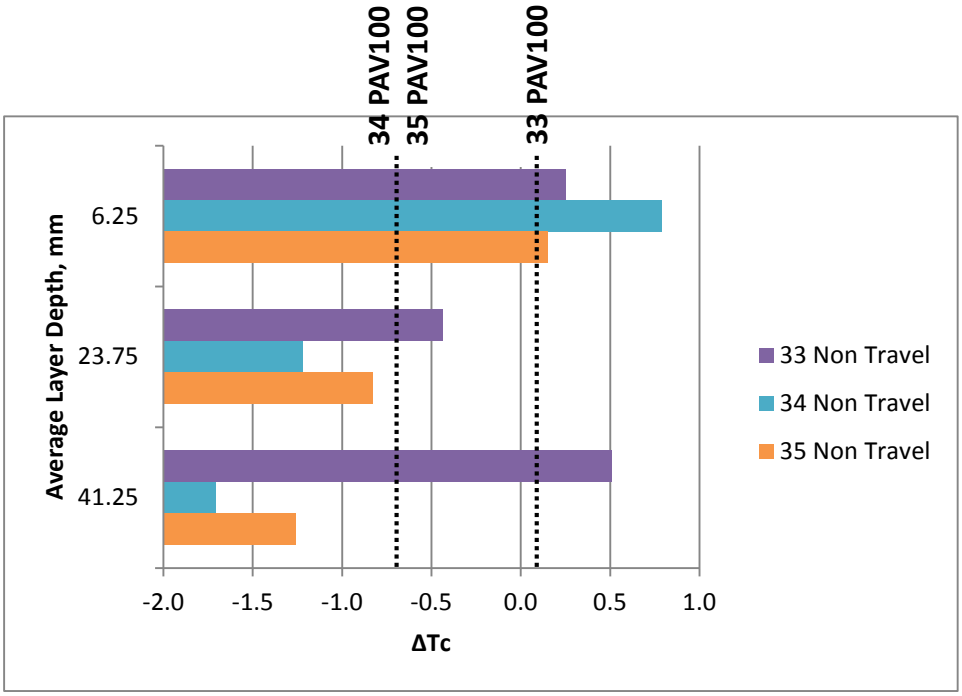

Figure 3.8 BBR ΔTc as a Function of Layer Depth - Acid Modification Study Cells (with PAV-aged results shown)

From Figure 3.8, it can be observed that the ΔT_c values of the Top layer of all three cells exceed the measured ΔT_c values from the PAV-aged asphalt binders, indicating that the in-service aging of the Top layers has exceeded the aging simulated by the PAV. Except for the apparently anomalous ΔT_c value obtained for the Bottom layer of Cell 33, the ΔT_c values of the Middle and Bottom layers of all three cells are less than the measured ΔT_c values from the PAV-aged asphalt binders.

One of the findings from the study conducted by the research team for the Airfield Asphalt Pavement Technology Program (Project 06-01) was that the DSR Parameter derived from temperature-frequency sweep testing was related to the ΔT_c parameter derived from BBR testing [5]. Figure 3.9 shows the relationship between the DSR parameter, $G'/(\eta'/G')$ at 15°C and 0.005 rad/s, and the ΔT_c parameter. A third-order polynomial fits the data of the logarithm of $G'/(\eta'/G')$ and ΔT_c and provides an equation relating the two parameters with an R-squared value of 0.98 as shown below:

$$\text{Log}\,[G'/(\eta'/G')\,] = 0.0034(\Delta T_c)^3 - 0.0542(\Delta T_c)^2 + 0.4315(\Delta T_c) - 3.8249 \qquad \text{[Eq. 1]}$$

If this predictive equation is used with the ΔT_c data shown in Tables 3.5 and 3.6, the $G'/(\eta'/G')$ parameter at 15°C and 0.005 rad/s can be estimated. This data is shown in Tables 3.7 and 3.8 below.

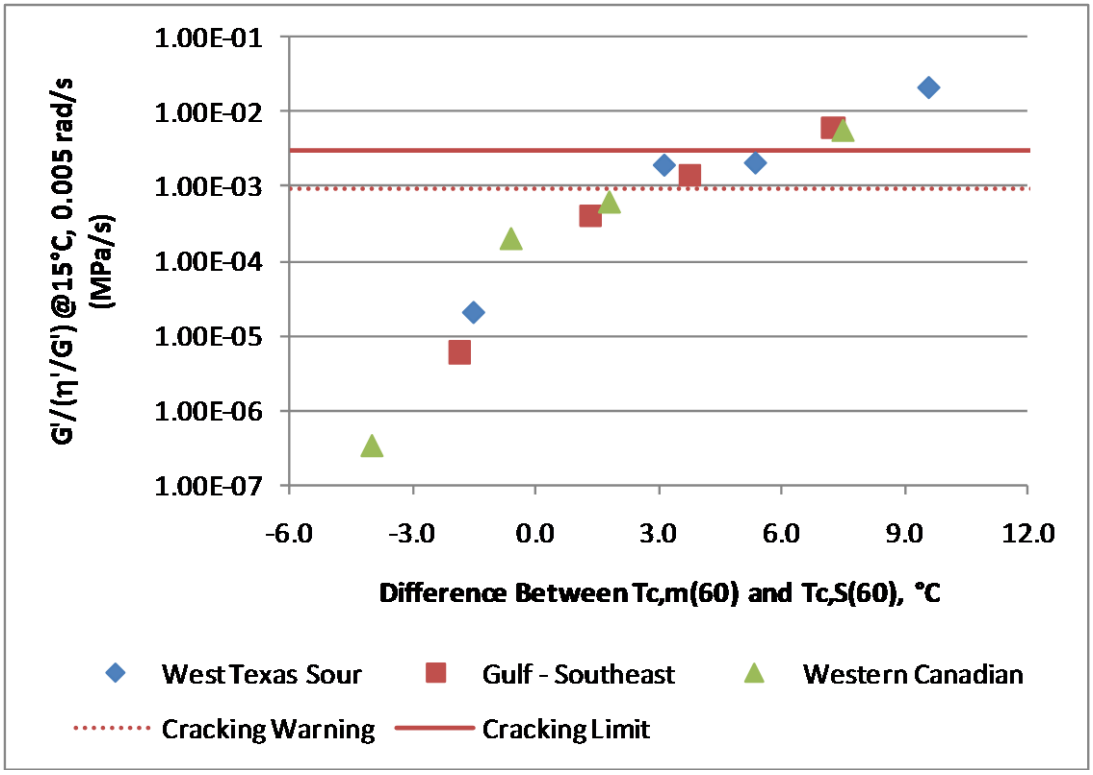

Figure 3.9 DSR Parameter, G′/(η′/G′), as a Function of BBR ΔTc Value

Table 3.7 2010 MnROAD Recovered Asphalt Binders – ΔTc and Estimated G′/(η′/G′)

Cell	Lane	Layer	T_c(S) °C	T_c(m) °C	ΔT_c °C	Estimated G′/(η′/G′) MPa/s
24A	Non-Travel	Top	-33.7	-33.9	-0.2	1.33E-04
		Mid	-34.7	-36.2	-1.4	3.15E-05
		Bot	-35.2	-36.4	-1.3	3.95E-05
	Travel	Top	-33.0	-32.9	0.1	1.75E-04
		Mid	-34.6	-35.7	-1.1	4.90E-05
		Bot	-34.0	-35.6	-1.7	2.15E-05
24B	Non-Travel	Top	-34.9	-35.7	-0.8	6.65E-05
		Mid	-34.2	-35.6	-1.4	3.16E-05
		Bot	-34.9	-36.7	-1.8	1.81E-05
	Travel	Top	-33.2	-33.6	-0.4	1.16E-04
		Mid	-34.5	-36.1	-1.6	2.39E-05
		Bot	-34.5	-36.2	-1.7	2.09E-05
24F	Non-Travel	Top	-35.0	-35.5	-0.5	9.88E-05
		Mid	-35.2	-36.9	-1.7	2.08E-05
		Bot	-35.4	-37.2	-1.8	1.80E-05
	Travel	Top	-34.0	-35.2	-1.2	4.28E-05
		Mid	-35.1	-36.5	-1.4	3.10E-05
		Bot	-35.1	-37.0	-1.9	1.47E-05
33	Non-Travel	Top	-33.7	-33.5	0.3	2.11E-04
		Mid	-35.0	-35.5	-0.4	1.06E-04
		Bot	-34.5	-34.0	0.5	2.64E-04
34	Non-Travel	Top	-34.1	-33.3	0.8	3.32E-04
		Mid	-35.4	-36.6	-1.2	4.12E-05
		Bot	-36.1	-37.8	-1.7	2.07E-05
35	Non-Travel	Top	-34.3	-34.2	0.2	1.92E-04
		Mid	-36.2	-37.0	0.8	6.78E-05
		Bot	-36.3	-37.6	-1.3	3.91E-05

T_c(S) is the temperature at which S(60) is equal to the specification limit (300 MPa).
T_c(m) is the temperature at which m(60) is equal to the specification limit (0.300).
ΔT_c is the difference between T_c(m) and T_c(S).

Table 3.8 2010 MnROAD Asphalt Binders – ΔTc and Estimated G′/(η′/G′)

Cell	Material	Cond.	T_c(S) °C	T_c(m) °C	ΔT_c °C	Estimated G′/(η′/G′) MPa/s
27	PG 52-34 Binder	RTFO	n/a	n/a	n/a	n/a
		PAV	-34.8	-37.3	-2.5	6.15E-06
		PAV 90°C	-35.6	-38.4	-2.7	3.62E-06
33	PG 58-34 Binder 0.75% PPA	RTFO	n/a	n/a	n/a	n/a
		PAV	-36.4	-36.3	0.1	1.86E-04
34	PG 58-34 Binder 0.3% PPA + 1% SBS	RTFO	n/a	n/a	n/a	n/a
		PAV	-36.6	-37.2	-0.7	8.29E-05
35	PG 58-34 Binder 2% SBS	RTFO	n/a	n/a	n/a	n/a
		PAV	-35.7	-36.4	-0.7	7.58E-05

An entry of "n/a" is used to indicate that testing is not anticipated to be conducted.
T_c(S) is the temperature at which S(60) is equal to the specification limit (300 MPa).
T_c(m) is the temperature at which m(60) is equal to the specification limit (0.300).
ΔT_c is the difference between T_c(m) and T_c(S).

3.3.2 DSR Temperature-Frequency Sweep Results

As previously discussed, the temperature-frequency response of the recovered asphalt binder was determined using the DSR at intermediate temperatures of 5, 15, and 25°C and loading frequencies from 0.1 to 100 rad/s. Data from the temperature-frequency sweep testing can be combined into a mastercurve at a reference temperature. Research conducted as part of the AAPTP 06-01 project validated findings from earlier research at Texas A&M University that a durability parameter, G′/(η′/G′) at 15°C and 0.005 rad/s was related to asphalt binder ductility, which, in turn, was related to durability.

Results from the temperature-frequency sweep testing were input into the Abatech RHEA™ software to generate a mastercurve from the isotherms. An example of the results from the DSR temperature-frequency sweep test is shown in Figure 3.10.

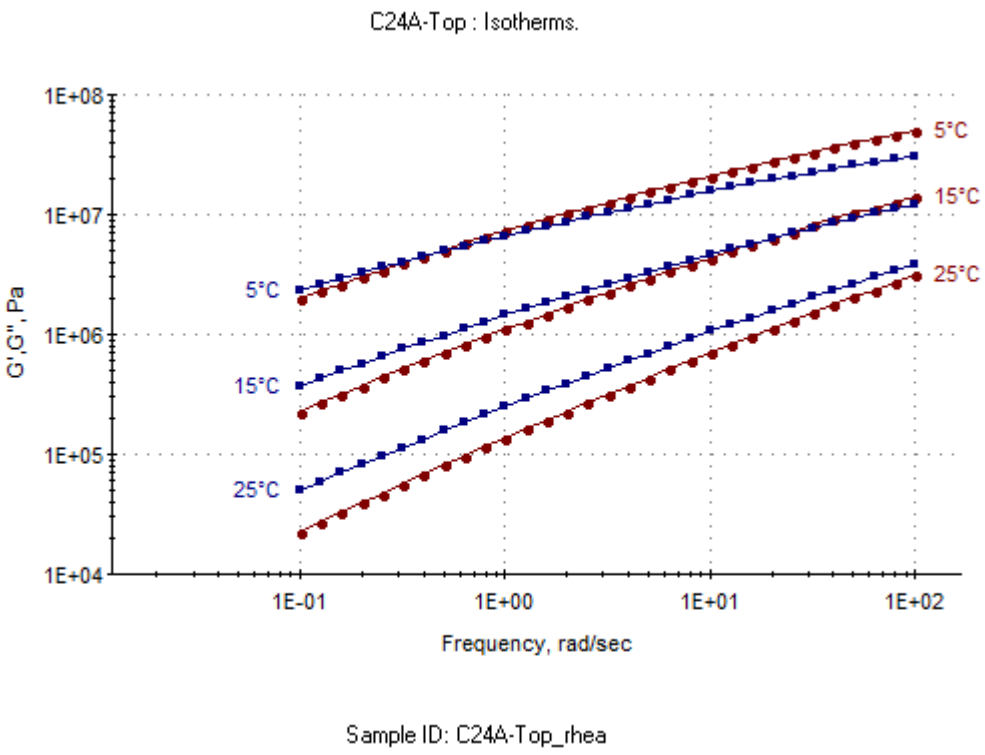

Figure 3.10 Example Output from DSR Temperature-Frequency Sweep Testing (Isotherms)

The mastercurve was generated by shifting the data to a reference temperature (in this case, 15°C) and fitting the data using a rheological model. For asphalt binders, the CAM (Christensen-Anderson-Marasteanu) model is often used. The equations for complex modulus and phase angle are given below:

$$G^*(\omega) = G_o[1+(\omega_o / \omega)^{\beta}]^{-\kappa/\beta} \quad \text{[Eq. 2]}$$

$$\delta(\omega) = 90 / [1+(\omega / \omega_o)^{\beta}] \quad \text{[Eq. 3]}$$

where:

$G^*(\omega)$ = Complex shear modulus as a function of frequency, Pa
$\delta(\omega)$ = Phase angle as a function of frequency, degrees
G_0 = Glassy shear modulus, Pa
ω = Loading frequency, rad/s
ω_0 = Crossover frequency, rad/s
β = Width parameter
κ = log:log asymptote gradient

An example of the fitted complex modulus and phase angle curves are shown in Figure 3.11.

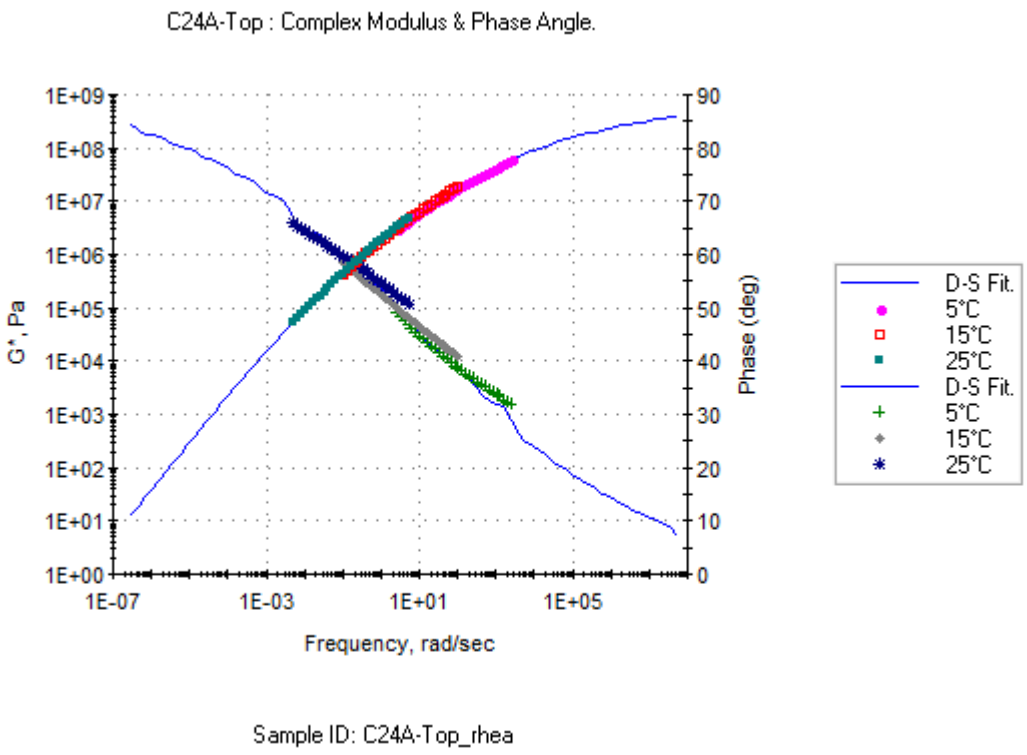

Figure 3.11 Example Mastercurve Generated from DSR Temperature-Frequency Sweep Testing

In Figure 3.11, the complex shear modulus, G*, curve is shown starting at the lower left of the graph (low modulus at slow loading frequency) and increasing to the upper right of the graph (high modulus at fast loading frequency). The G* curve uses the scaling shown on the left vertical axis. The phase angle, δ, curve is shown starting at the upper left of the graph (high phase angle at slow loading frequency) and decreasing to the lower right of the graph (low phase angle at fast loading frequency). The δ curve uses the scaling shown on the right vertical axis.

Once the mastercurve is fitted, data can be determined at any point within the range of temperatures and frequencies bounded by the mastercurve.

Fitted mastercurves can be plotted as a function of depth within a given cell or between cells at a given layer depth. As an example, Figure 3.12 shows the fitted mastercurves as a function of depth for Cell 24F (Non-Travel Lanes). Similar curves can be developed for the Non-Travel lanes of Cells 24A, 24B, 33, 34, and 35, as well as the Travel lanes of Cells 24A, 24B, and 24F.

In Figure 3.12, it can be seen that the recovered asphalt binder from the Top layer of Cell 24F has a consistently higher G* at a range of frequencies compared to the recovered asphalt binder from the Middle and Bottom layers (which are virtually identical). This is an indication that the Top layer has aged more than the Middle or Bottom layers.

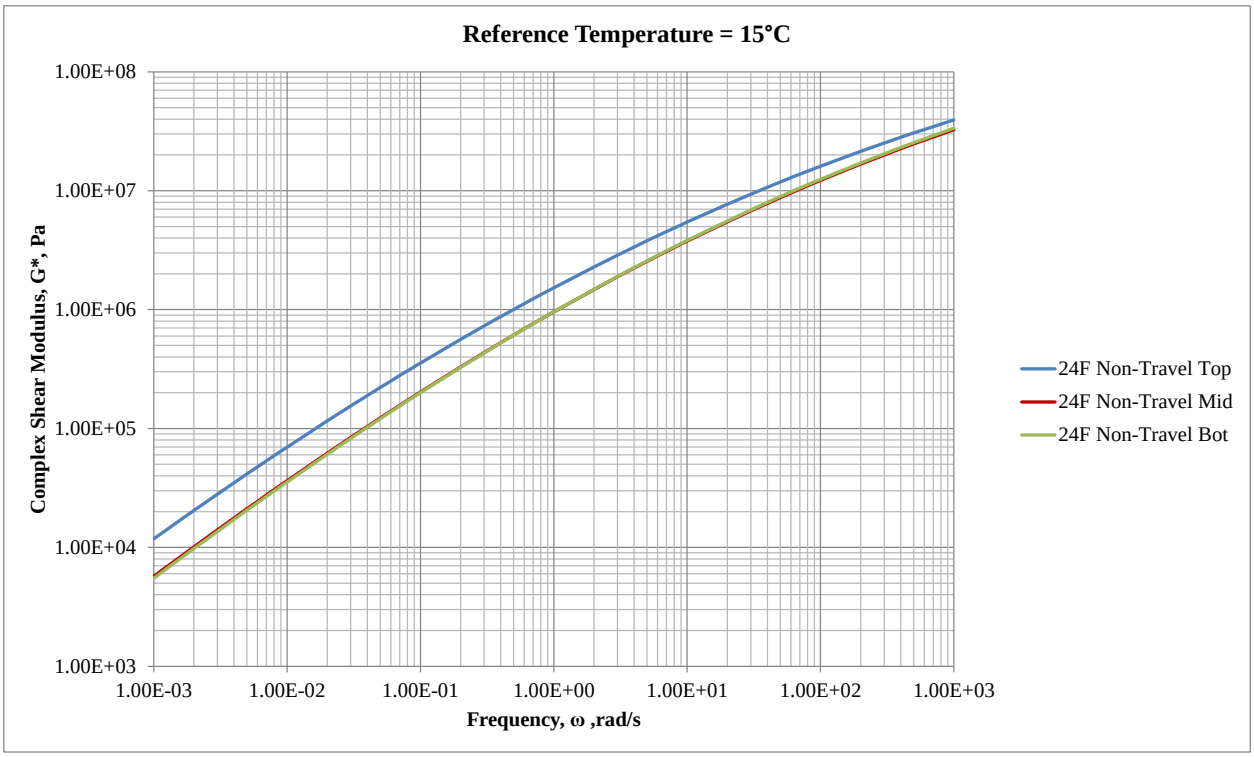

Figure 3.12 Fitted Mastercurves for Different Layers of Cell 24F (Non-Travel Lanes)

Another way of looking at the data is to show the fitted mastercurves for just the Top layers of the different cells. Figure 3.13 shows the mastercurves for the Top layers of the Non-Travel lanes of Cells 24A, 24B, and 24F. Figure 3.14 shows the mastercurves for the Top layers of the Travel lanes of Cells 24A, 24B, and 24F. Figures 3.15-3.17 compare the Top layers of the Travel and Non-Travel lanes for Cells 24A, 24B, and 24F, respectively. Finally, Figure 3.18 shows the mastercurves for the Top layers of the Non-Travel lanes of Cells 33, 34, and 35.

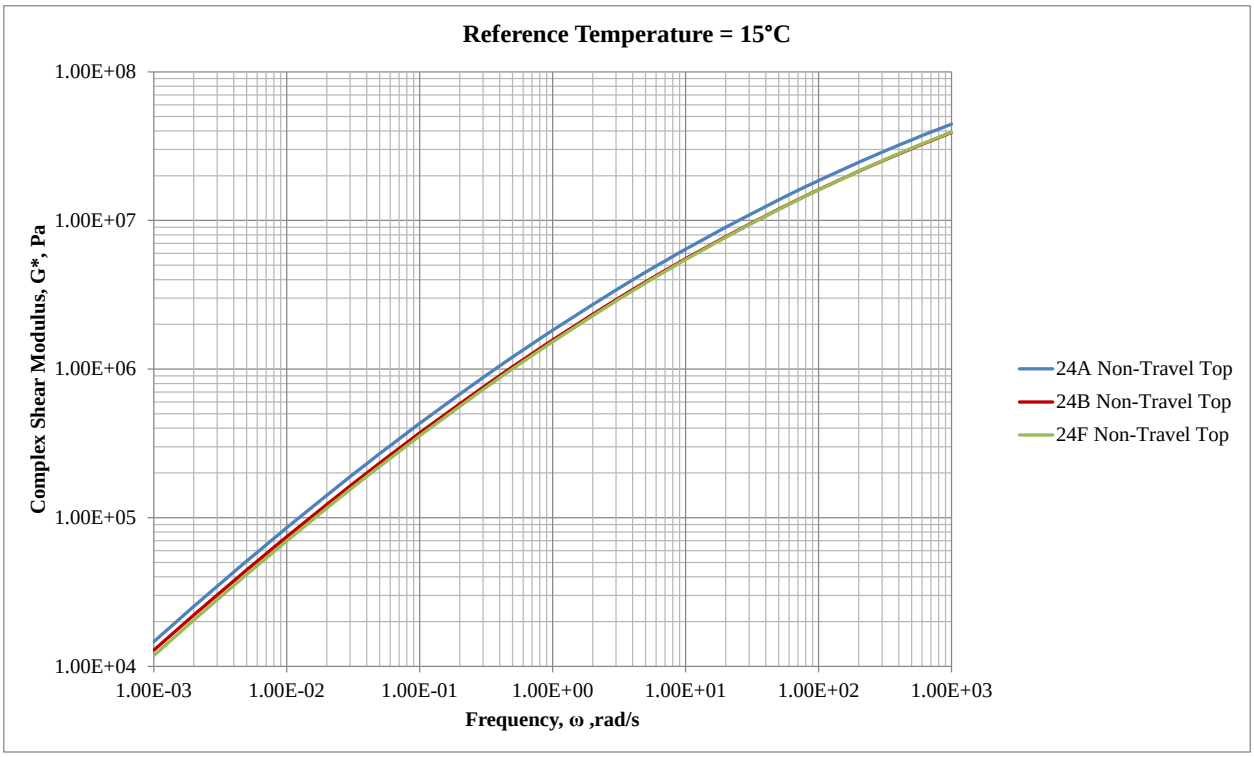

Figure 3.13 Fitted Mastercurves for Top Layers of Cells 24A, 24B, and 24F (Non-Travel)

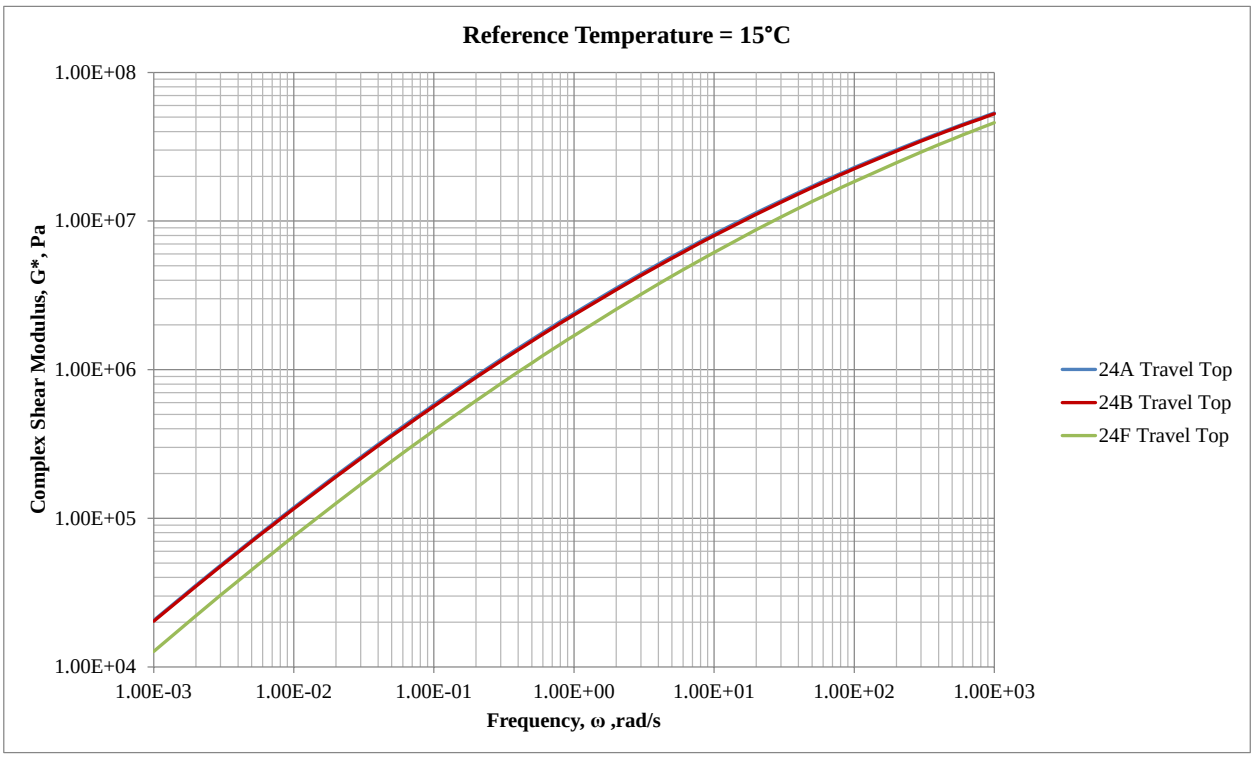

Figure 3.14 Fitted Mastercurves for Top Layers of Cells 24A, 24B, and 24F (Travel)

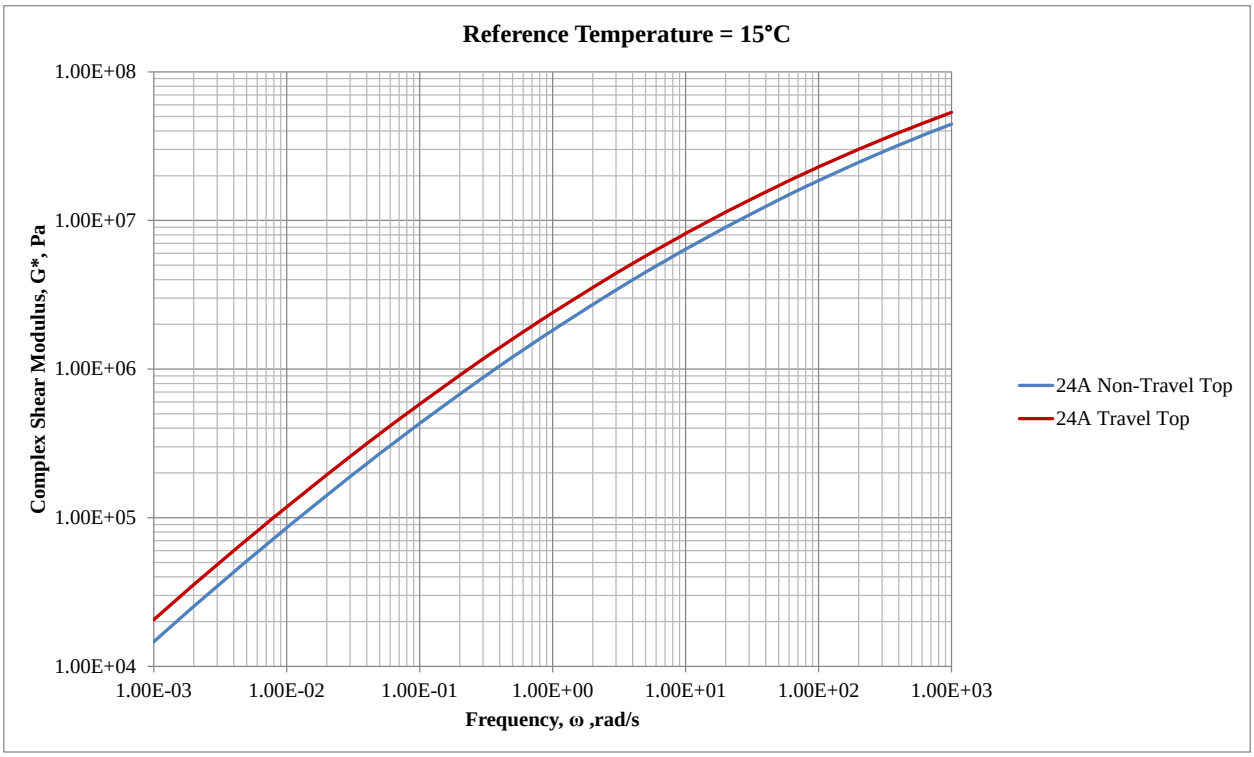

Figure 3.15 Fitted Mastercurves for Top Layers of Cell 24A, Travel vs. Non-Travel

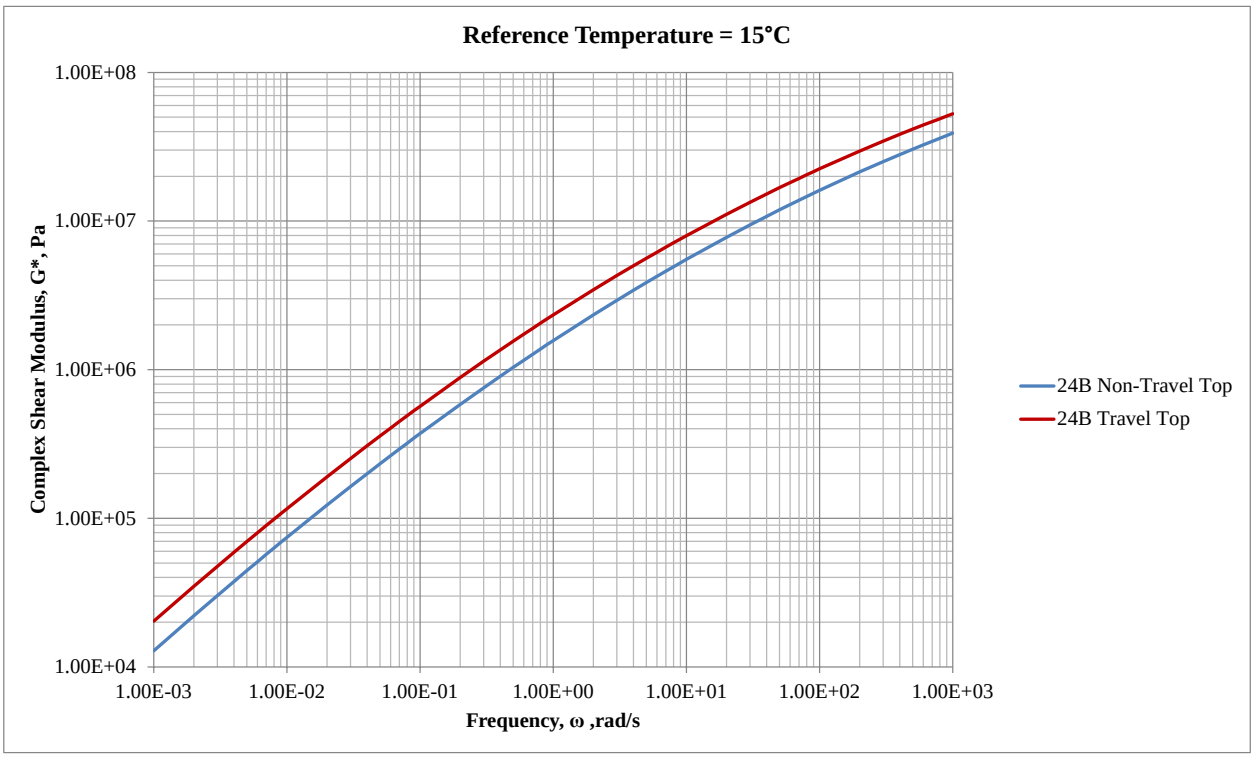

Figure 3.16 Fitted Mastercurves for Top Layers of Cell 24B, Travel vs. Non-Travel

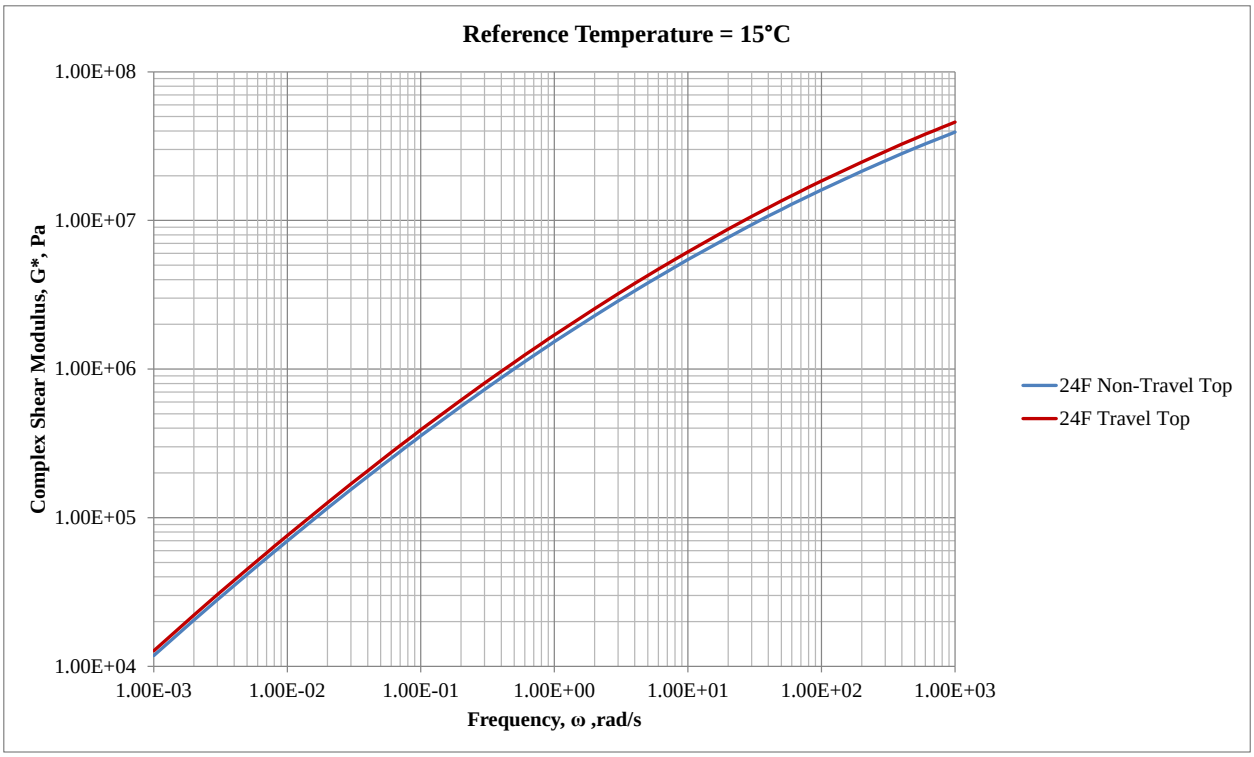

Figure 3.17 Fitted Mastercurves for Top Layers of Cell 24F, Travel vs. Non-Travel

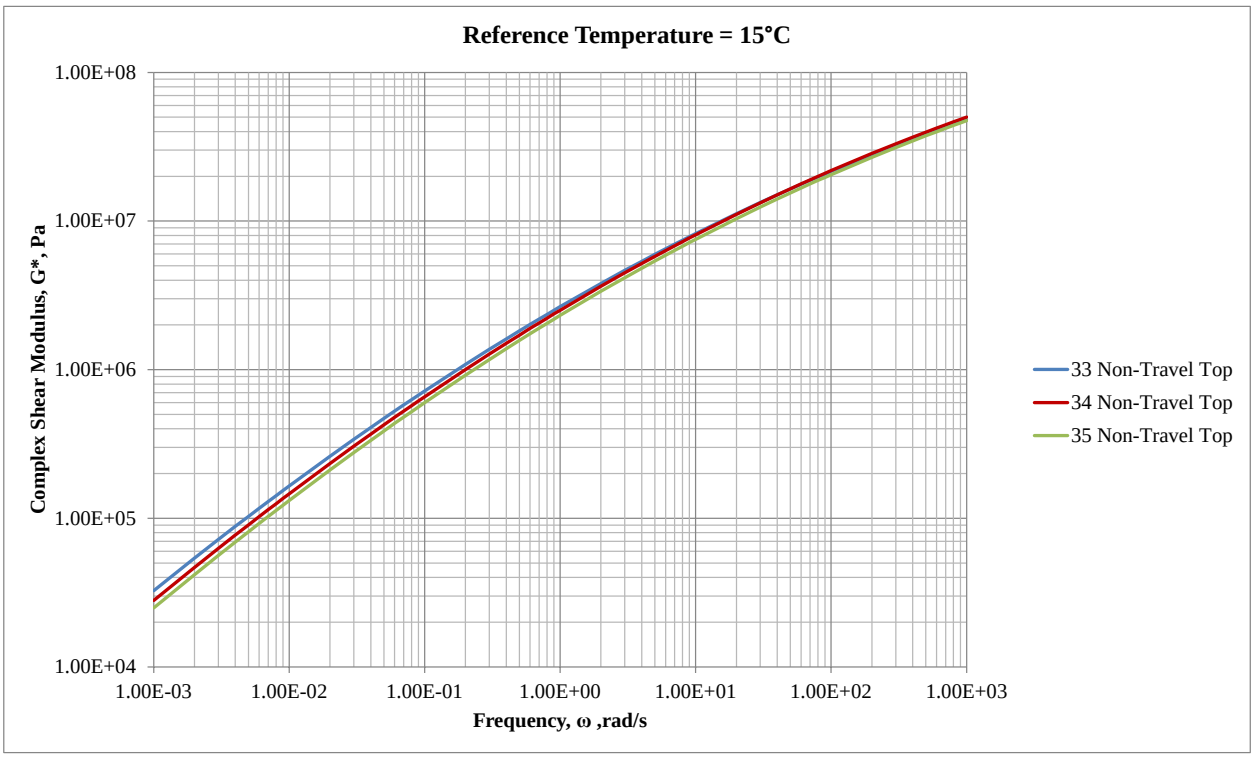

Figure 3.18 Fitted Mastercurves for Top Layers of Cells 33, 34, and 35 (Non-Travel)

In Figures 3.13 and 3.14, the mastercurve data generally confirms the BBR ΔT_c data shown in Figures 3.5 and 3.6. For an unknown reason, the mastercurve of the recovered asphalt binder from the Top layer of Cell 24A is higher than the mastercurves of the recovered asphalt binder from the Top layers of Cells 24B and 24F.

The data in Figures 3.15-3.17 show that the mastercurves from the Top layers of the Travel lanes are generally higher than the mastercurves from the Non-Travel lanes (although Figure 3.17 doesn't indicate much of a difference for Cell 24F).

The data in Figure 3.18 shows that the mastercurves of the recovered asphalt binder from the Top layers of Cells 33, 34, and 35 are essentially the same.

Another potentially useful parameter that can be determined from a mastercurve is the Rheological Index, R, which generally represents the shape of the mastercurve. As discussed in SHRP and other reports, the Rheological Index, R, is the difference between the glassy modulus and the complex shear modulus at the crossover frequency (where tan $\delta = 1$). According to SHRP Report A-369, "…[R] is directly proportional to the width of the relaxation spectrum and indicates rheologic type. R is not a measure of temperature, but reflects the change in modulus with frequency or loading time and therefore is a measure of the shear rate dependency of asphalt cement. R is asphalt specific."[29] The determination of R is illustrated in Figure 3.19.

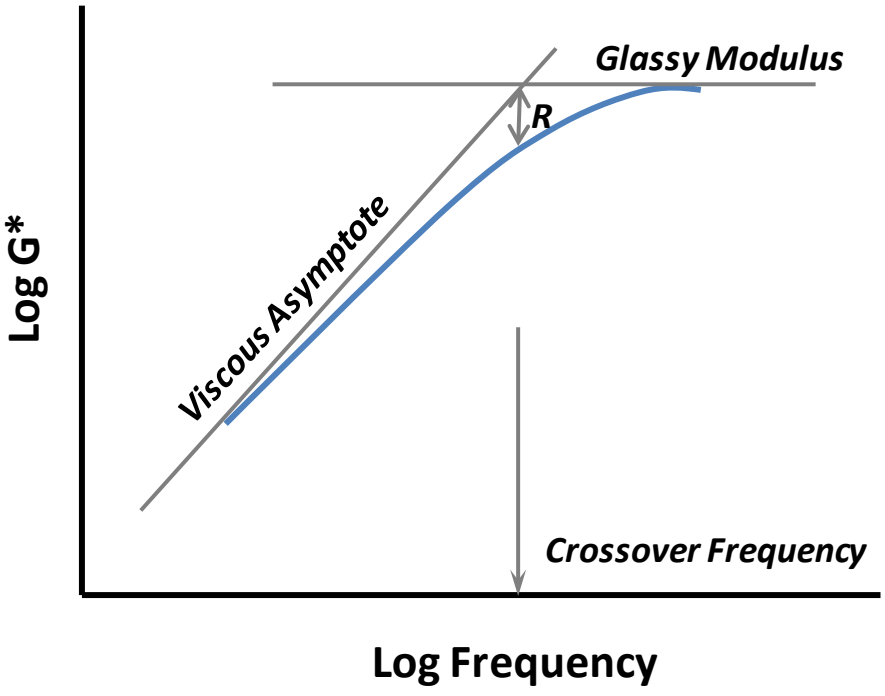

Figure 3.19 Definition of Rheological Index, R, from the Mastercurve

Since R is a measure of shear rate dependency, it was hypothesized that it should relate to $G'/(\eta'/G')$ at the same temperature. Using equations developed during SHRP [29], R can be calculated for each of the mastercurves as follows:

$$R = \frac{\log(2) * \log\left(\frac{G^*(\omega)}{G_0}\right)}{\log\left(1 - \frac{\delta(\omega)}{90}\right)} \qquad \text{[Eq. 4]}$$

where: $G^*(\omega)$ = complex shear modulus at frequency ω (rad/s), Pa
G_0 = glassy modulus, Pa (assumed to be 1E+09 Pa)
$\delta(\omega)$ = phase angle at frequency ω (rad/s), degrees (valid between 10 and 70°)

By observation, one can see that R becomes larger as the phase angle decreases at a given value of G*. By converse, R becomes smaller at a given phase angle as G* increases. This response is similar to the type of response seen with the G′/(η′/G′) parameter.

From the fitted mastercurve data, the DSR Parameter, G′/(η′/G′) , was calculated at 15°C and 0.005 rad/s. The calculated values are shown in Table 3.9 along with the calculated R values for each of the asphalt binders in Table 3.3.

Table 3.9 2010 MnROAD Recovered Asphalt Binder – Calculated G′/(η′/G′) and R Values

Cell	Lane	Layer	Calculated G′/(η′/G′) MPa/s	R
24A	Non-Travel	Top	4.27E-05	2.153
		Mid	1.40E-05	2.065
		Bot	1.09E-05	2.052
	Travel	Top	6.43E-05	2.142
		Mid	1.78E-05	2.094
		Bot	2.19E-05	2.105
24B	Non-Travel	Top	3.81E-05	2.203
		Mid	2.36E-05	2.086
		Bot	1.01E-05	2.049
	Travel	Top	6.50E-05	2.165
		Mid	1.58E-05	2.087
		Bot	1.35E-05	2.043
24F	Non-Travel	Top	3.37E-05	2.180
		Mid	1.35E-05	2.130
		Bot	1.22E-05	2.097
	Travel	Top	3.57E-05	2.138
		Mid	1.16E-05	2.042
		Bot	9.04E-06	2.047
33	Non-Travel	Top	1.31E-04	2.371
		Mid	6.12E-05	2.320
		Bot	7.67E-05	2.315
34	Non-Travel	Top	1.07E-04	2.322
		Mid	2.66E-05	2.239
		Bot	1.56E-05	2.190
35	Non-Travel	Top	9.34E-05	2.316
		Mid	2.50E-05	2.267
		Bot	2.05E-05	2.239

G′/(η′/G′) and R values calculated at 15°C and 0.005 rad/s.

Calculated values of G′/(η′/G′) and R at 15°C and 0.005 rad/s are shown in Table 3.10 for each of the asphalt binders in Table 3.4.

Table 3.10 2010 MnROAD Asphalt Binders – Calculated G′/(η′/G′) and R Values

Cell	Material	Cond.	Calculated G′/(η′/G′) MPa/s	R
27	PG 52-34 Binder	RTFO	1.18E-06	1.969
		PAV	3.65E-05	2.418
		PAV 90°C	1.20E-05	2.218
33	PG 58-34 Binder 0.75% PPA	RTFO	2.63E-05	2.759
		PAV	3.98E-04	3.323
34	PG 58-34 Binder 0.3% PPA + 1% SBS	RTFO	1.82E-05	2.653
		PAV	2.24E-04	3.104
35	PG 58-34 Binder 2% SBS	RTFO	4.83E-06	2.260
		PAV	8.88E-05	2.585

G′/(η′/G′) and R values calculated at 15°C and 0.005 rad/s.

As with Figures 3.5 and 3.6, the calculated value of G′/(η′/G′) at 15°C and 0.005 rad/s can be plotted as a function of layer depth. Figure 3.20 illustrates the G′/(η′/G′) values for the Cell 24 cores taken from the Non-Travel lane of the MnROAD Low Volume loop. Figure 3.21 illustrates the G′/(η′/G′) values for the Cell 24 cores taken from the Travel lane of the MnROAD Low Volume loop. In both Figures, the plot is arranged so that pavement depth is illustrated by moving down the y-axis from the origin in the top left corner. Pavement aging is represented by increasing G′/(η′/G′) values, progressing from left to right on the x-axis.

The data in Figures 3.20 and 3.21, generated from the calculated value of G′/(η′/G′) at 15°C and 0.005 rad/s, confirm the results shown in Figures 3.5 and 3.6, generated from BBR ΔT_c values. Even though the behavior of the data for Cell 24A cannot be readily explained, at the least the two parameters from DSR and BBR tests are corroborated. Likewise, the data in Figure 3.22 corroborates the data in Figure 3.7 for the Acid Modification Study cells.

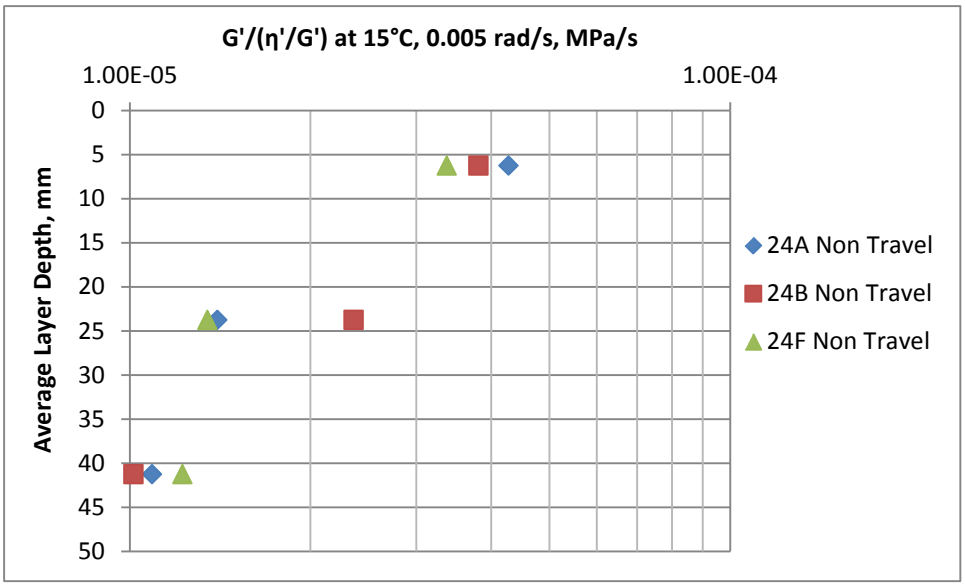

Figure 3.20 G′/(η′/G′) Value as a Function of Layer Depth – Cell 24 Non-Travel Lane

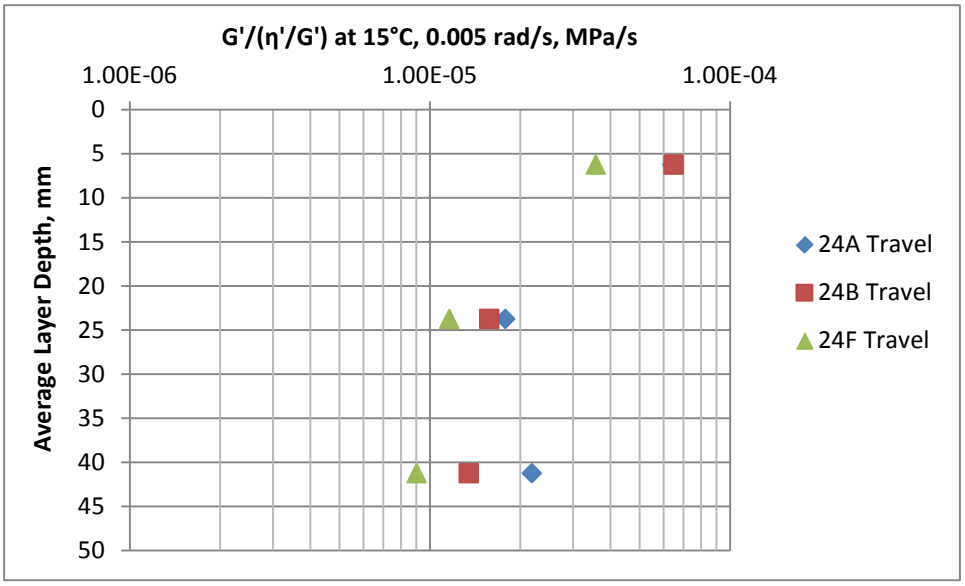

Figure 3.21 G′/(η′/G′) Value as a Function of Layer Depth – Cell 24 Travel Lane

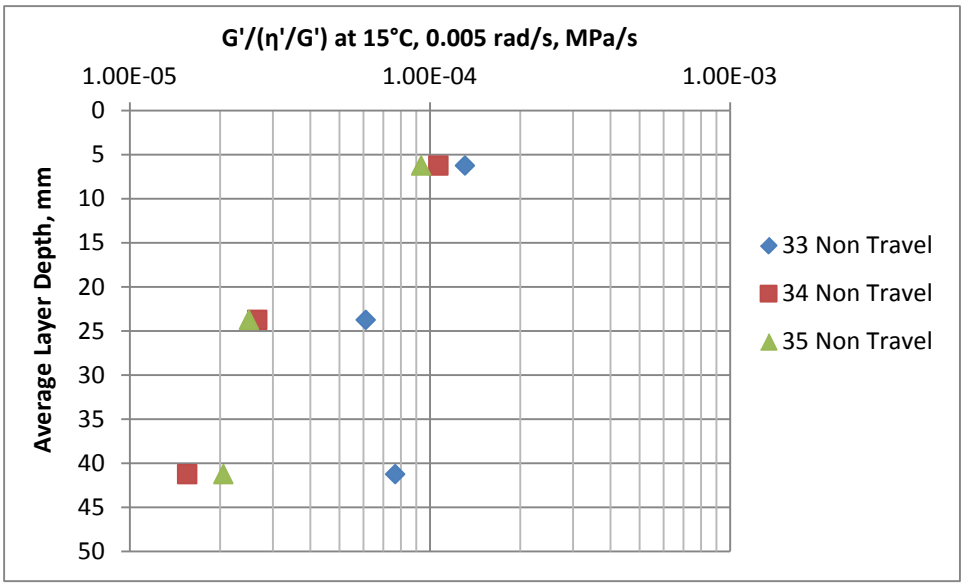

Figure 3.22 G′/(η′/G′) Value as a Function of Layer Depth – Acid Modification Study Cells

In explaining the data in Figures 3.5 and 3.6, four possible explanations were offered as follows:

1. The ΔT_c parameter may not be indicative of aging as previously thought.
2. After only two years of in-service aging, the data is still far enough below the expected cracking warning limit ($\Delta T_c = 2.5$ from previous research), that the ΔT_c parameter is not indicating significant aging.
3. Material or construction variability (pavement density, percentage of RAP used, and stiffness of RAP) may be affecting results.
4. Testing variability (single operator variability of BBR Stiffness and m-value)

The fact that the data in Figures 3.20-3.22 generally corroborates the data in Figures 3.5-3.7, suggests that neither Explanation #1 (parameter not indicative of aging) or Explanation #4 (testing variability) is correct. If testing variability in either the BBR or DSR tests were the problem than the data in Figures 3.5-3.7 should look different than the data in Figures 3.20-3.22. Material or construction variability (Explanation #3) is still a possibility for the anomalous responses, as is the fact that the aging hasn't been significant enough after only two years (Explanation #2). Testing after additional years of in-service aging should be expected to prove/disprove Explanation #2.

One possibility that is related to test procedure variability is the variability in the recovery procedure. Although the testing appears to be consistent, an error in the recovery procedure (such as leaving residual solvent in the recovered asphalt binder sample) could also account for any anomalous results.

As confirmation that the BBR and DSR data are providing similar information, the calculated value of G′/(η′/G′) determined from BBR testing and Equation 1 was plotted as a function of the measured value of G′/(η′/G′) determined from DSR testing. This data is shown in Figure 3.23.

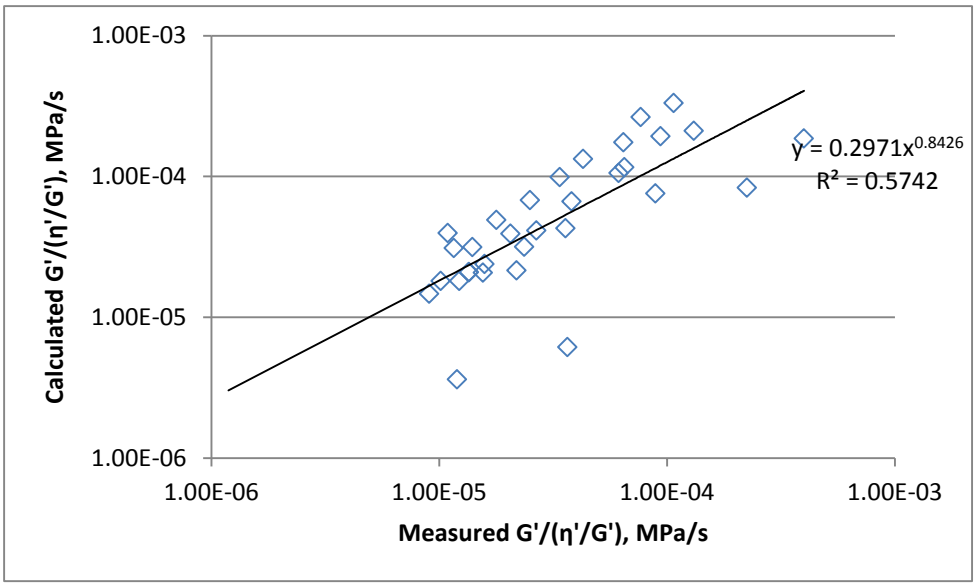

Figure 3.23 Comparison of Calculated and Measured Values of G′/(η′/G′)

As seen in Figure 3.23, there is a decent correlation between the calculated and measured values of G′/(η′/G′), but with some apparent outliers. Upon further review of the data, it was observed that the apparent outliers were from values determined from PAV-aged asphalt binders and not recovered asphalt binders. Removing the PAV-aged samples from the data set, leaving only the recovered asphalt binders, results in Figure 3.24.

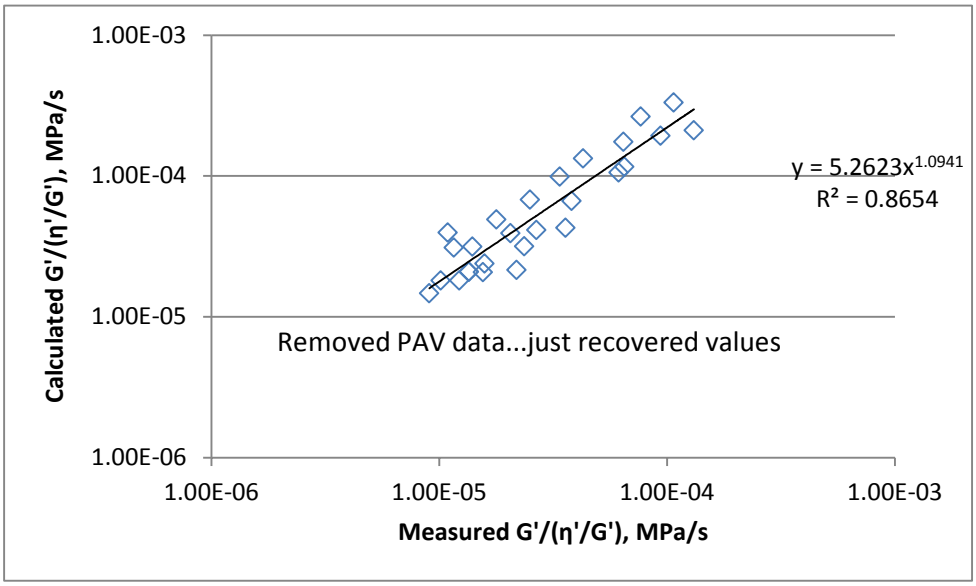

Figure 3.24 Comparison of Calculated and Measured Values of G′/(η′/G′) – PAV Data Removed

In Figure 3.24, the correlation becomes much stronger, indicating a definite relationship between the calculated G′/(η′/G′) value, determined from BBR testing, and the measured G′/(η′/G′) value, determined from DSR testing. This can also be seen in Figure 3.25, which compares the G′/(η′/G′) value from DSR testing with the BBR ΔT_c value.

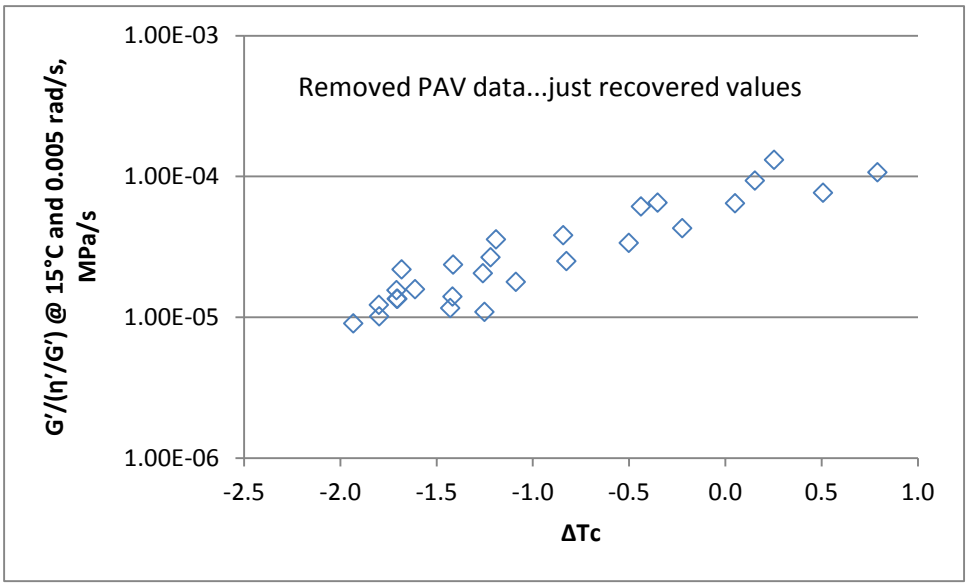

Figure 3.25 Comparison of G′/(η′/G′) and ΔTc – Recovered Binder Data

As discussed earlier, the Rheological Index, R, obtained from the fitted mastercurve has also been hypothesized to be related to aging/durability since R increases as the phase angle decreases. Calculated R values are shown in Tables 3.9 and 3.10. It should be noted that the calculated values for R were determined from the mastercurve at 15°C and 0.005 rad/s. At this temperature-frequency combination, the phase angle, δ, is in many cases close to 70 degrees – the limit of the acceptable range provided in Equation 4. A more accurate representation for the R value could be obtained by determining R at the crossover frequency. Nonetheless, the relative trend for R should stay approximately the same.

Figures 3.26-3.28 illustrate the effect of layer depth on R value for the different recovered asphalt binders tested.

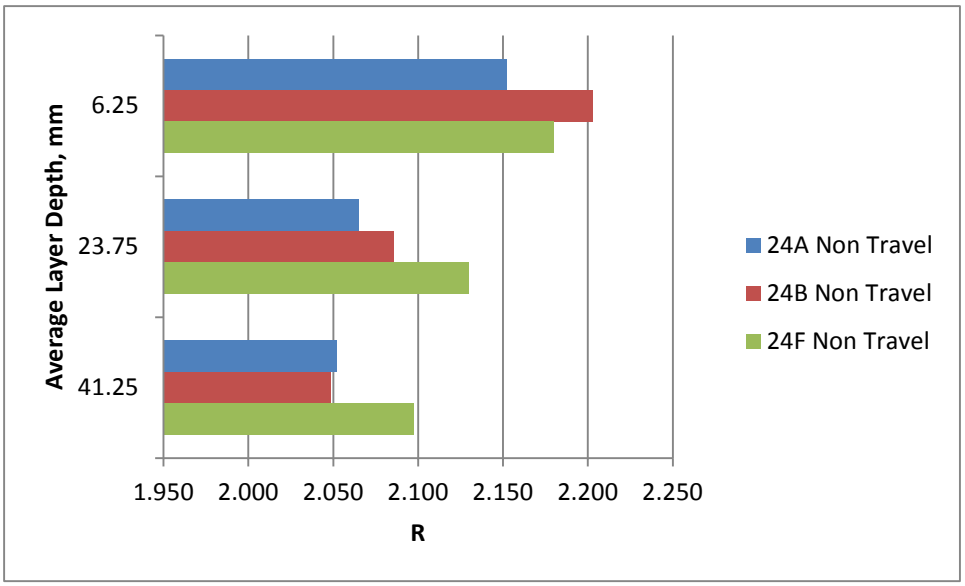

Figure 3.26 R as a Function of Layer Depth – Cell 24 Non-Travel Lane

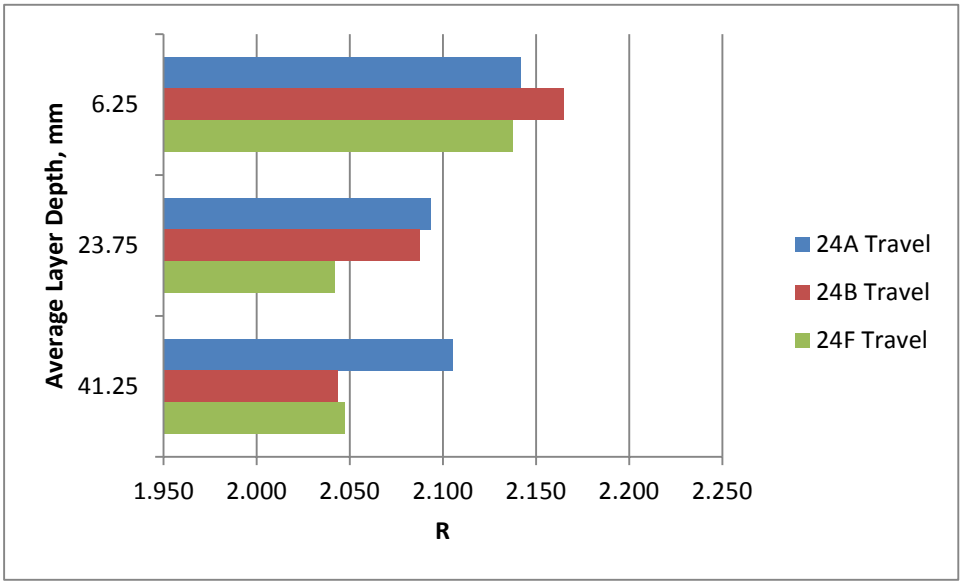

Figure 3.27 R as a Function of Layer Depth – Cell 24 Travel Lane

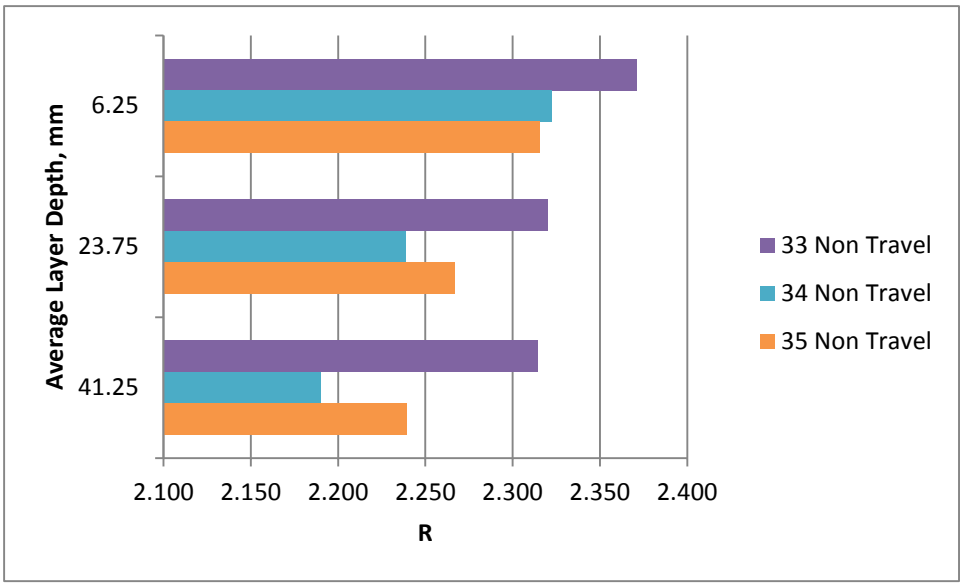

Figure 3.28 R as a Function of Layer Depth – Acid Modification Study Cells

Figures 3.26-3.28 show, as in earlier figures, that the R value generally decreases with increasing layer depth, indicating less aging at lower layers than in the Top layer. Interestingly, in Figure 3.26, the R value of the Top layer of Cell 24A is less than the R values of Cells 24B and 24F, indicating potentially less aging. This does not match the data in Figures 3.5 or 3.20.

3.3.3 Single Point DSR Results

Research conducted at Texas A&M University indicated that the durability parameter, G′/(η′/G′), could be determined directly at 44.7°C and 10 rad/s and would provide equivalent results as G′/(η′/G′) determined at 15°C and 0.005 rad/s [4]. The advantage of this approach is that it uses a direct measurement and does not rely on temperature-frequency sweep testing and determination of a mastercurve to derive the durability parameter. The disadvantage of this approach is that it assumes that the time-temperature superposition principle (TTSP) will result in a similar shift for all asphalt binders. Findings during the AAPTP 06-01 research indicated that the single point test did not work as well for determining the durability parameter as the mastercurve approach [5].

An alternative method that was considered was to directly measure G′/(η′/G′) at 15°C and 0.005 rad/s. The disadvantage of this approach is that the slow loading means that each cycle would take approximately 20 minutes. To collect 10 cycles would require nearly 3.5 hours per test. Considering that temperature-frequency sweep testing as described previously can be accomplished in less than two hours (with some additional time required to generate the mastercurve and derive the durability parameter) and the single point DSR test at 10 rad/s can be conducted in 20 minutes, the alternative direct measurement approach was considered as an untenable alternative.

Single Point DSR test results at 45°C and 10 rad/s are shown in Tables 3.11 and 3.12 for the cores and asphalt binders, respectively. Note that the temperature is not exactly the same as specified by the Texas A&M research, but it was felt that the small difference in temperature, 0.3°C, would have a negligible effect on the results. To convert data from 45°C and 10 rad/s, the value of G′/(η′/G′) is first determined, then divided by 2000 to convert from 10 rad/s to 0.005 rad/s.

Table 3.11 2010 MnROAD Recovered Asphalt Binder – Calculated G′/(η′/G′) Values at 15°C and 0.005 rad/s from Data at 45°C and 10 rad/s

Cell	Lane	Layer	Measured G* at 45°C, 10 rad/s, Pa	Measured δ at 45°C, 10 rad/s, degrees	Calculated G′/(η′/G′) at 15°C, 0.005 rad/s MPa/s
24A	Non-Travel	Top	61,200	67.4	4.89E-05
		Mid	34,700	70.5	2.05E-05
		Bot	32,900	71.0	1.84E-05
	Travel	Top	69,300	66.9	5.80E-05
		Mid	37,100	69.9	2.33E-05
		Bot	41,000	69.6	2.66E-05
24B	Non-Travel	Top	59,700	66.6	5.13E-05
		Mid	23,000	71.1	1.28E-05
		Bot	35,600	70.5	2.10E-05
	Travel	Top	65,900	66.5	5.71E-05
		Mid	34,600	70.3	2.09E-05
		Bot	32,400	70.9	1.84E-05
24F	Non-Travel	Top	52,600	68.2	3.91E-05
		Mid	32,100	70.4	1.92E-05
		Bot	33,700	70.4	2.01E-05
	Travel	Top	53,600	68.0	4.06E-05
		Mid	29,300	71.2	1.61E-05
		Bot	28,600	70.9	1.62E-05
33	Non-Travel	Top	91,700	64.0	9.80E-05
		Mid	57,900	66.5	5.02E-05
		Bot	66,100	65.7	6.14E-05
34	Non-Travel	Top	80,700	64.4	8.35E-05
		Mid	44,700	67.8	3.45E-05
		Bot	32,200	69.2	2.17E-05
35	Non-Travel	Top	87,600	63.0	1.01E-04
		Mid	41,400	66.6	3.56E-05
		Bot	38,200	66.8	3.22E-05

G′/(η′/G′) calculated at 15°C and 0.005 rad/s.

Table 3.12 2010 MnROAD Asphalt Binders – Calculated G′/(η′/G′) Values at 15°C and 0.005 rad/s from Data at 45°C and 10 rad/s

Cell	Material	Cond.	Measured G* at 45°C, 10 rad/s, Pa	Measured δ at 45°C, 10 rad/s, degrees	Calculated G′/(η′/G′) at 15°C, 0.005 rad/s MPa/s
27	PG 52-34 Binder	RTFO	9,410	77.4	2.29E-06
		PAV	46,900	65.6	4.39E-05
		PAV 90°C	29,200	69.9	1.84E-05
33	PG 58-34 Binder 0.75% PPA	RTFO	41,600	62.3	5.08E-05
		PAV	174,000	50.4	4.59E-04
34	PG 58-34 Binder 0.3% PPA + 1% SBS	RTFO	34,000	61.9	4.28E-05
		PAV	127,000	53.1	2.86E-04
35	PG 58-34 Binder 2% SBS	RTFO	23,700	66.6	2.04E-05
		PAV	77,400	59.7	1.14E-04

G′/(η′/G′) calculated at 15°C and 0.005 rad/s.

Figure 3.29 illustrates a comparison of the G′/(η′/G′) value determined at 15°C and 0.005 rad/s using the binder mastercurve and the G′/(η′/G′) value determined at 15°C and 0.005 rad/s using the direct, single point DSR measurement at 45°C and 10 rad/s. The solid red diagonal line represents the line of equality between the two parameters.

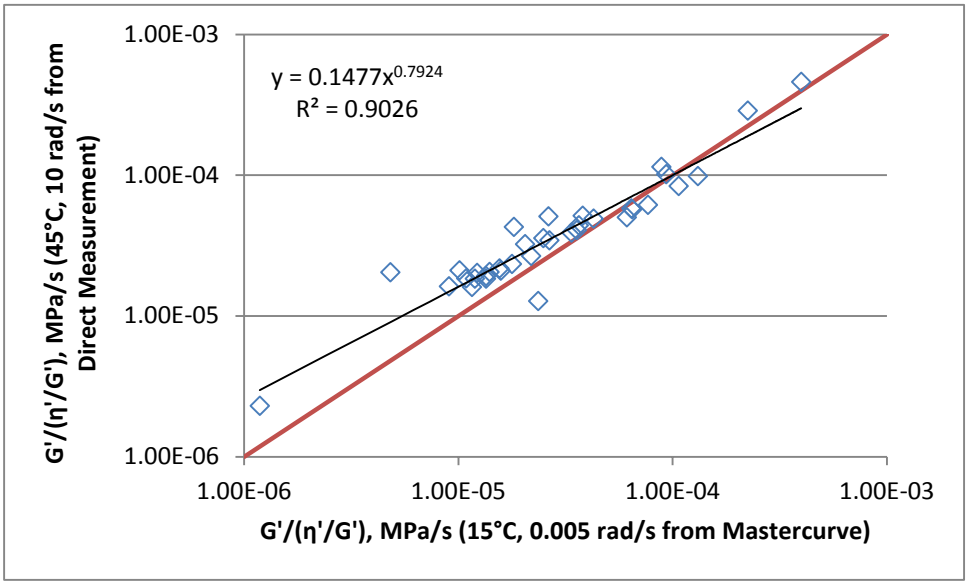

Figure 3.29 Comparison of G′/(η′/G′) Values Determined by Mastercurve and Single-Point DSR

The data illustrated in Figure 3.29 indicates that the two parameters are related – as indicated by the relatively high R-squared value (0.90) – but not exactly the same – as indicated by the difference in slope (0.7924) and variance from the line of equality. Although the relationship is better than was found in the previous research, the time advantage offered by the Single-Point

DSR measurement over the Temperature-Frequency Sweep and mastercurve calculation may not be worth the "error" in test result. Note that "error" in this case presumes that the mastercurve provides the "true" value since it represents a modelled fit of various temperature and frequencies joined to produce a mastercurve at 15°C while the Single-Point DSR represents testing conducted at a temperature that was determined based on the assumption that all asphalt binders will exhibit the same TTSP principles.

3.3.4 Linear Amplitude Sweep (LAS) Results

The Linear Amplitude Sweep test was proposed by Dr. Hussain Bahia at the University of Wisconsin-Madison as a possible intermediate temperature test related to asphalt binder fatigue. The test is conducted by first performing a frequency sweep at small strain (0.1%) and a range of loading frequencies to determine the parameter α, which is related to the slope of the log storage modulus (G′) versus log frequency. The second part of the test involves testing at a fixed loading frequency of 10 Hz and a linearly increasing strain from 1% to a maximum of 30%. In its original form, the test was performed for 10 seconds at each discrete strain level and the average data collected. The dissipated energy is calculated per data point and used in a viscoelastic continuum damage (VECD) analysis. VECD analysis has been used for asphalt mixtures to relate to fatigue cracking. Dr. Bahia and his colleagues have published several papers discussing the relevance of the LAS test to fatigue cracking and aging [30,31].

In this study, the LAS test was conducted at 16°C to represent the approximate intermediate temperature grade for MnROAD (assuming a PG 58-34 climate). The temperature is also very close to the temperature used in the G′/(η′/G′) determination (15°C). VECD analysis is used to determine the LAS parameters A and B that are used in the equation to determine the number of cycles to failure:

$$N_f = A\gamma^B \qquad \text{[Eq. 5]}$$

where: N_f = number of cycles to failure (at a user-defined damage level, such as 0.35)
A = LAS power-law parameter representing the intercept at 1% strain
γ = shear strain, expressed as a percent (e.g. γ=2 for 2% shear strain)
B = LAS power-law parameter representing the slope of the N_f-Strain curve

LAS test results at 16°C are shown in Tables 3.13 and 3.14 for the cores and asphalt binders, respectively.

Table 3.13 2010 MnROAD Recovered Asphalt Binder – LAS at 16°C

			LAS Parameter		N_f	
Cell	**Lane**	**Layer**	**A**	**B**	**γ = 2%**	**γ = 5%**
24A	Non-Travel	Top	1.900E+05	-3.537	16,369	640
		Mid	1.624E+05	-3.203	17,633	937
		Bot	1.604E+05	-3.159	17,966	994
	Travel	Top	1.283E+05	-3.622	10,424	377
		Mid	1.329E+05	-3.228	14,177	736
		Bot	1.147E+05	-3.262	11,952	602
24B	Non-Travel	Top	1.514E+05	-3.574	12,706	480
		Mid	1.156E+05	-3.273	11,954	596
		Bot	1.079E+05	-3.196	11,777	630
	Travel	Top	1.499E+05	-3.607	12,299	451
		Mid	1.118E+05	-3.179	12,338	670
		Bot	1.048E+05	-3.135	11,928	675
24F	Non-Travel	Top	1.333E+05	-3.475	11,981	496
		Mid	1.201E+05	-3.168	13,362	733
		Bot	1.124E+05	-3.163	12,545	691
	Travel	Top	1.194E+05	-3.459	10,861	457
		Mid	1.045E+05	-3.110	12,105	700
		Bot	1.061E+05	-3.067	12,657	762
33	Non-Travel	Top	2.441E+05	-3.957	15,716	418
		Mid	2.238E+05	-3.678	17,493	602
		Bot	2.317E+05	-3.769	16,993	537
34	Non-Travel	Top	2.170E+05	-3.837	15,188	451
		Mid	1.836E+05	-3.442	16,889	721
		Bot	1.672E+05	-3.233	17,775	919
35	Non-Travel	Top	2.375E+05	-3.878	16,159	463
		Mid	1.941E+05	-3.366	18,825	862
		Bot	1.962E+05	-3.335	19,434	915

Table 3.14 2010 MnROAD Asphalt Binders – LAS at 16°C

			LAS Parameter		N_f	
Cell	**Material**	**Cond.**	**A**	**B**	**γ = 2%**	**γ = 5%**
27	PG 52-34 Binder	RTFO	1.257E+05	-2.676	19,671	1,694
		PAV	2.423E+05	-3.561	20,530	786
		PAV 90°C	1.716E+05	-3.247	18,075	922
33	PG 58-34 Binder 0.75% PPA	RTFO	4.924E+05	-3.547	42,120	1,632
		PAV	1.893E+06	-4.714	72,138	960
34	PG 58-34 Binder 0.3% PPA + 1% SBS	RTFO	3.855E+05	-3.358	37,603	1,734
		PAV	9.571E+05	-4.327	47,700	905
35	PG 58-34 Binder 2% SBS	RTFO	2.108E+05	-3.031	25,788	1,604
		PAV	3.355E+05	-3.836	23,499	699

Figure 3.30 illustrates the N_f-Strain curve for the Top layers of Cells 24A, 24B, and 24F. The curves are relatively close to each other, but it can be seen that Cell 24F looks to have a slightly lower number of cycles to failure (N_f) at all strain levels than Cell 24A. This can be seen more clearly by looking at the N_f for a given strain. Figure 3.31 illustrates the N_f for Cells 24A, 24B, and 24F at 2% shear strain.

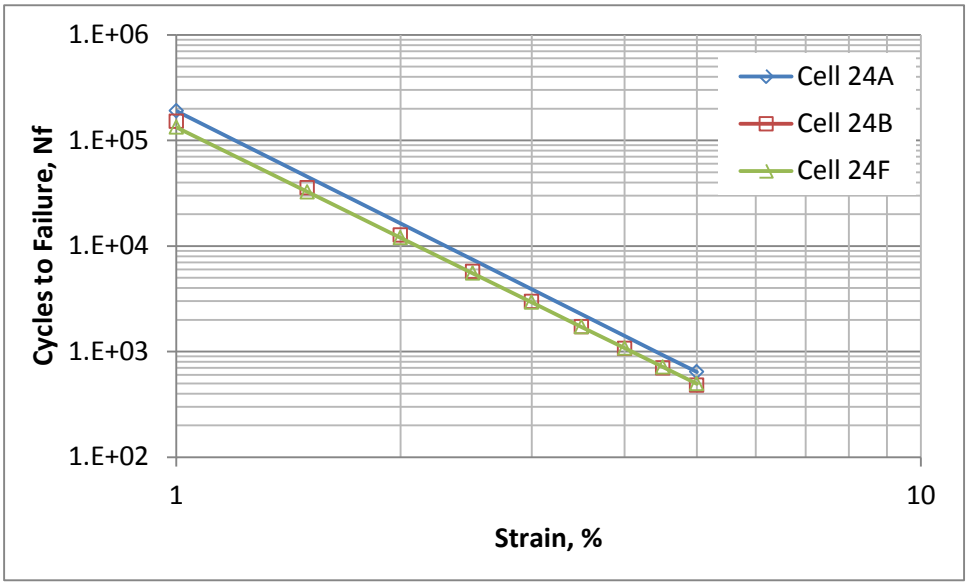

Figure 3.30 LAS Nf-Strain Curves for Top Layer of Cells 24A, 24B, and 24F

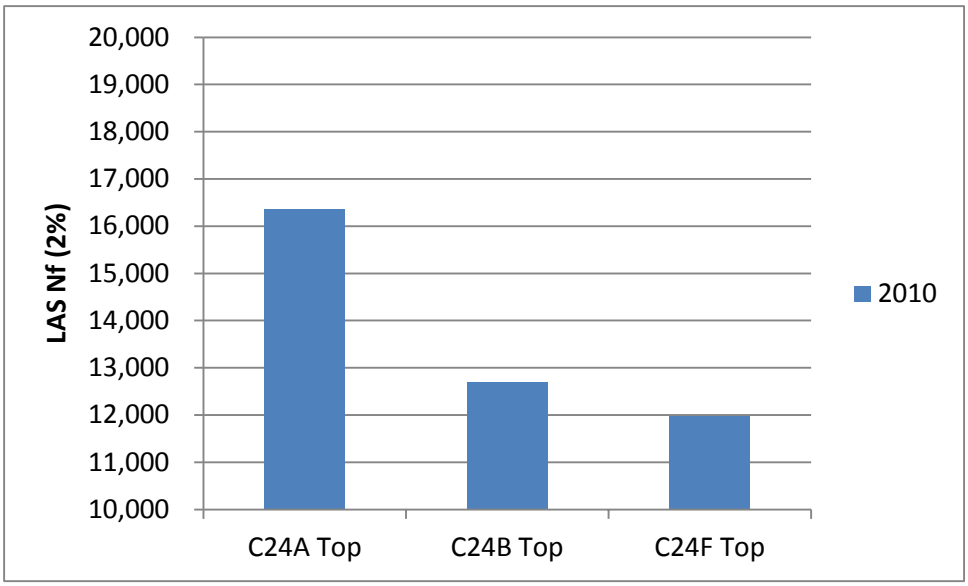

Figure 3.31 LAS Nf Values at 2% Shear Strain for Top Layer of Cells 24A, 24B, and 24F

Figures 3.30 and 3.31 support the hypothesis that sealing an asphalt pavement early in its life reduces the aging that occurs and improves cracking resistance – in this case by increasing the number of cycles to failure.

The slope parameter, B, from the LAS test is derived from the frequency sweep test that is conducted prior to the strain sweep test in the LAS procedure. Since B simply represents the slope of the G*-frequency curve at a given temperature (isotherm) it is expected that it will relate to the other DSR parameters such as R and G′/(η′/G′). As such, the LAS B parameter should also be related to aging. The absolute value of B from the LAS test is shown in Figure 3.32 for the Top layers of Cells 24A, 24B, and 24F.

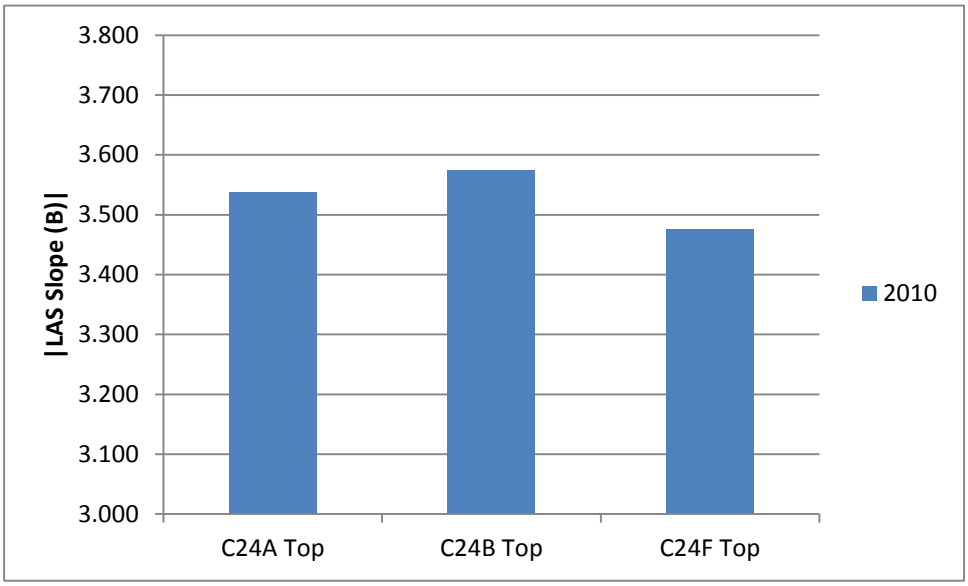

Figure 3.32 Absolute Value of LAS B for Top Layer of Cells 24A, 24B, and 24F

The data in Figure 3.32 somewhat contradicts the conclusions drawn from Figures 3.30 and 3.31 that earlier sealing reduces aging. Cell 24B does indeed show a higher B value than Cell 24A – indicating that Cell 24B is more "aged" – but Cell 24F has the lowest B value – suggesting that it is the least aged. The reason for this response is not quite clear but could be attributed to a couple of factors:

1. Variability in test results – the B values for all three cells are very similar from -3.475 to -3.574. This could simply be within the range of testing variability.
2. The LAS B is a binder-specific parameter. Cell 24A had a CSS-1 emulsion applied to it after construction. Since the fog seal was not removed prior to testing, it is possible that the base asphalt in the emulsion co-mingled with the PG 58-34 asphalt binder. Depending on the stiffness of the emulsion base asphalt binder this co-mingling could have resulted in a stiffer binder than would be present in Cell 24F (with only the PG 58-34 binder)
3. Material or construction variability (pavement density, percentage of RAP used, and stiffness of RAP) may be affecting results.

Despite the conflicting results, it does appear that the absolute value of the LAS slope, B, measured at 16°C is related to the G′/(η′/G′) parameter measured at 15°C and 0.005 rad/s. This relationship is shown in Figure 3.33 with an R-squared value of 0.95.

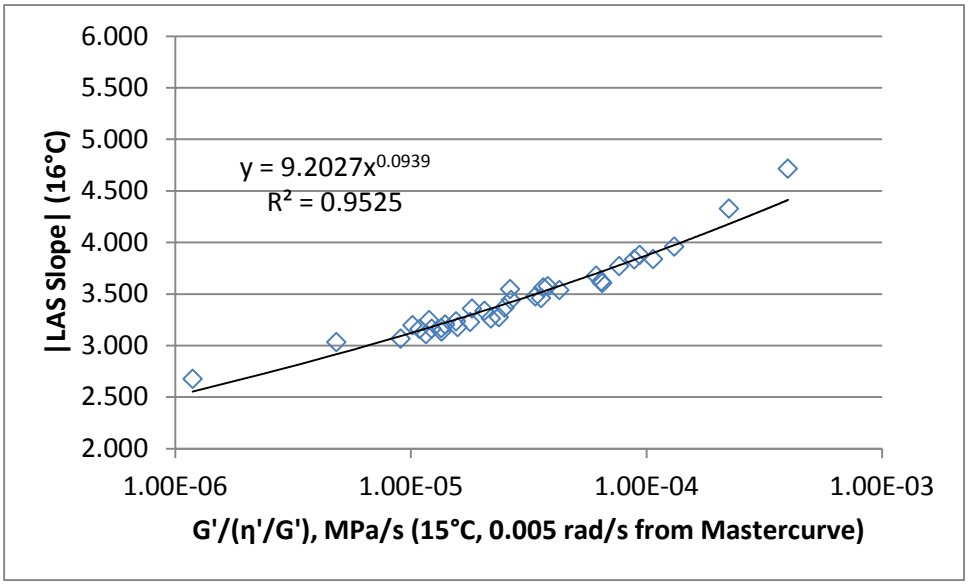

Figure 3.33 Comparison of Absolute Value of LAS Slope (B) to G′/(η′/G′) Parameter

Given the strong relationship exhibited in Figure 3.33, it does appear that the LAS test could be used as a substitute for the Temperature-Frequency Sweep test with mastercurve determination.

Figures 3.34-3.36 illustrate the N_f-Strain curves for Cells 24A, 24B, and 24F, respectively.

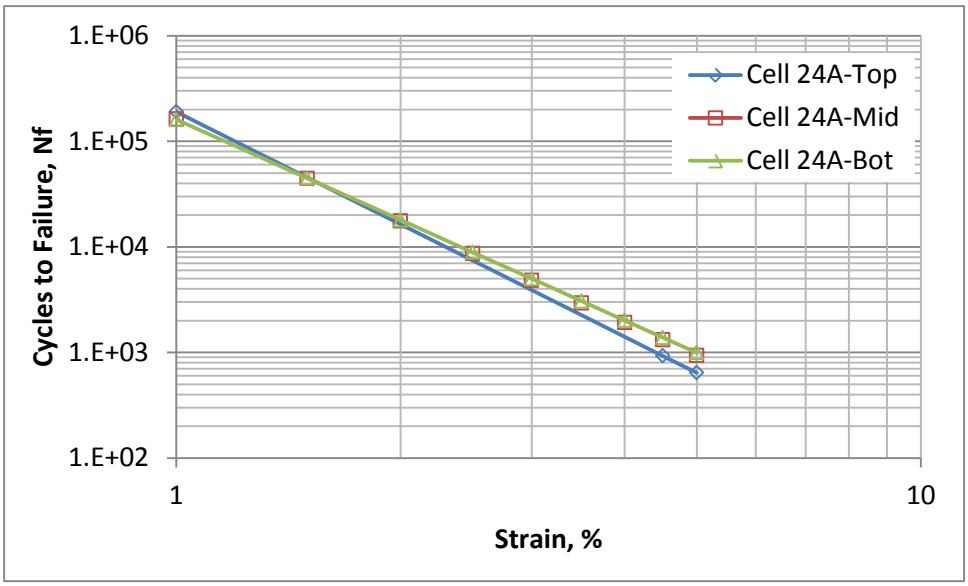

Figure 3.34 LAS Nf-Strain Curves at 16°C for Cell 24A

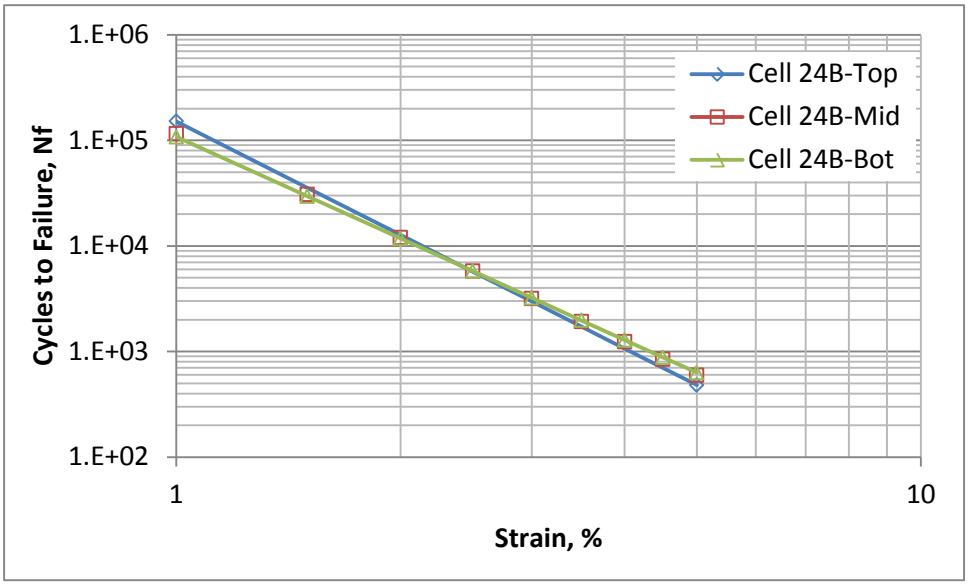

Figure 3.35 LAS Nf-Strain Curves at 16°C for Cell 24B

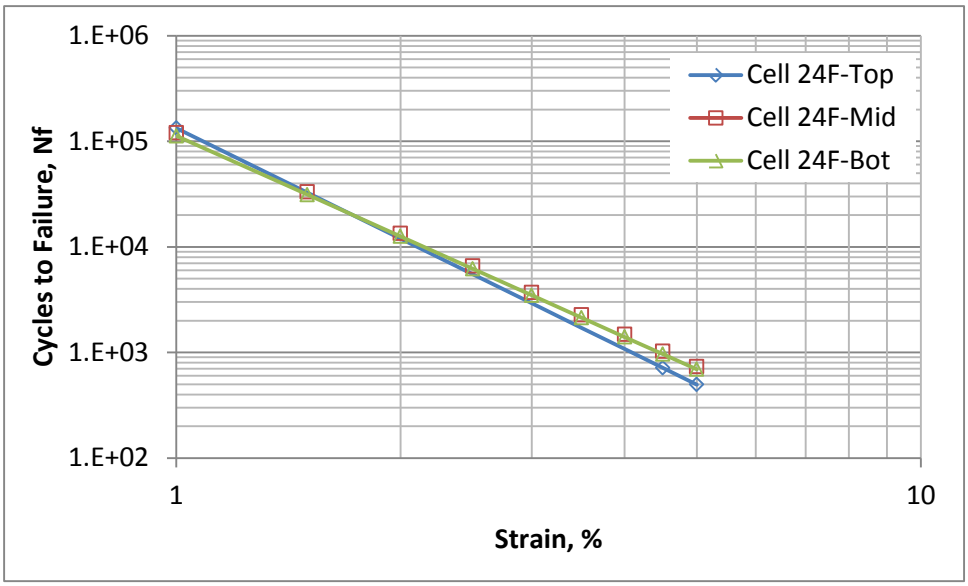

Figure 3.36 LAS Nf-Strain Curves at 16°C for Cell 24F

In each of Figures 3.34-3.36, it can be seen that the Top layer has the steepest slope and generally the lowest N_f for a given shear strain. At low strain levels, the Top layer appears to have a higher N_f in some instances despite the steeper slope. Figure 3.37 illustrates the change in LAS slope (B) as a function of depth in the pavement core.

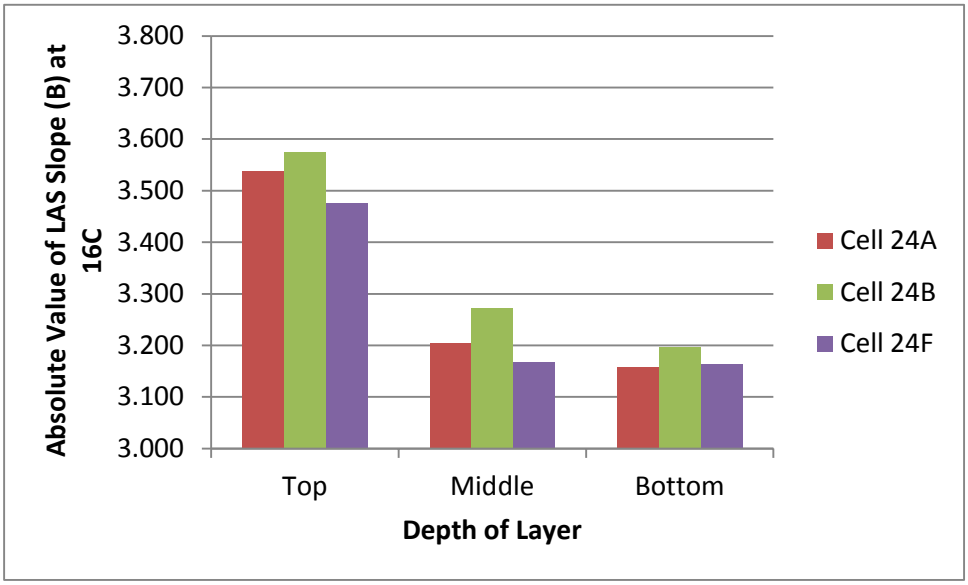

Figure 3.37 Absolute Value of LAS Slope (B) at 16°C for Cells 24A, 24B, and 24F

Figure 3.37 clearly shows a reduction in LAS Slope as a function of depth, suggesting less aging is occurring deeper in the pavement structure.

Lastly, Figure 3.38 illustrates for Cell 24A the effect of depth in the pavement structure on N_f. As can be seen in the figure, the Top layer has the lowest N_f value followed by the Middle and Bottom layers.

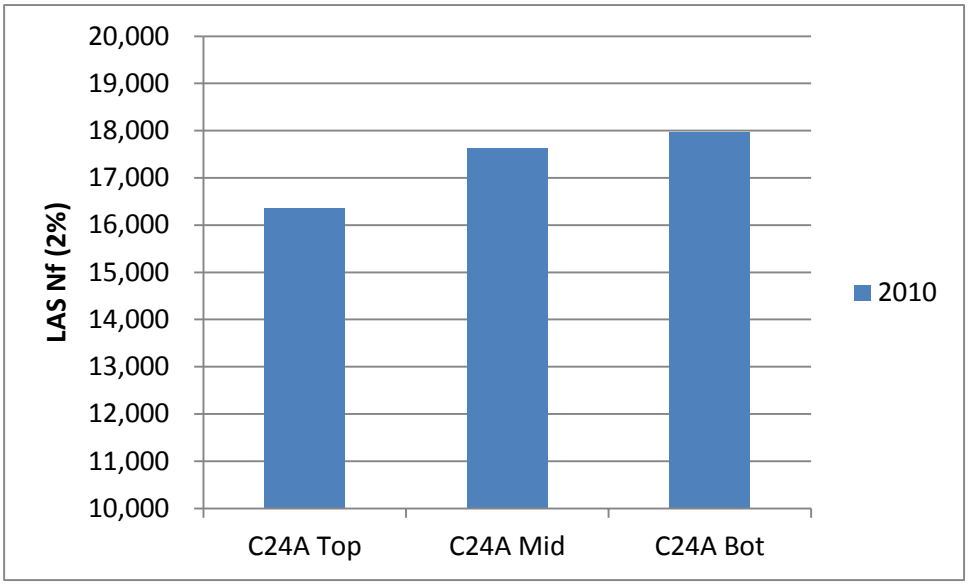

Figure 3.38 LAS Nf Values at 2% Shear Strain and 16°C for Cell 24A

3.3.5 Using Asphalt Binder Properties to Quantify Aging

Although at the time of initial testing only two years of in-service aging had occurred, it appeared that recovered asphalt binder properties could possibly be used to indicate aging and relate to durability. Each of the properties evaluated – BBR ΔT_c value, DSR $G'/(\eta'/G')$ value at 15°C and 0.005 rad/s, DSR Rheological Index (R), LAS N_f, and LAS Slope (B) – showed rational responses of expected aging with layer depth.

To examine the effects of aging, $G'/(\eta'/G')$ values were compared for the Acid Modification Study cells. In this study, recovered asphalt binder properties from the Top layer of each Cell were compared to the RTFO- and PAV-aged properties of the project asphalt binder. This data is shown in Figure 3.39.

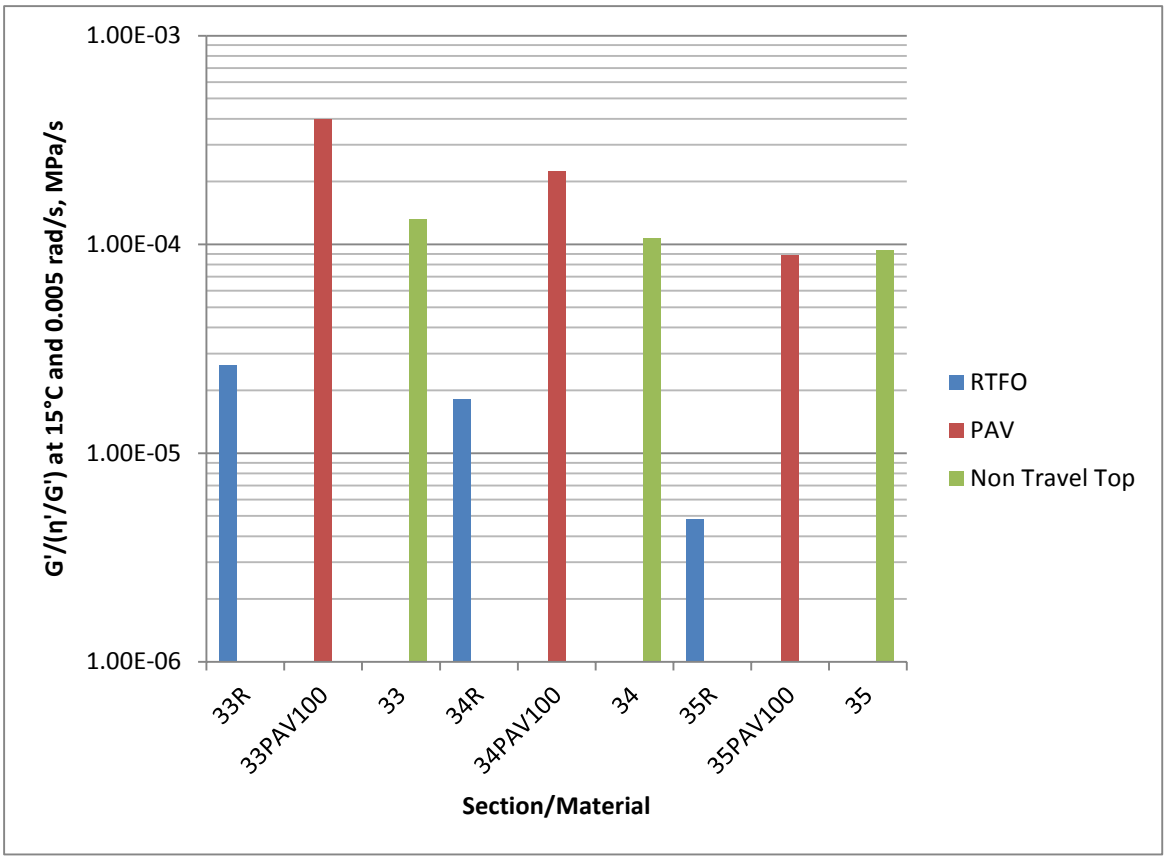

Figure 3.39 Comparison of G′/(η′/G′) Values for Acid Modification Study Cells

In Figure 3.39, within each cell the G′/(η′/G′) value of the RTFO-aged asphalt binder is the lowest, indicating the least amount of aging. Within each cell, the G′/(η′/G′) value of the PAV-aged asphalt binder is generally the highest, indicating the most amount of aging. Within each cell, the G′/(η′/G′) value of the recovered asphalt binder from the Top layer is generally between the RTFO-aged and PAV-aged values, indicating an asphalt binder that is stiffer than RTFO-aging (which is appropriate considering that the recovered asphalt binder has undergone three years of in-service aging), but not quite as stiff as PAV-aging (once again, likely appropriate). The other observation from Figure 3.39 is that the relative ranking of the G′/(η′/G′) values stays the same between the cells regardless of aging. The RTFO-aged G′/(η′/G′) value is highest for Cell 33, followed by Cell 34, followed by Cell 35 as the lowest. The G′/(η′/G′) values for the PAV-aged binder and recovered binder follow the same pattern. This indicates that initial properties of the asphalt binder can have an effect on how quickly the recovered asphalt binder reaches a critical value for durability concerns.

One other parameter that was not discussed in the previous sections, but is introduced in Chapter 2, is the Glover-Rowe (G-R) parameter. The G-R parameter uses the same information contained in the G′/(η′/G′) parameter, but restates it in a more rheologically-familiar manner and in more familiar units (kPa). The G-R parameter is defined as follows:

$$\text{G-R Parameter at 15C, 0.005 rad/s, kPa} = \frac{G^*(\cos\delta)^2}{1000^*(\sin\delta)} \qquad \text{[Eq. 6]}$$

where: G^* = Complex Shear Modulus at 15°C and 0.005 rad/s, Pa
δ = Phase Angle at 15°C and 0.005 rad/s, degrees

Because it is essentially the same information as provided by the G′/(η′/G′) parameter it has not been discussed in this section, but will be used in discussions in Chapter 4.

3.3.6 Error in Aging/Durability Parameter Due to Testing Variability

As discussed earlier, variability in the extraction/recovery procedure and in the tests used to characterize recovered asphalt binder properties can lead to anomalous results. Since the G′/(η′/G′) parameter is derived from a mastercurve, there have been no studies to examine within-lab or between-lab variability. In the AAPTP project, triplicate specimens were tested for each condition of lab-aged (not recovered) asphalt binder, providing some indication of testing repeatability. In that study, the single-operator coefficient of variation (1s%) was generally less than 10% for the aged asphalt binder samples. This is comparable to the single-operator coefficient of variation reported in AASHTO T315 (DSR test procedure) for RTFO-aged asphalt binders.

In the AASHTO T313 (BBR) test procedure, the single-operator d2s% values – representing the acceptable range between two results at a 95% confidence level – are 7.2% for Stiffness and 2.9% for m-value. Individual Stiffness and m-value results at two temperatures are used to calculate the $T_c(S)$ and $T_c(m)$ values, which are then used to calculate the ΔT_c values. Table 3.15 illustrates the effect of testing variability on the $T_c(S)$, $T_c(m)$, and ΔT_c values for a specific recovered asphalt binder (Cell 24A, Bottom Layer, Non-Travel Lane).

Table 3.15 Effect of Variability on Calculated ΔTc Values

	Stiffness, MPa			**m-value**		
	-24°C	**-30°C**	**$T_c(S)$, °C**	**-24°C**	**-30°C**	**$T_c(m)$, °C**
Actual	261	530	-35.2	0.332	0.253	-36.4
- d2s	243	494	-35.8	0.323	0.246	-35.8
+ d2s	280	569	-34.6	0.341	0.260	-37.0

As shown in Table 3.15, for this data set the $T_c(S)$ and $T_c(m)$ values can change by ±0.6°C. Depending on how the values change the ΔT_c value could either be unaffected or, in the worst case, changed by ±1.2°C. To get to this worst case scenario, the m-values would have to be on one end of the limit (e.g., at the d2s limit on the high side) while the Stiffness values would be on the other end of the limit (e.g., at the d2s limit on the low side). This would seem to be a

somewhat unlikely scenario. Nevertheless, it is important to consider the effects of testing variability on the results used to assess durability.

3.4 Asphalt Mixture Testing

The majority of work conducted in the initial testing program was focused on quantifying the effects of aging/durability through recovered asphalt binder testing as opposed to asphalt mixture testing – even though it is recognized that mixture testing provides a true indication of the in-situ properties. This was the selected approach for a couple of reasons:

1. Mix testing requires more material (cores) and is generally more costly than binder testing.
2. The testing variability of mixture tests is usually higher than the variability of binder tests.
3. Aging will manifest itself in the asphalt binder, not the aggregate, meaning that a mixture test should provide essentially the same information as a binder test.

Nevertheless, there was a limited selection of asphalt mixture tests performed to characterize mix properties that could be related to aging/durability. Specifically, low temperature stiffness (using the Indirect Tensile Creep test) and fracture energy (using the Disk-Shaped Compact Tension test) were determined for some of the cores.

In preparation for testing, selected cores were cut to generate a specimen thickness of 25 millimeters. This is different than the preparation used with the cores for asphalt binder extraction/recovery (which were cut into three 12.5-mm thick layers). The selected thickness, 25 mm, is the minimum thickness that can be used for the Disk-Shaped Compact Tension test and is actually thinner than is specified for the Indirect Tensile Creep test (minimum of 38 mm). However, to assess the effect of aging on the top layer without too much influence from the lower, lesser-aged layers, the research team decided to keep the specimen thickness at no more than 25 millimeters.

For each set to be evaluated, three cores were selected and cut to the desired thickness. After determining the bulk specific gravity, specimens were allowed to dry completely before gauge points were attached in the center of the specimen to allow extensometers to be placed for measuring deformation during the Indirect Tensile Creep test. After performing the Indirect Tensile Creep tests at three temperatures, one of the specimens was tested at a single temperature using the Indirect Tensile Strength test. The remaining two specimens were then prepared for the Disk-Shaped Compact Tension test. Details on the procedures are described in the following sections.

3.4.1 Indirect Tensile Creep Test

The Indirect Tensile Creep test is a low temperature test used to determine the creep compliance of an asphalt mixture specimen at low temperatures. The procedure, AASHTO T 322, was developed from research conducted for the Strategic Highway Research Program (SHRP). The researchers found that data from the Indirect Tensile Creep test could be used with prediction models to estimate the low temperature cracking performance of an asphalt mixture. As mixtures age, it is expected that the stiffness of the mix will increase (the compliance of the mix will decrease) and the slope of the compliance curve will decrease.

In the Indirect Tensile Creep test procedure (AASHTO T 322), the specimen is loaded in an indirect tensile testing frame at a low temperature. The specimen then is subjected to a static load to induce deformation during the course of the test. The load is selected to induce sufficient horizontal deformation for a reasonable measurement while maintaining the test within the linear viscoelastic range (typically below 500 x 10^{-6} mm/mm horizontal strain). Testing is usually conducted at three temperatures on the same test specimen. At the conclusion of creep testing, the specimen may be used to determine the asphalt mixture tensile strength by performing the Indirect Tensile Strength test at a single temperature (usually the middle temperature used in the testing program). In this test, the specimen is loaded at a fixed deformation rate of 12.5 mm/min until failure. The tensile strength is determined from the measured peak stress.

In this research, Indirect Tensile Creep testing was conducted at -20, -30, and -40°C, with Indirect Tensile Strength testing conducted on one specimen at -30°C. AASHTO T 322 indicates that the Indirect Tensile Creep test is usually run for 100 seconds, but may also be run for 1000 seconds to create a more complete creep compliance curve (i.e., better overlap in the data allowing for a better curve fit). Experimental testing indicated that electronic noise generated from the environmental chamber could cause poor quality data from the extensometers – particularly at the lowest test temperature. The electronic noise problem was exacerbated at 1000 seconds. As a compromise between avoiding excessive electronic noise (and poorer quality data) and allowing for sufficient compliance overlap for curve-fitting, the research team elected to conduct Indirect Tensile Creep testing for 300 seconds. Data from the three specimens were combined according to the procedures described in AASHTO T 322 and the creep compliance values determined at each temperature. The data was then shifted and fit to a master creep compliance curve having the form:

$$D(t) = D_0 + D_1 t^m \qquad \text{[Eq. 7]}$$

where:

$D(t)$ = creep compliance at time, t

D_0, D_1, m = creep compliance curve-fitting values

Table 3.16 includes the shift coefficients and curve-fit coefficients from Indirect Tensile Creep data for the Non-Travel Lanes of Cells 24A, 24B, and 24F. The creep compliance curves for the three mixtures are shown in Figure 3.40. Table 3.17 includes the indirect tensile strength at -30°C and creep compliance value at -34°C (at 7200 seconds) for the three mixtures.

Table 3.16 Indirect Tensile Creep – Shift and Curve-Fit Coefficients for Cell 24 (Non-Travel)

	Shift Coefficients		Curve-Fit Coefficients		
Cell	a_0	a_1	D_0	D_1	m
24A	0.0123	1.19E+04	2.25E-05	2.65E-06	0.256
24B	-0.2855	9.76E+03	2.36E-05	1.72E-06	0.294
24F	-0.1139	1.16E+04	2.46E-05	3.46E-06	0.253

Table 3.17 Indirect Tensile Creep Compliance and Strength for Cell 24 (Non-Travel)

Cell	D(7200) at -34°C, MPa^{-1}	Strength at -30°C, MPa
24A	7.69E-05	3.63
24B	8.14E-05	3.40
24F	9.71E-05	3.51

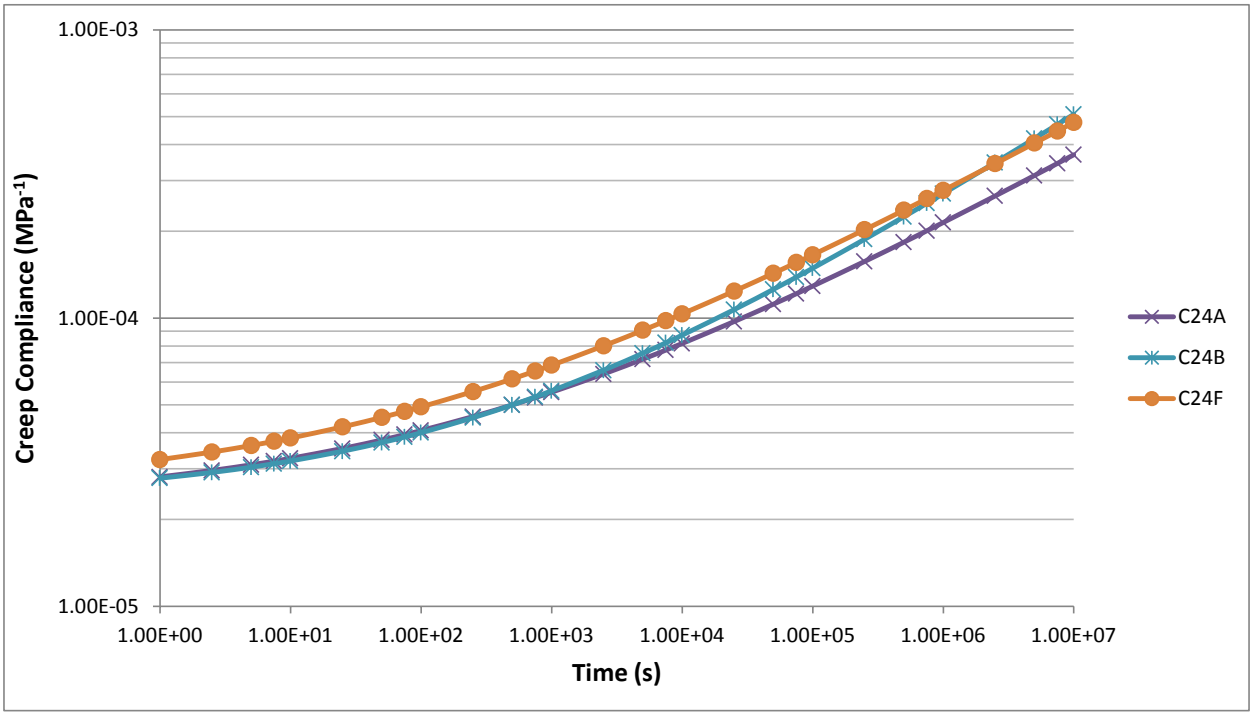

Figure 3.40 Indirect Tensile Creep Compliance – Cell 24 (Non-Travel)

The indirect tensile strength of the three sections of Cell 24 are essentially the same, which is to be expected as the mixture is the same for all three sections with the only exception being that the aging could be different due to the difference in time of sealing the sections. At -30°C and a loading rate of 12.5 mm/min., the stiffness of the asphalt binder might be sufficiently similar such that the tensile strength is unaffected, regardless of aging differences.

Unlike the indirect tensile strength, the creep compliance of the three mixtures is different as shown in Table 3.16 and Figure 3.40. At a temperature of -34°C and a loading time of 7200 seconds (two hours), the creep compliance of Cell 24F was higher than the creep compliance of Cell 24B and Cell 24A. Higher creep compliance values indicate materials that have lower stiffness at the specified temperature and time of loading. This generally matches the findings from the recovered asphalt binder testing, with Cell 24A having the highest value of ΔT_c and $G'/(\eta'/G')$, indicating a stiffer material, and Cell 24F having the lowest value of ΔT_c and $G'/(\eta'/G')$, indicating a less stiff material.

Table 3.18 includes the shift coefficients and curve-fit coefficients from Indirect Tensile Creep data for the Non-Travel Lanes of Cells 33, 34, and 35 – the Acid Modification Study Cells. The creep compliance curves for the three mixtures are shown in Figure 3.41. Table 3.19 includes the indirect tensile strength at -30°C and creep compliance value at -34°C (at 7200 seconds) for the three mixtures.

Table 3.18 Indirect Tensile Creep – Shift and Curve-Fit Coefficients for Acid Modification Study Cells

	Shift Coefficients		Curve-Fit Coefficients		
Cell	a_0	a_1	D_0	D_1	m
33	0.0235	7.78E+03	2.09E-05	3.35E-06	0.323
34	-0.1158	1.12E+04	2.09E-05	1.58E-06	0.302
35	-0.1440	1.08E+04	2.45E-05	1.52E-06	0.302

Table 3.19 Indirect Tensile Creep Compliance and Strength for Acid Modification Study Cells

Cell	D(7200) at -34°C, MPa^{-1}	Strength at -30°C, MPa
33	1.29E-04	3.01
34	7.87E-05	3.22
35	7.99E-05	4.09

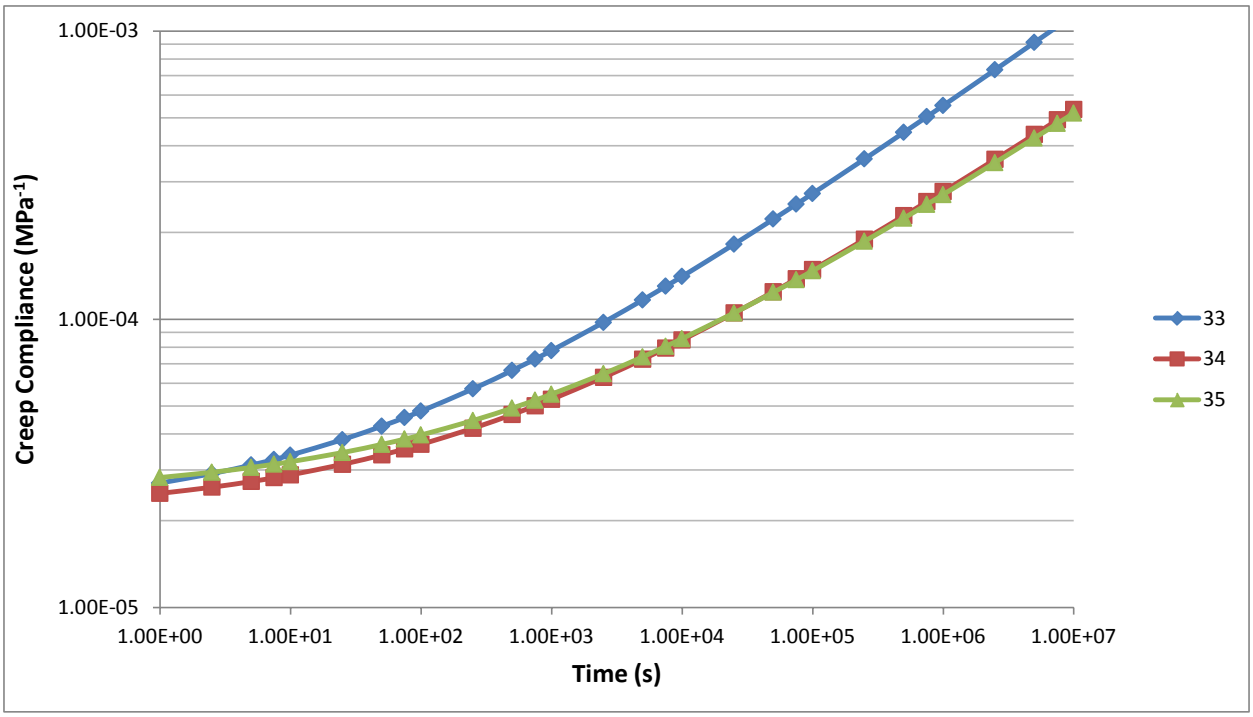

Figure 3.41 Indirect Tensile Creep Compliance – Acid Modification Study Cells

Unlike the Cell 24 mixtures, the indirect tensile strength values of the three sections of the Acid Modification Study are not the same. In this case, Cell 35 appears to have a significantly higher indirect tensile strength compared to Cells 33 and 34. Since the aging on these Cells is the same, the difference is likely attributable to the asphalt binder. Cell 35 has the highest concentration of SBS modification, which could be responsible for the higher tensile strength. Assuming similar development of thermal stress in the mixture, a higher tensile strength will translate to a lower critical temperature before cracking occurs.

The creep compliance of the three mixtures is different as shown in Table 3.19 and Figure 3.41. At a temperature of -34°C and a loading time of 7200 seconds (two hours), the creep compliance of Cell 33 was higher, with a steeper slope, than the creep compliance of Cells 34 and 35. Higher creep compliance values indicate materials that have lower stiffness at the specified temperature and time of loading. This does not match the findings from the recovered asphalt binder testing, with Cell 33 having generally higher values of ΔT_c and $G'/(\eta'/G')$, indicating a stiffer material.

3.4.2 Disk-Shaped Compact Tension Test – DC(T)

The Disk-Shaped Compact Tension, or DC(T), test is a fracture energy test for asphalt mixtures that is performed at low temperatures, usually 10°C warmer than the low temperature of the project where the mix is used. In lab testing used to compare mixtures, the temperature is usually 10°C warmer than the low temperature performance grade (PG) of the asphalt binder. Research

studies have shown the fracture energy obtained from the DC(T) test to be related to the cracking performance – thermal, reflective and/or block cracking – of the mixture [32].

An abbreviated description of the test procedure follows. More complete details of the test procedure are described in ASTM D7313.

The test specimen is similar in size to an IDT specimen – usually 150-mm diameter by 50-mm height – with cut faces. The specimen undergoes a sequence of preparation steps as follows:

1. A template is used to mark the location of two 25-mm diameter loading holes on the face of the specimen. The two loading holes are drilled through the specimen.
2. A masonry saw is used to cut the rounded edge of the specimen closest to the loading holes to provide a flat face.
3. A notch is cut from the flat face towards the center of the specimen, bisecting the loading holes.
4. Gage points are placed on the flat face on either side of the notch to provide for placement of the crack mouth opening displacement (CMOD) gage.
5. Metal pins are fitted into the loading holes to allow for the testing fixture to grip the specimen in an indirect tension configuration.

After specimen preparation is complete, the test specimen is conditioned at the proper test temperature and loaded in the fixture. The CMOD gage is attached to the test specimen and the test is executed by controlling displacement from the CMOD at a rate of 1 mm/min. Testing is continued until the specimen is completely failed. The fracture energy is calculated using the area under the load-displacement curve and the specimen dimensions. Higher values of fracture energy have been correlated to a lower propensity for cracking. Figures 3.42 and 3.43 illustrate the DC(T) test configuration with specimen. Figure 3.44 shows a test specimen after testing.

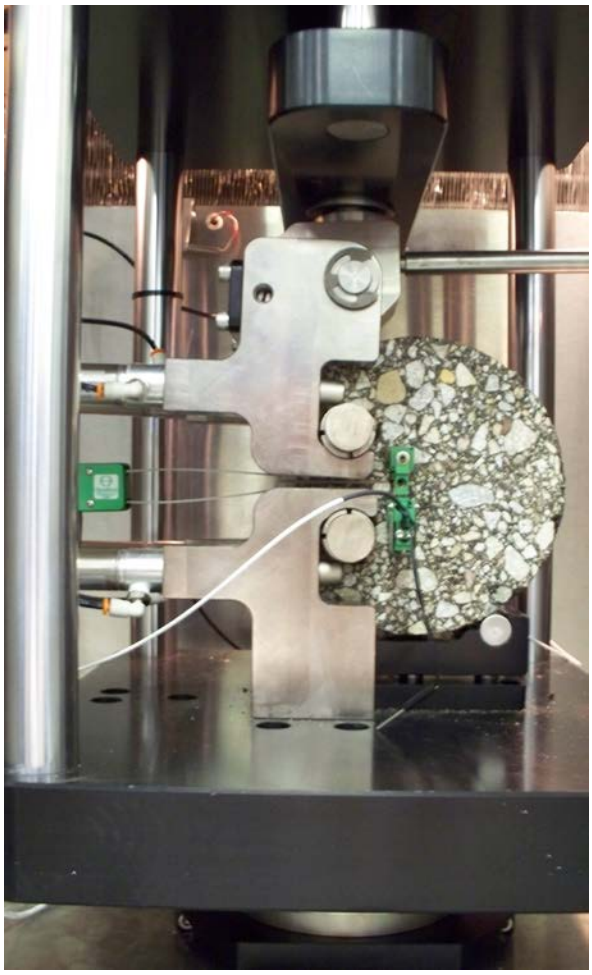

Figure 3.42 DC(T) Test Configuration

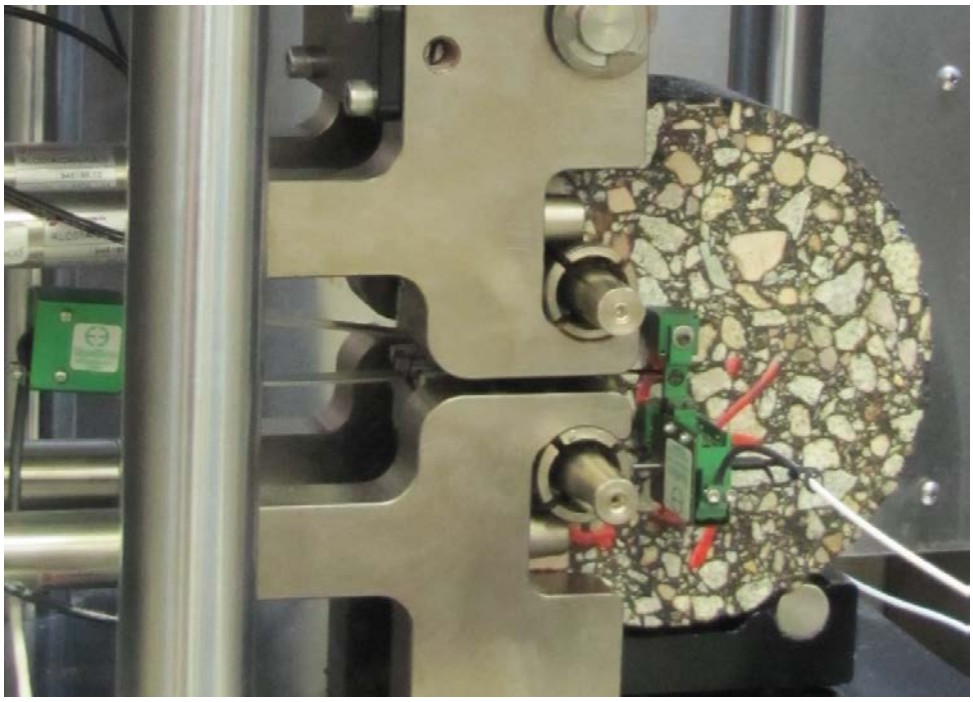

Figure 3.43 DC(T) Test Configuration – Closer View

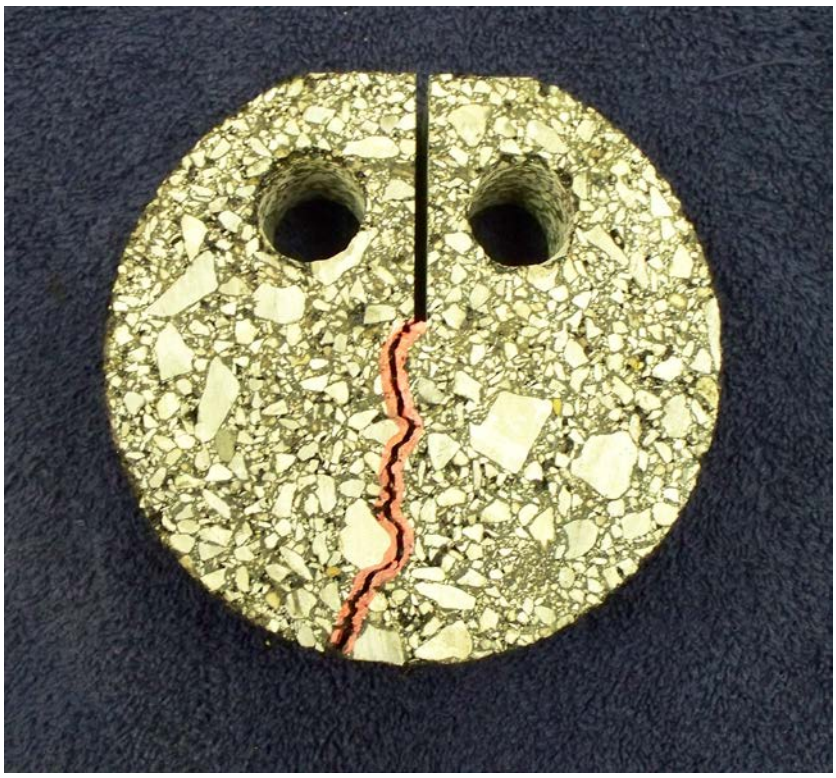

Figure 3.44 DC(T) Specimen after Testing

Table 3.20 shows the test results from DC(T) testing at -24°C for Cell 24 (24A, 24B, and 24C) and the Cells used in the Acid Modification Study (33, 34, and 35). The data is also illustrated in Figures 3.45 and 3.46. Unfortunately, the limited number of cores available after extraction/recovery testing meant that a maximum of two tests were performed for each mixture. Consequently, it is difficult to draw any conclusions from the DC(T) data.

Table 3.20 DC(T) Results at -24°C

			Fracture Energy from CMOD, J/m^2		
Cell	**Sample**	**Gmb**	**Measured**	**Average**	**1s%**
24A	1	2.332	723.4	750.1	5%
	2	2.343	776.8		
24B	1	2.347	874.3	874.3	n/a
24F	3	2.343	619.9	619.9	n/a
33	2	2.296	667.3	573.5	23%
	3	2.328	479.6		
34	2	2.347	426.6	450.8	8%
	3	2.375	474.9		
35	1	2.315	348.7	541.6	50%
	2	2.340	734.5		

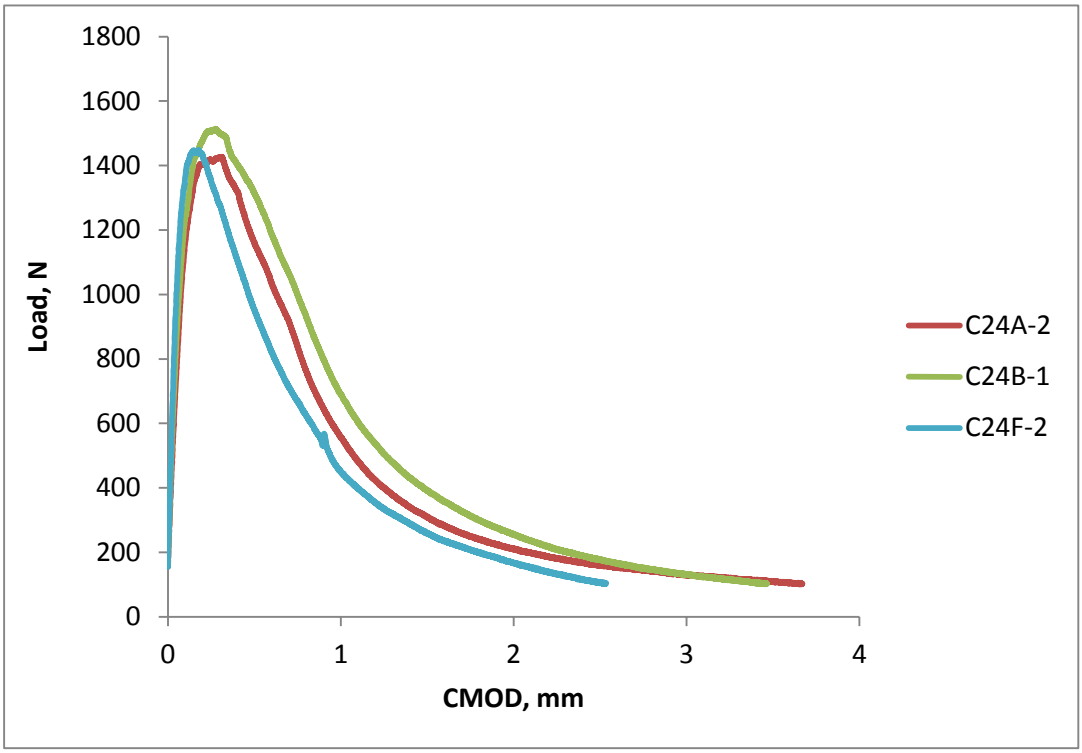

Figure 3.45 DC(T) Load vs. CMOD Curves for Cell 24

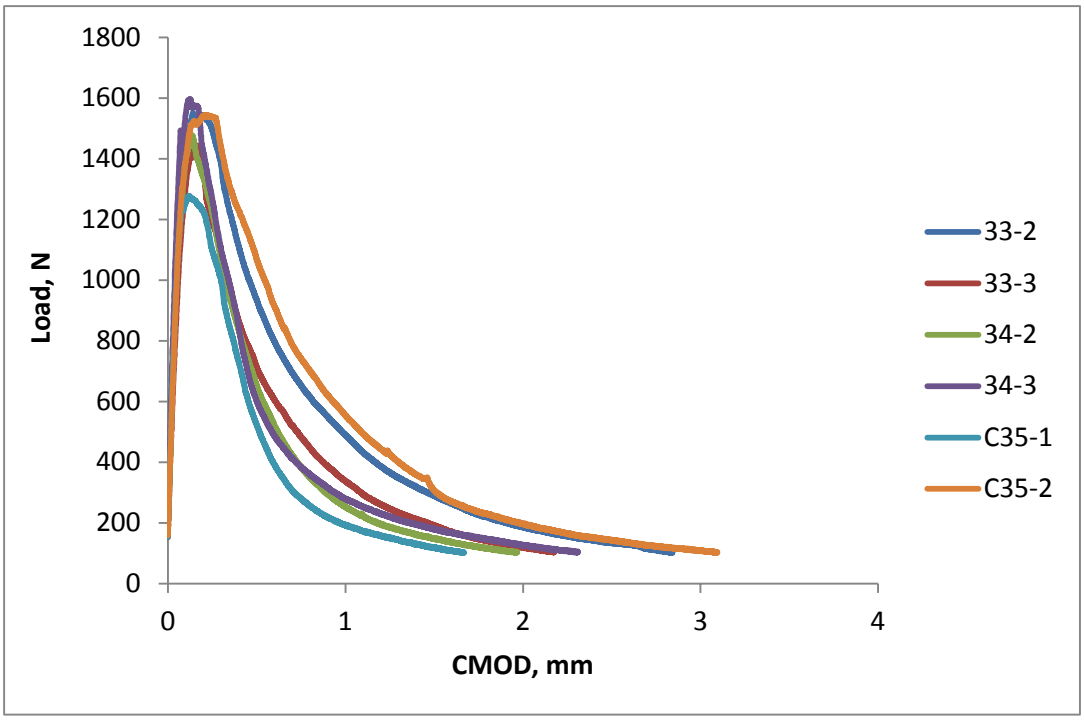

Figure 3.46 DC(T) Load vs. CMOD Curves for Cells 33-35

3.5 Summary of Findings from Initial MnROAD Testing

From the initial testing, it appeared that recovered asphalt binder testing may be sufficient to characterize the aging of the asphalt mixture in-service. The evaluated binder parameters from the BBR – ΔT_c – and the DSR – $G'/(\eta'/G')$ value at 15°C and 0.005 rad/s, DSR Rheological Index (R), LAS N_f, and LAS Slope (B) – show rational responses of expected aging with layer depth. There was some indication of environmental aging, but there had not been sufficient aging time before coring to fairly evaluate the parameters in that regard. The binder parameters that were evaluated can be derived using conventional asphalt binder testing equipment (Bending Beam Rheometer and Dynamic Shear Rheometer). The ΔT_c parameter has the advantage of being a temperature-independent parameter, but requires more recovered asphalt binder. The $G'/(\eta'/G')$ parameter is temperature-dependent (some work may be needed to select the proper temperature), but can be determined using a much smaller recovered asphalt binder sample. The $G'/(\eta'/G')$ parameter determined from a mastercurve developed using Temperature-Frequency Sweep data requires a longer testing and analysis time – approximately 2.5 hours – but provides a more complete rheological characterization of the binder. The Single-Point DSR test is a fast test (approximately 20 minutes) conducted at higher test temperatures and can provide an estimate of the $G'/(\eta'/G')$ parameter, but doesn't offer a direct measurement at the temperature of interest and depends on the assumption that the Time-Temperature Superposition Principle is valid and provides a constant shift for all asphalt binders. The LAS test may provide a good compromise to the Temperature-Frequent Sweep test with mastercurve development. The LAS

test can be performed at intermediate temperatures and provides a parameter – the LAS Slope (B) – that appears to be highly correlated to the G′/(η′/G′) parameter. The test is relatively quick (approximately 30 minutes), but variability is unknown.

Limited mixture testing did not provide an indication of any different behavior than was already identified by the binder test results. Considering that mixture tests require more material, are more costly, and generally have higher variability, mixture testing in the field evaluation phase of the study should be limited.

Chapter 4 - Field Evaluation of Pavements for Aging/Durability

4.1 MnROAD Low Volume Road – Cell 24

As discussed in Chapter 3.1, Cell 24 of the MnROAD Low Volume Road (Figure 3.1) was established as a test section to study the effects of aging on asphalt pavements, with the goal of identifying the best timing for preventive maintenance treatments. This test section was built in October 2008 and immediately subdivided into five 100-foot test sections with an additional control section. The plan was to seal one of the test subsections each year so that the timing of the sealing and its effect on environmental aging could be studied.

In 2008, immediately after construction the first subsection, identified as Cell 24A in this study, was sealed using a CSS-1 emulsion, diluted 1:1, applied at a rate of 0.03 gallons per square yard. The intent was to use a CRS-2P emulsion but it was too late in the year to obtain the product [27]. It was decided to not use aggregate (chips) on any of the subsections to complete the chip seals due to concerns that the aggregate could impact any subsequent testing that would occur.

Approximately one year after construction in 2009 a second 100-ft subsection, identified as Cell 24B, was sealed using a CRS-2P emulsion at an application rate of 0.1 gallons per square yard.

Approximately two years after construction in 2010 a third 100-ft subsection, identified as Cell 24C, was sealed using a CRS-2P emulsion at an application rate of 0.1 gallons per square yard. Coring operations also began in 2010 to provide initial testing of Cell 24 for evaluation of environmental aging. Six cores were taken from the travel and non-travel lanes of each of Cells 24A, 24B, 24C, and 24F. As discussed in Chapter 3, no testing was conducted on the cores taken in 2010 from Cell 24C since this subsection had just been sealed prior to coring. It was believed that the data from Cell 24C would be the same as data from the Control subsection (Section 24F).

Approximately three years after construction in 2011 a fourth 100-ft subsection, identified as Cell 24D, was sealed using a CRS-2P emulsion at an application rate of 0.1 gallons per square yard. Six cores were taken from the non-travel lanes of each of Cells 24A, 24B, 24C, 24D, and 24F. As was done with Cell 24C in 2010, no testing was conducted on the cores taken in 2011 from Cell 24D since this subsection had just been sealed prior to coring.

Approximately four years after construction in 2012 a fifth 100-ft subsection, identified as Cell 24D, was sealed using a CRS-2P emulsion at an application rate of 0.1 gallons per square yard. Six cores were taken from the non-travel lanes of each of Cells 24A, 24B, 24C, 24D, 24E, and 24F. As was done with Cell 24C in 2010 and Cell 24D in 2011, no testing was conducted on the cores taken in 2012 from Cell 24E since this subsection had just been sealed prior to coring.

Finally, approximately five years after construction in 2013 six cores were taken from the non-travel lanes of each of Cells 24A, 24B, 24C, 24D, 24E, and 24F. After the seal was applied to

Cell 24E in 2012, all the subsections were complete. Cell 24F, the control subsection, remained unsealed during the life of the pavement.

As described in Chapter 3, two cores from each subsection, for each year of coring, were designated for asphalt binder testing and were cut into four layers starting at the top of the core. The "Top" layer represented the surface of the core to a depth of 12.5 millimeters. The "Middle" layer represented the portion of the core from approximately 17.5 millimeters to 30 millimeters depth from the surface. Finally, the "Bottom" layer represented the portion of the core from approximately 35 millimeters to 47.5 millimeters depth from the surface

As noted, the saw blade used in cutting was thick enough so that five millimeters of each cut was lost. As such the cuts didn't provide layers that were exactly at depths of 12.5, 25, and 37.5 millimeters as might have been expected.

After cutting, like layers from the two cores were combined to use for solvent extraction and recovery testing. Solvent extraction was conducted following AASHTO T 164, *Quantitative Extraction of Asphalt Binder from Hot-Mix Asphalt (HMA)*, except that toluene was used as the solvent. Recovery of the asphalt binder from solution was accomplished using the recovery procedure described in AASHTO T 319, *Quantitative Extraction and Recovery of Asphalt Binder from Asphalt Mixtures*. At the completion of the recovery procedure, the recovered asphalt binder was poured into a container and identified by pavement section and layer.

Based on results from the initial testing program plan, it was determined that testing should be focused on DSR tests – specifically Temperature-Frequency Sweep and Linear Amplitude Sweep Tests. Temperature-Frequency Sweep testing could provide a more complete look at the rheological behavior of the asphalt binder at intermediate temperatures, and, through the use of mastercurves derived from the test data, could offer more potential analysis options. LAS testing could provide information on the slope of the Complex Shear Modulus-Frequency curve which was shown to be related to the rheological parameters derived from the Temperature-Frequency Sweep testing and also provide an estimate of fatigue resistance through the use of Viscoelastic Continuum Damage theory. BBR testing would require more time and material and did not appear to provide any substantially different information than could have been obtained with the DSR tests. The Single-Point DSR test was quick, but relied on assumptions to provide an estimate of the same parameter that could be derived from Temperature-Frequency Sweep tests.

Testing for the recovered asphalt binder samples in the field evaluation is shown below:

- **DSR Temperature-Frequency Sweep** – Testing to determine the temperature-frequency response of the recovered asphalt binder using intermediate temperatures of 5, 15, and 25°C and loading frequency from 0.1 to 100 rad/s. Data from the temperature-frequency sweep testing can be combined into a mastercurve at a reference temperature (15°C) and used to derive various rheological parameters. AASHTO T 315 is used as the reference procedure for Temperature-Frequency Sweep testing.
- **Linear Amplitude Sweep (LAS) Test** – Shear strain sweep testing conducted at an intermediate temperature appropriate to the climate (16°C) and 10 Hz (62.9 rad/s) loading frequency. The test is conducted by first performing a frequency sweep at small strain (0.1%) and a range of loading frequencies to determine the slope of the modulus-

frequency curve. The second part of the test involves testing at a fixed loading frequency of 10 Hz and linearly increasing the strain from 1% to a maximum of 30%. Dissipated energy is calculated per data point and used in a viscoelastic continuum damage (VECD) analysis.

The remaining four cores from each subsection/year were designated for mixture testing. Because mixture testing required a minimum specimen thickness of 25 mm, the cutting operation was slightly different. Instead of separating each core into three 12.5-mm layers, the cores were cut at a depth of 25 millimeters from the surface, representing the "Top" layer, and another 25 millimeters deeper (with five millimeters removed by the saw blade), representing the "Bottom" layer. It was understood that direct comparisons with binder test results would prove difficult since the Mixture "Top" layer would include material that was in the Binder "Top" and most of the Binder "Middle" layers. The Mixture "Bottom" layer would include material that was in the Binder "Bottom" layer, but would also include material that was a little deeper in the pavement core not characterized by binder testing.

After cutting, three of the specimens from each subsection and layer were instrumented and subjected to the Indirect Tensile Creep Test at -20, -30, and -40°C following the procedures in AASHTO T 322, as described in Chapter 3. One core was then instrumented and subjected to the Indirect Tensile Strength test at -30°C following the procedures in AASHTO T 322. This core was discarded after fracture. The results of the indirect tensile creep and strength tests were used as inputs into the PIDT/MONARCH™ software program developed by Abatech, Inc. The PIDT/MONARCH software is used to inspect the quality of data from the Indirect Tensile Creep and Strength tests and then perform an analysis to estimate the predicted cracking temperature of an asphalt pavement.

After testing at the third temperature, the three specimens that had been subjected to Indirect Tensile Creep testing were re-used for DC(T) testing. The specimens were not considered damaged by the indirect tensile creep testing since the testing occurred at a sufficiently low load to induce a low strain over the relatively short duration of the test. The gage points used for the indirect tensile creep testing were removed and the specimen subjected to the additional preparation procedures needed to make the specimen into a proper DC(T) test specimen. DC(T) testing was then conducted at -24°C following the procedure described in ASTM D7313 for three specimens of each subsection/layer/year. Data from the DC(T) tests was input into the PDC(T)™ software program developed by Abatech to calculate the fracture energy of the specimen.

4.1.1 Binder Testing Results

Test results from the temperature-frequency sweep tests on each subsection/layer for each coring year were used to generate a mastercurve at 15°C. Results are shown in Tables 4.1-4.4. The data is also illustrated graphically in Figures 4.1 and 4.2 showing the $G'/(\eta'/G')$ parameter and the G-R parameter – both calculated at 15°C and 0.005 rad/s – as a function of depth in the pavement layer for each subsection/year.

Table 4.1 2010 MnROAD Recovered Asphalt Binder: Mastercurve-Derived Parameters

			15°C, 0.005 rad/s				15°C, 10 rad/s	
Cell	**Lane**	**Layer**	**Calculated G′/(η′/G′) MPa/s**	**G-R Parameter, kPa**	**R**	**δ, degrees**	**G*, kPa**	**δ, degrees**
24A	Non-Travel	Top	4.27E-05	8.55	2.153	67.3	6,415	45.2
		Mid	1.40E-05	2.80	2.065	70.8	4,149	49.5
		Bot	1.09E-05	2.18	2.052	71.5	3,709	50.2
24B	Non-Travel	Top	3.81E-05	7.62	2.203	67.0	5,477	45.6
		Mid	2.36E-05	4.72	2.086	69.4	5,407	48.8
		Bot	1.01E-05	2.03	2.049	71.7	3,575	50.3
24F	Non-Travel	Top	3.37E-05	6.75	2.180	67.6	5,416	45.9
		Mid	1.35E-05	2.69	2.130	70.2	3,788	49.8
		Bot	1.22E-05	2.45	2.097	70.8	3,778	49.6

Table 4.2 2011 MnROAD Recovered Asphalt Binder: Mastercurve-Derived Parameters

			15°C, 0.005 rad/s				15°C, 10 rad/s	
Cell	**Lane**	**Layer**	**Calculated G′/(η′/G′) MPa/s**	**G-R Parameter, kPa**	**R**	**δ, degrees**	**G*, kPa**	**δ, degrees**
24A	Non-Travel	Top	7.698E-05	15.40	2.110	66.3	8,280	41.3
		Mid	1.926E-05	3.85	1.940	71.6	5,500	46.4
		Bot	2.250E-05	4.50	1.957	71.0	5,870	46.6
24B	Non-Travel	Top	1.163E-04	23.26	2.181	64.4	8,883	39.4
		Mid	2.087E-05	4.17	1.967	71.1	5,492	46.2
		Bot	2.360E-05	4.72	1.999	70.4	5,587	46.6
24C	Non-Travel	Top	1.061E-04	21.21	2.163	64.8	8,733	39.8
		Mid	2.107E-05	4.21	1.995	70.7	5,316	47.1
		Bot	1.669E-05	3.34	1.973	71.5	4,659	47.2
24F	Non-Travel	Top	5.762E-05	11.52	2.086	67.3	7,090	42.1
		Mid	2.180E-05	4.36	1.994	70.7	5,421	46.5
		Bot	2.334E-05	4.67	1.977	70.7	5,579	46.3

Table 4.3 2012 MnROAD Recovered Asphalt Binder: Mastercurve-Derived Parameters

			15°C, 0.005 rad/s				15°C, 10 rad/s	
Cell	**Lane**	**Layer**	**Calculated G′/(η′/G′) MPa/s**	**G-R Parameter, kPa**	**R**	**δ, degrees**	**G*, kPa**	**δ, degrees**
24A	Non-Travel	Top	6.731E-05	13.46	2.186	65.8	7,711	43.7
		Mid	4.423E-05	8.85	2.136	67.4	6,546	44.3
		Bot	3.368E-05	6.74	2.098	68.5	6,262	46.5
24B	Non-Travel	Top	5.475E-05	10.95	2.169	66.5	7,141	44.2
		Mid	3.609E-05	7.22	2.097	68.3	6,098	44.7
		Bot	2.981E-05	5.96	2.080	69.0	5,955	46.1
24C	Non-Travel	Top	4.208E-05	8.42	2.139	67.5	6,495	44.9
		Mid	2.931E-05	5.86	2.041	69.5	5,935	45.7
		Bot	2.950E-05	5.90	2.097	68.8	5,953	46.4
24D	Non-Travel	Top	5.231E-05	10.46	2.161	66.7	6,978	44.0
		Mid	3.553E-05	7.11	2.093	68.4	6,267	45.1
		Bot	3.115E-05	6.23	2.081	68.9	6,051	46.2
24F	Non-Travel	Top	4.147E-05	8.29	2.116	67.8	6,598	45.1
		Mid	3.248E-05	6.50	2.047	69.2	6,265	45.2
		Bot	3.095E-05	6.19	2.073	69.0	6,098	46.2

Table 4.4 2013 MnROAD Recovered Asphalt Binder: Mastercurve-Derived Parameters

			15°C, 0.005 rad/s				15°C, 10 rad/s	
Cell	**Lane**	**Layer**	**Calculated G′/(η′/G′) MPa/s**	**G-R Parameter, kPa**	**R**	**δ, degrees**	**G*, kPa**	**δ, degrees**
24A	Non-Travel	Top	6.036E-05	12.07	2.184	66.1	7,536	43.2
		Mid	4.950E-05	9.90	2.082	67.7	7,201	43.4
		Bot	3.123E-05	6.25	2.038	69.3	6,339	45.7
24B	Non-Travel	Top	4.908E-05	9.82	2.164	66.8	6,571	44.1
		Mid	3.952E-05	7.90	2.088	68.2	6,739	45.2
		Bot	2.728E-05	5.46	1.994	70.2	6,145	45.9
24C	Non-Travel	Top	5.306E-05	10.61	2.143	66.9	7,212	44.1
		Mid	3.113E-05	6.23	2.046	69.3	5,974	45.4
		Bot	3.462E-05	6.92	2.067	68.8	6,530	45.8
24D	Non-Travel	Top	5.678E-05	11.36	2.161	66.5	7,297	43.9
		Mid	4.434E-05	8.87	2.119	67.6	6,891	45.0
		Bot	2.895E-05	5.79	2.001	69.9	6,180	45.5
24E	Non-Travel	Top	5.172E-05	10.34	2.095	67.5	7,315	44.3
		Mid	4.187E-05	8.37	2.111	67.8	6,679	45.1
		Bot	3.051E-05	6.10	2.059	69.2	5,841	45.2
24F	Non-Travel	Top	5.198E-05	10.40	2.143	66.9	7,189	44.2
		Mid	3.326E-05	6.65	1.994	69.7	6,097	44.4
		Bot	3.000E-05	6.00	2.065	69.1	6,073	46.5

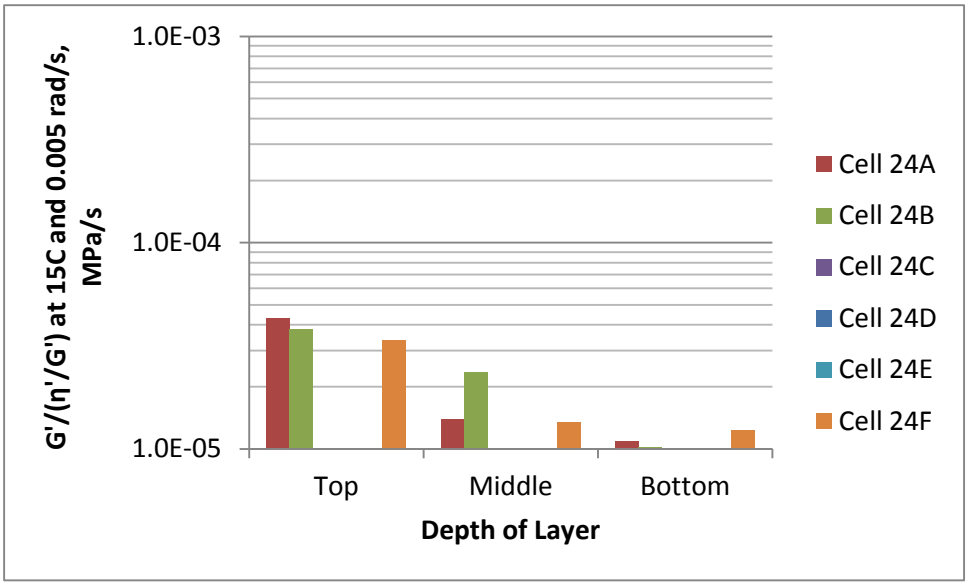

Figure 4.1(a) G′/(η′/G′) Parameter as a Function of Subsection and Layer – 2010

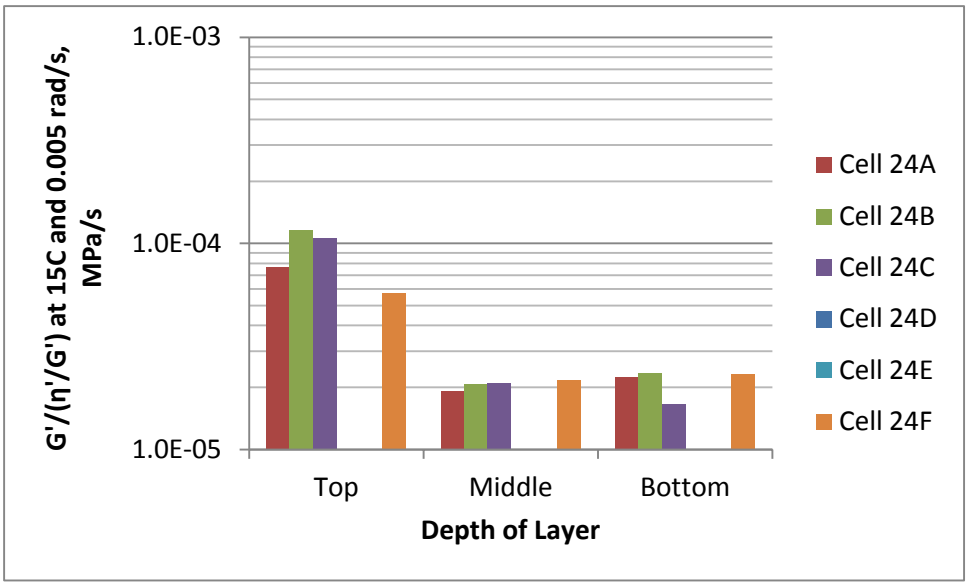

Figure 4.1(b) G'/(η'/G') Parameter as a Function of Subsection and Layer – 2011

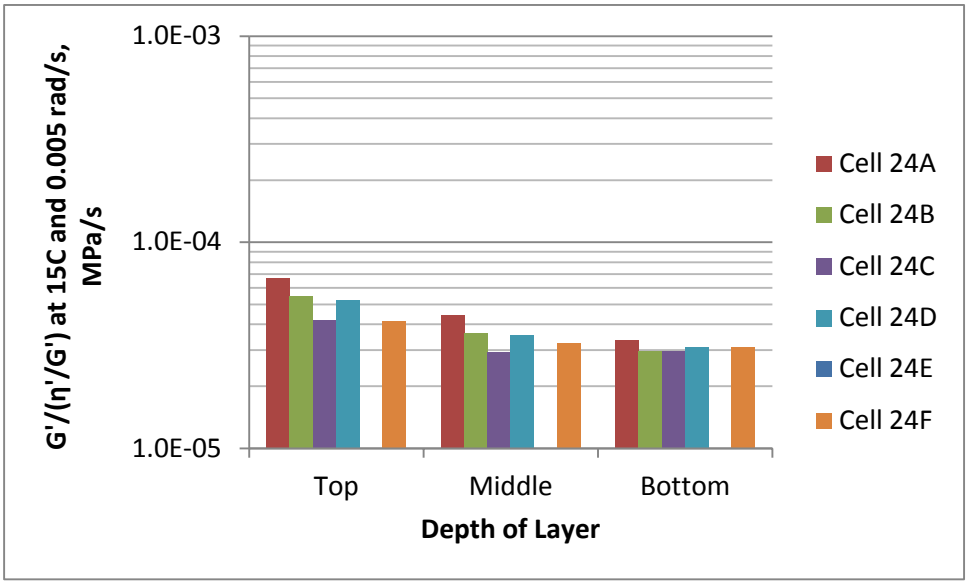

Figure 4.1(c) G'/(η'/G') Parameter as a Function of Subsection and Layer – 2012

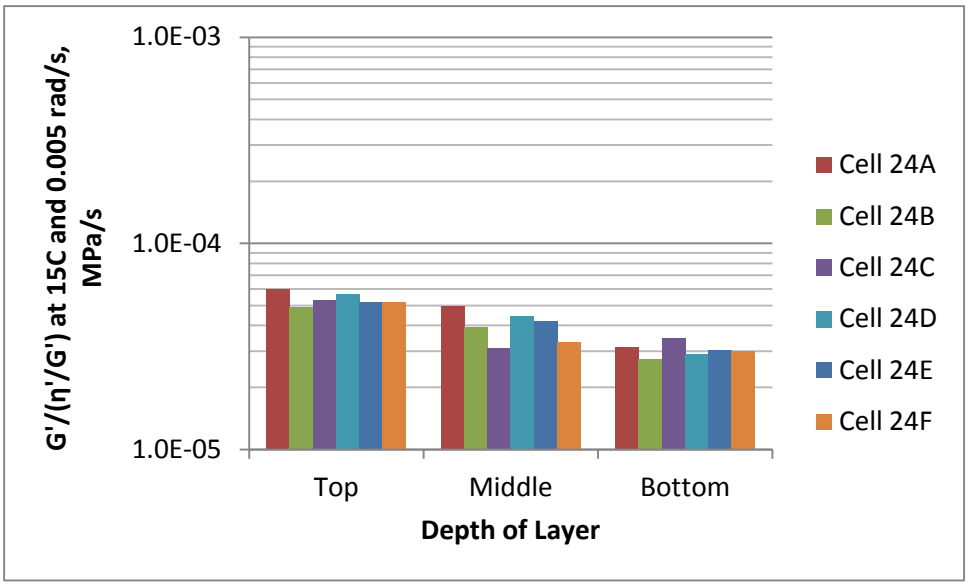

Figure 4.1(d) G′/(η′/G′) Parameter as a Function of Subsection and Layer – 2013

Figure 4.1 G′/(η′/G′) Parameter as a Function of Subsection and Layer, 2010-2013

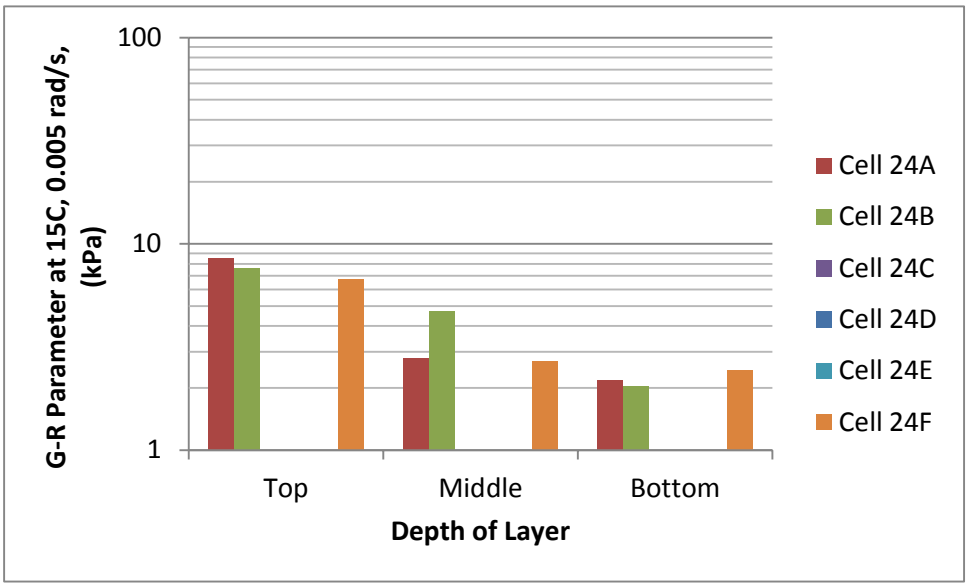

Figure 4.2(a) G-R Parameter as a Function of Subsection and Layer – 2010

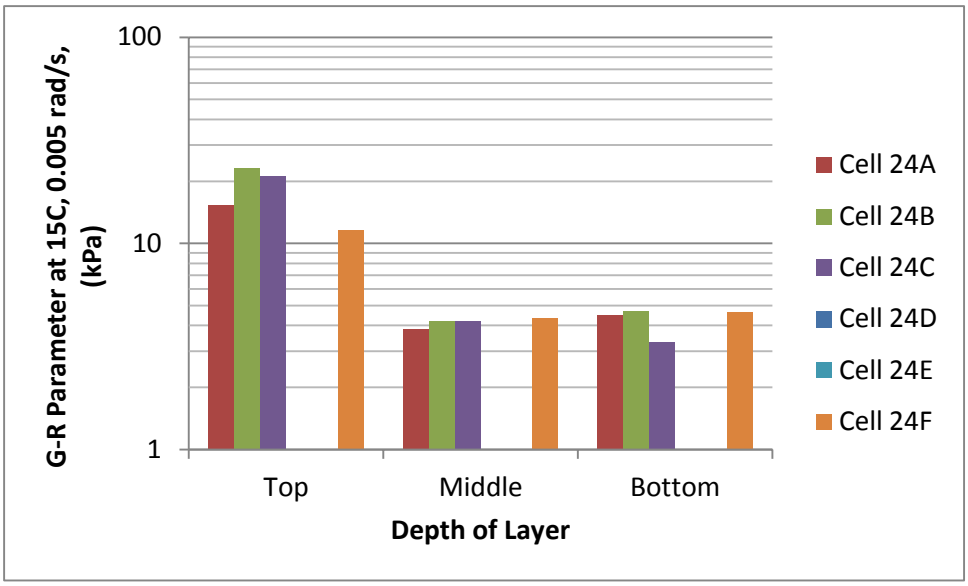

Figure 4.2(b) G-R Parameter as a Function of Subsection and Layer – 2011

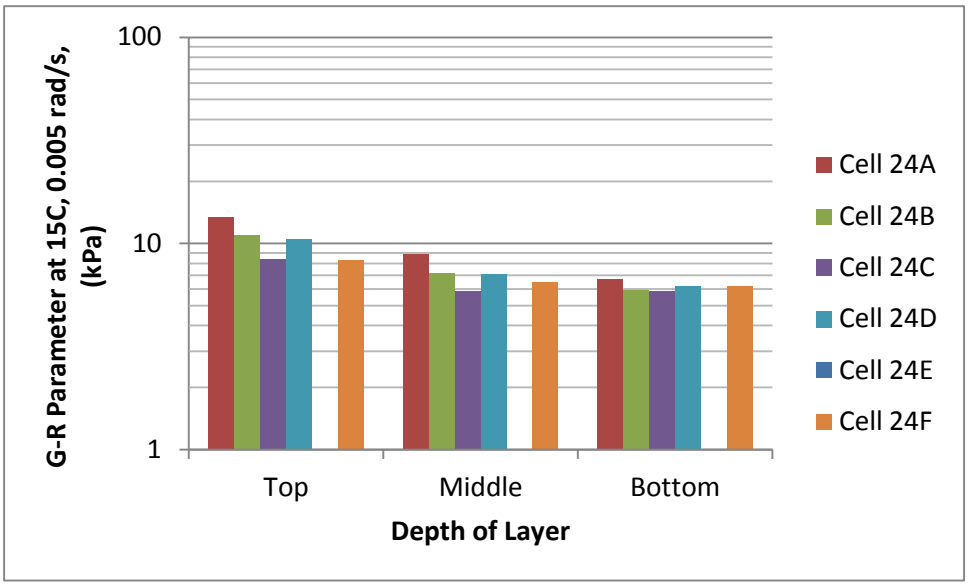

Figure 4.2(c) G-R Parameter as a Function of Subsection and Layer – 2012

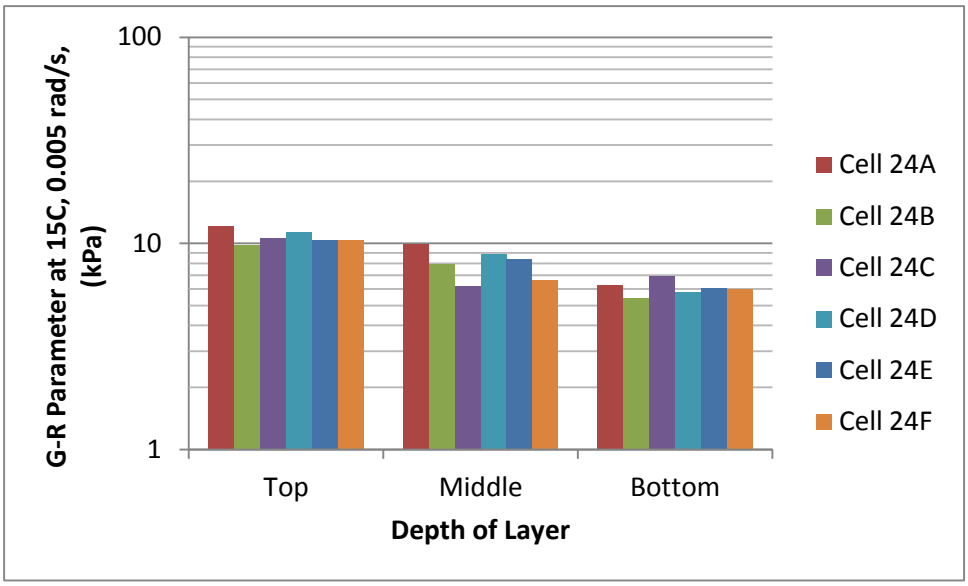

Figure 4.2(d) G-R Parameter as a Function of Subsection and Layer – 2013

Figure 4.2 G-R Parameter as a Function of Subsection and Layer, 2010-2013

In Tables 4.1-4.4 and Figures 4.1-4.2, it can be seen that the derived parameters from the asphalt binder mastercurves show a rational response with depth. Near the surface (the "Top" layers), the asphalt binder shows an increase in stiffness and a decrease in phase angle, indicating a loss of relaxation properties as the binder ages. Further down in the pavement, the asphalt binder exhibits less aging as exhibited by lower stiffness and higher phase angle. Both the $G'/(\eta'/G')$ parameter and the G-R parameter – calculated at 15°C and 0.005 rad/s – capture the effects of increased stiffness and decreased phase angle seen with aging.

It appears from the data that the asphalt binder properties generally exhibit rational behavior as time progresses. For any given combination of subsection and layer, it can be seen that the $G'/(\eta'/G')$ and G-R parameters generally increase as time increases – indicating an increase in aging. Despite this general trend, it should be noted that the data from the Top layers of the cores taken in 2011 shows an increase in the values of the $G'/(\eta'/G')$ and G-R parameters from 2010, as expected, but a subsequent decrease in values for 2012. For most of the 2013 subsections the values return to the expected trend of being higher as aging progresses.

The anomalous behavior exhibited in the Top layers of the 2011 cores was not exhibited in the Bottom layers of the 2011 cores. The data for the Bottom layers generally indicates a rational progression to higher values with increased time.

Figures 4.3 and 4.4 show how the value of the $G'/(\eta'/G')$ parameter changes with time for the Top and Bottom layers. Figures 4.5 and 4.6 show how the value of the G-R parameter changes with time for the Top and Bottom layers.

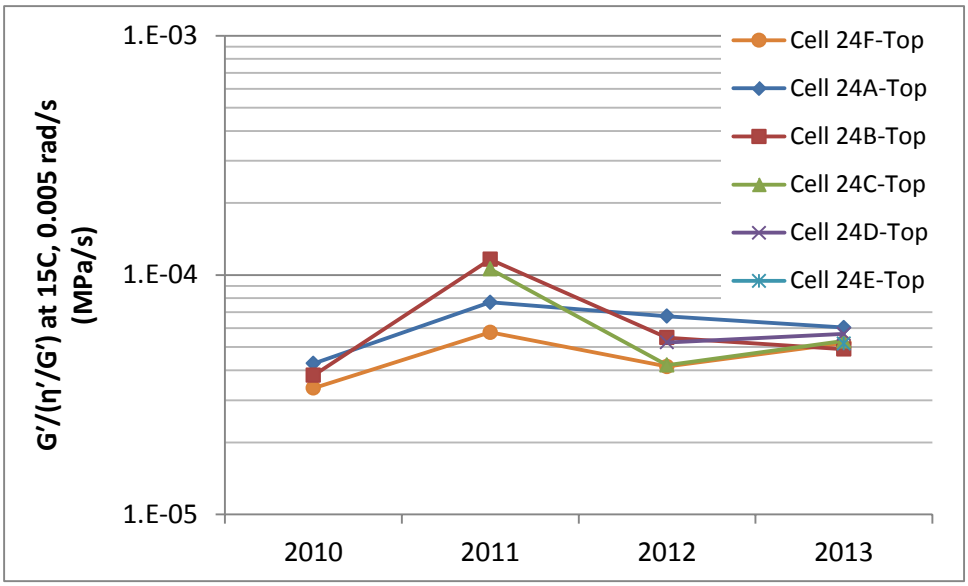

Figure 4.3 G′/(η′/G′) Parameter as a Function of Time – Top Layer

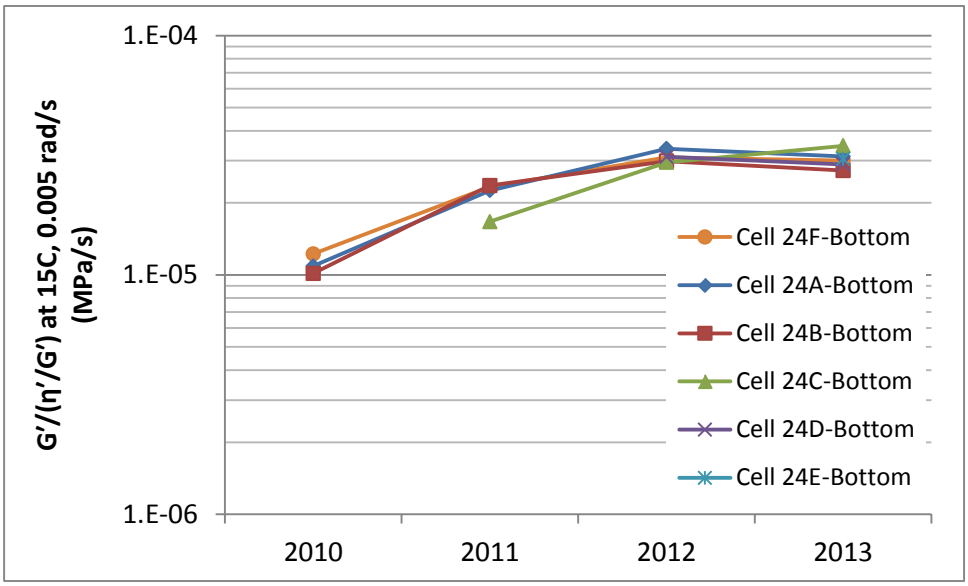

Figure 4.4 G′/(η′/G′) Parameter as a Function of Time – Bottom Layer

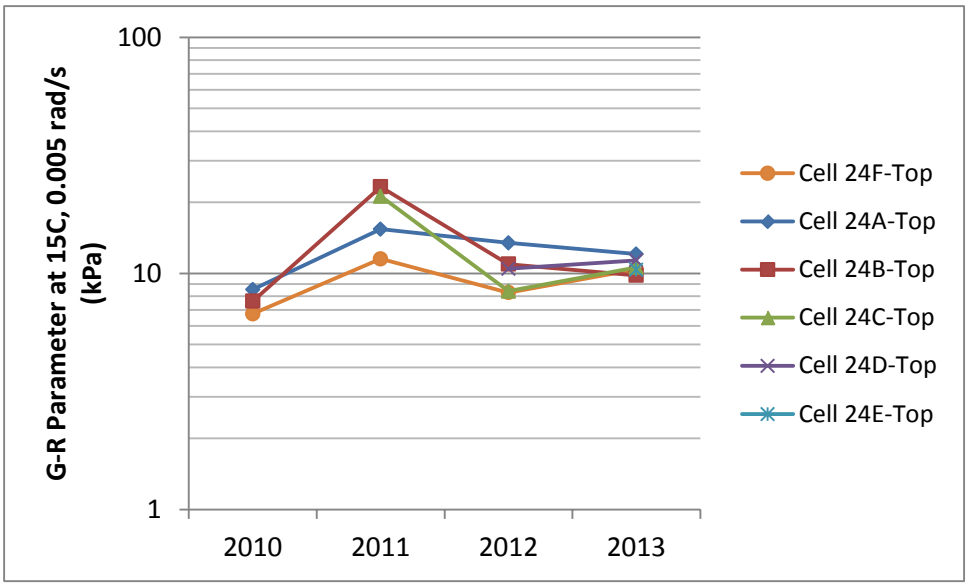

Figure 4.5 G-R Parameter as a Function of Time – Top Layer

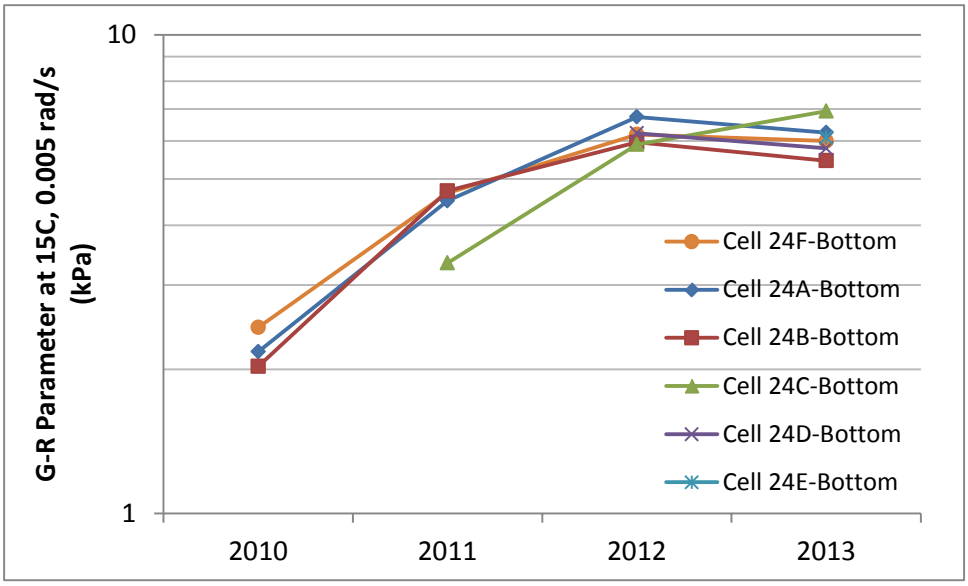

Figure 4.6 G-R Parameter as a Function of Time – Bottom Layer

It is not clear why the Top layers of the 2011 cores showed such a significant increase in the G′/(η′/G′) and G-R parameters from 2010 followed by a reduction in 2012. The fact that the Bottom layers did not exhibit this behavior would suggest that it was not due to an error in the extraction/recovery or testing procedures.

In Figures 4.3 and 4.5, Cell 24A-Top and Cell 24B-Top exhibit a slight decrease in value from 2012 to 2013. Cells 24C-Top and 24F-Top exhibit an increase as expected from 2012 to 2013. Cell 24D-Top exhibits a slight increase. Cell 24E-Top represents only a single data point, so no conclusions can be drawn regarding its behavior.

In Figures 4.4 and 4.6, the trend is much clearer, showing an increase in value with time. Similar to the Top layers in Figures 4.3 and 4.5, the Bottom layers also show a slight decrease in values for nearly all of the Cells. Once again, if testing error were the consideration, then it would have been expected to see a more random pattern among all the subsections.

One possibility could be any differential aging that occurred from the time the cores were taken and shipped out for testing to the time when the extraction/recovery process occurred. Each year once the cores from Cell 24 arrived at the Asphalt Institute, they were cataloged and stored in the lab storage area until scheduling allowed for their testing. While the lab storage area was temperature-controlled, the cores were not sealed in bags and so were continuing to be exposed to oxidation. When testing on an annual basis, this additional aging could cause data between two years to look similar, although the overall trend would continue in the proper direction. Although this is just a hypothesis, it seems prudent to suggest that future research into the effects of aging of pavements should strongly consider vacuum sealing specimens until such time as they are tested.

For reference, a PG 52-34 asphalt binder was tested after RTFO and PAV aging at 90°C and 100°C. Although this was not the project asphalt binder that was used on Cell 24 it can provide a reference point for how the binder specification mimics aging compared to in-place aging. Figures 4.7 and 4.8 show the aging of the Top and Bottom layers of the Cell 24 subsections as a function of time compared to the aged asphalt binder.

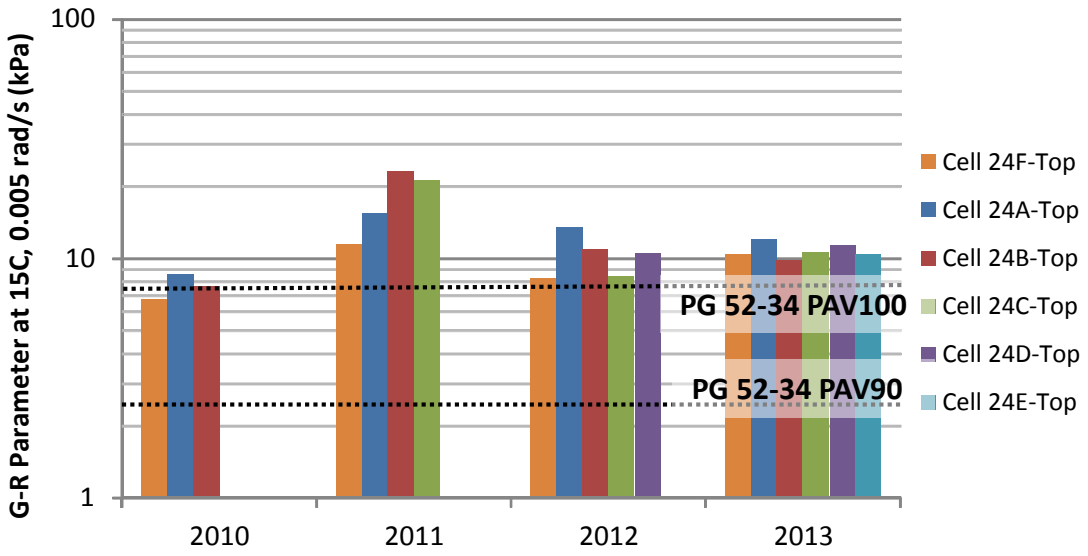

Figure 4.7 G-R Parameter as a Function of Time (with PG 52-34 shown) – Top Layer

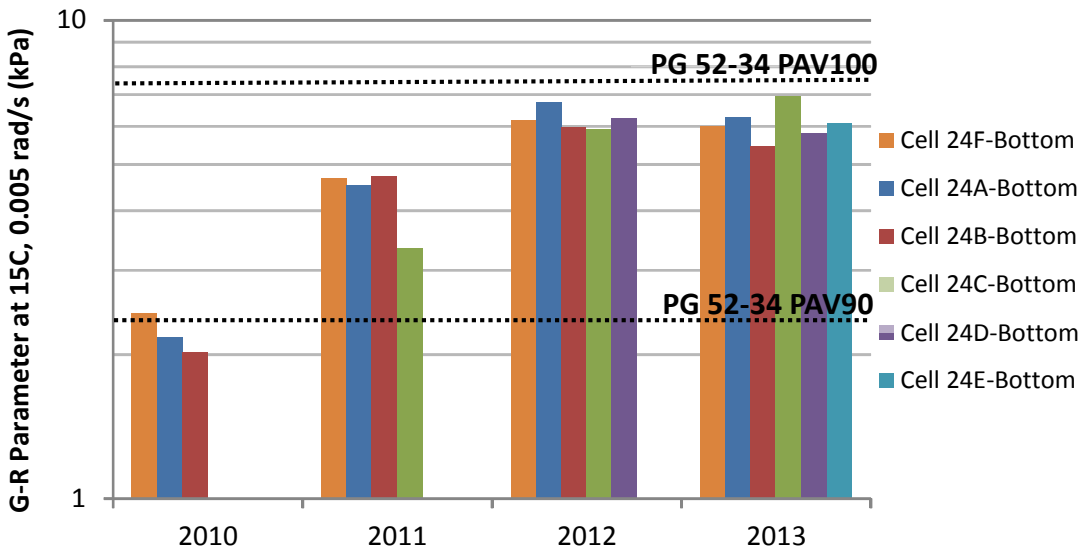

Figure 4.8 G-R Parameter as a Function of Time (with PG 52-34 shown) – Bottom Layer

In Figure 4.7, it can be seen that all of the subsections exceeded the G-R value of the PG 52-34 asphalt binder (PAV100) after 2011. In Figure 4.8, as of 2013, none of the subsections had reached the G-R value of the PG 52-34 asphalt binder (PAV100). While it would have been useful to have tested the PG 58-34 asphalt binder that was actually used in the Cell 24 mixture, Figures 4.7 and 4.8 can at least provide a relative indication of how the asphalt binders in the Cell 24 subsections have aged compared to a control.

Another way of looking at the data is in a Black Space diagram as described in Chapter 2. In this representation, the relationship between complex shear modulus (G*) and phase angle (δ) can be seen. From previous research it can be seen that aging progresses along a path from lower stiffness and higher phase angle to higher stiffness and lower phase angle. Figure 4.9 shows a Black Space representation of the data from 2010-2013 for the Top and Bottom layers of Cell 24F. For reference, curves are shown where the G-R parameter is equal to 180 and 600 kPa at 15°C and 0.005 rad/s. These values correspond to the recommended cracking limits suggested by the Texas A&M research [4].

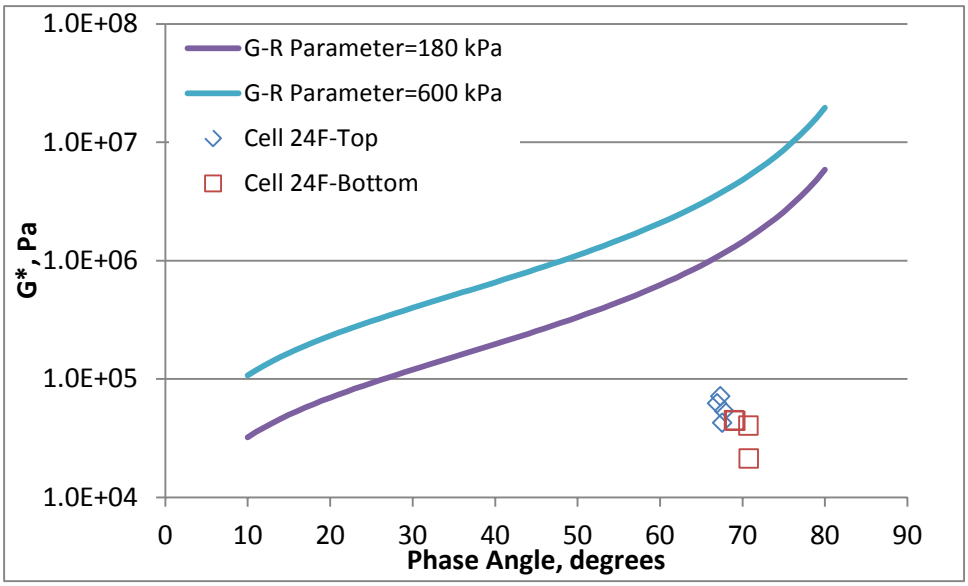

Figure 4.9 Black Space Representation of Cell 24F (Top and Bottom Layers) with Time

The data in Figure 4.9 shows the difference in the aging of the Top and Bottom layers. In Figure 4.10, the data from the PG 52-34 asphalt binder is added. The three data points for the PG 52-34 data represent (from lower right to upper left) the RTFO, PAV90, and PAV100 aging conditions.

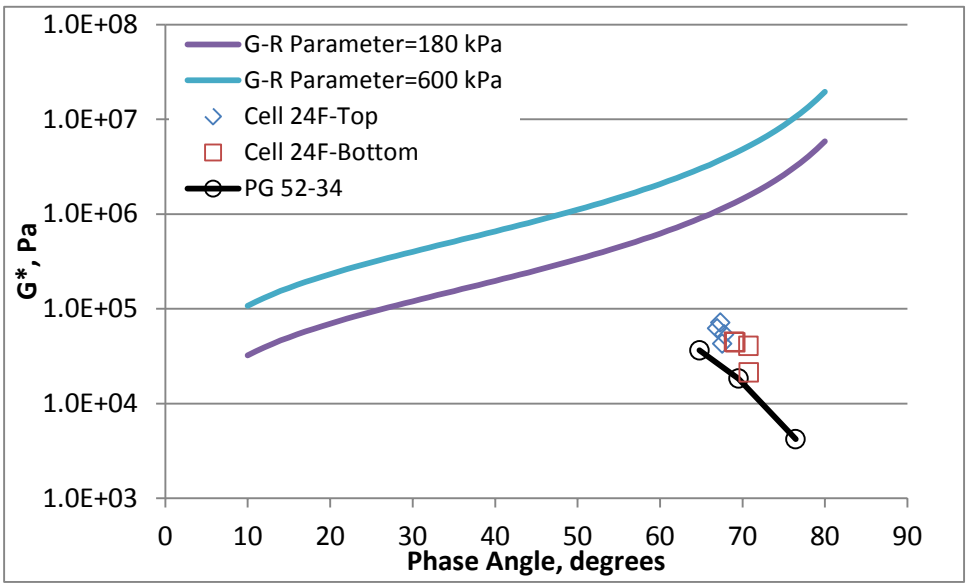

Figure 4.10 Black Space Representation of Cell 24F (Top and Bottom Layers) with Time – PG 52-34 Data Added

With only four data points representing a relatively short time period (4 years) it is difficult to tell how the aging will ultimately proceed. Aging could proceed following a linear path as demonstrated by Line A, or in a curvilinear path as demonstrated by Curve B in Figure 4.11. The

path of the PG 52-34 asphalt binder in Figure 4.10 provides some indication as to the possible aging path for the subsection layers, but further testing with time would be needed to see how the aging actually progresses. The most likely response would be somewhere between the two paths represented by "A" and "B" in Figure 4.11.

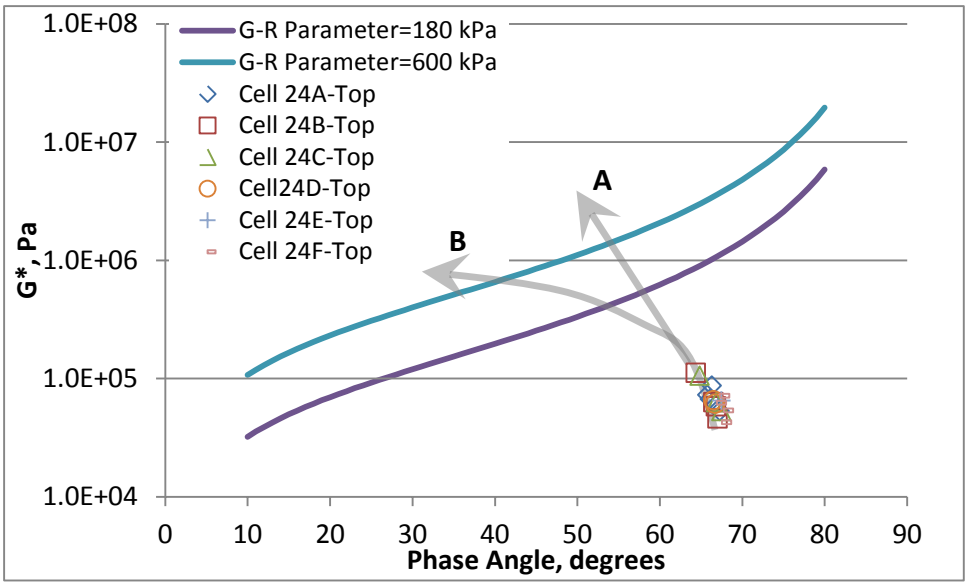

Figure 4.11 Black Space Representation of All Subsections (Top Layers only) with Time – Possible Aging Paths

In addition to the temperature-frequency sweep testing, the Linear Amplitude Sweep (LAS) test was conducted on the recovered asphalt binders at 16°C – the expected intermediate temperature grade for a PG 58-34 climate. Results are shown in Tables 4.5-4.8 for each year from 2010 to 2013.

Table 4.5 2010 MnROAD Recovered Asphalt Binder – LAS at 16°C

			LAS Parameter		N_f	
Cell	**Lane**	**Layer**	**A**	**B**	**γ = 2%**	**γ = 5%**
24A	Non-Travel	Top	1.900E+05	-3.537	16,369	640
		Mid	1.624E+05	-3.203	17,633	937
		Bot	1.604E+05	-3.159	17,966	994
24B	Non-Travel	Top	1.514E+05	-3.574	12,706	480
		Mid	1.156E+05	-3.273	11,954	596
		Bot	1.079E+05	-3.196	11,777	630
24F	Non-Travel	Top	1.333E+05	-3.475	11,981	496
		Mid	1.201E+05	-3.168	13,362	733
		Bot	1.124E+05	-3.163	12,545	691

Table 4.6 2011 MnROAD Recovered Asphalt Binder – LAS at 16°C

			LAS Parameter		N_f	
Cell	**Lane**	**Layer**	**A**	**B**	**γ = 2%**	**γ = 5%**
24A	Non-Travel	Top	2.666E+06	-3.725	201,555	6,637
		Mid	1.350E+06	-3.310	136,155	6,562
		Bot	3.731E+05	-3.279	38,444	1,906
24B	Non-Travel	Top	6.139E+05	-3.886	41,528	1,180
		Mid	1.346E+06	-3.310	135,758	6,543
		Bot	8.650E+05	-3.279	89,120	4,418
24C	Non-Travel	Top	6.105E+05	-3.852	42,293	1,240
		Mid	5.745E+05	-3.270	59,580	2,979
		Bot	5.301E+05	-3.234	56,322	2,908
24F	Non-Travel	Top	2.129E+06	-3.648	169,879	6,006
		Mid	3.808E+05	-3.289	38,974	1,915
		Bot	6.322E+05	-3.315	63,501	3,044

Table 4.7 2012 MnROAD Recovered Asphalt Binder – LAS at 16°C

			LAS Parameter		N_f	
Cell	**Lane**	**Layer**	**A**	**B**	**γ = 2%**	**γ = 5%**
24A	Non-Travel	Top	2.603E+06	-3.688	201,983	6,882
		Mid	1.838E+06	-3.559	155,951	5,978
		Bot	5.749E+05	-3.431	53,309	2,299
24B	Non-Travel	Top	2.218E+06	-3.625	179,781	6,489
		Mid	1.163E+06	-3.534	100,413	3,938
		Bot	6.009E+05	-3.453	54,873	2,319
24C	Non-Travel	Top	1.262E+06	-3.547	107,997	4,187
		Mid	1.529E+06	-3.491	136,058	5,555
		Bot	1.755E+06	-3.409	165,232	7,272
24D	Non-Travel	Top	2.244E+06	-3.629	181,313	6,520
		Mid	1.472E+06	-3.486	131,375	5,388
		Bot	5.728E+05	-3.456	52,189	2,199
24F	Non-Travel	Top	9.613E+05	-3.458	87,448	3,677
		Mid	8.135E+05	-3.387	77,751	3,490
		Bot	4.808E+05	-3.362	46,773	2,149

Table 4.8 2013 MnROAD Recovered Asphalt Binder – LAS at 16°C

			LAS Parameter		N_f	
Cell	**Lane**	**Layer**	**A**	**B**	**γ = 2%**	**γ = 5%**
24A	Non-Travel	Top	2.337E+06	-3.635	188,052	6,724
		Mid	2.149E+06	-3.618	174,939	6,353
		Bot	8.129E+05	-3.380	78,070	3,526
24B	Non-Travel	Top	6.608E+05	-3.519	57,628	2,292
		Mid	4.355E+05	-3.524	37,872	1,500
		Bot	1.376E+06	-3.458	125,150	5,262
24C	Non-Travel	Top	2.231E+06	-3.625	180,826	6,526
		Mid	1.606E+06	-3.520	139,955	5,560
		Bot	1.377E+06	-3.468	124,441	5,188
24D	Non-Travel	Top	1.596E+06	-3.641	127,937	4,552
		Mid	7.532E+05	-3.546	64,495	2,504
		Bot	1.545E+06	-3.499	136,668	5,538
24E	Non-Travel	Top	2.313E+06	-3.638	185,798	6,629
		Mid	1.746E+06	-3.542	149,890	5,837
		Bot	1.621E+06	-3.521	141,239	5,610
24F	Non-Travel	Top	2.181E+06	-3.608	178,879	6,558
		Mid	1.147E+06	-3.541	98,523	3,840
		Bot	5.811E+05	-3.431	53,901	2,325

The LAS "A" parameter in Table 4.5 for the 2010 cores is generally lower than the values in subsequent years, which results in the N_f values being lower in 2010 than in subsequent years. This difference in values may have been caused by a change in the analysis technique used for interpreting the LAS data.

Figure 4.12(a)-4.12(d) shows the absolute value of the LAS slope ("B") for each subsection, layer, and year.

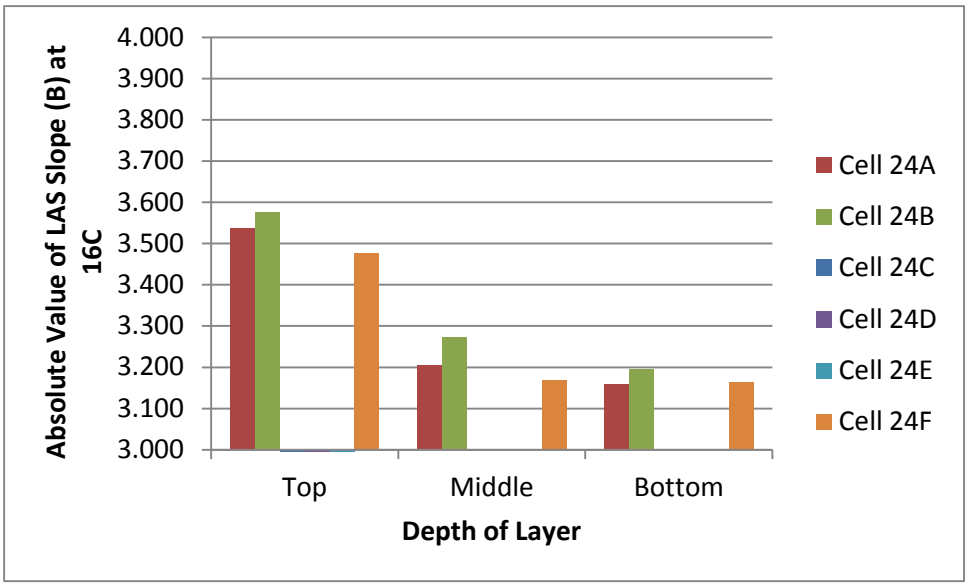

Figure 4.12(a) Absolute Value of LAS Slope (B) as a Function of Subsection and Layer – 2010

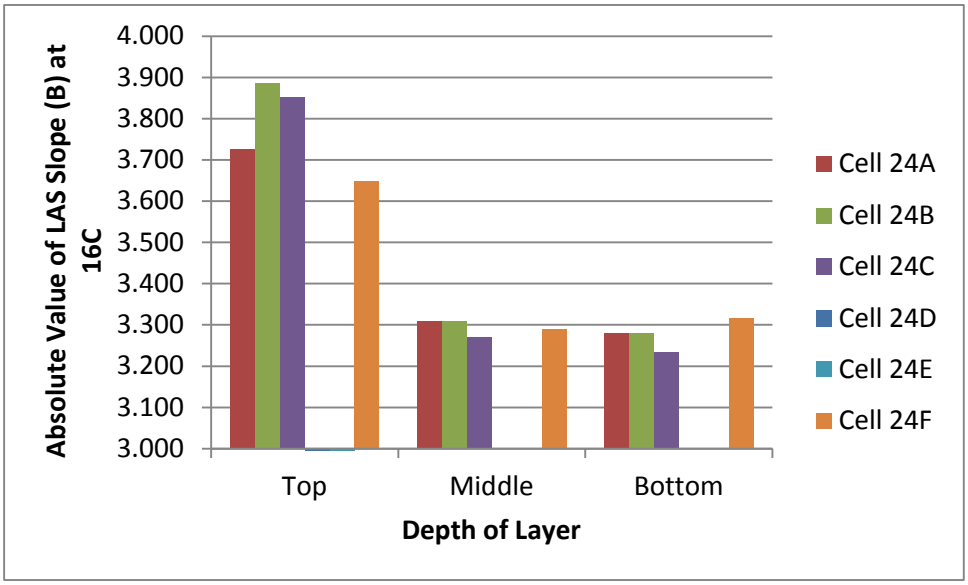

Figure 4.12(b) Absolute Value of LAS Slope (B) as a Function of Subsection and Layer – 2011

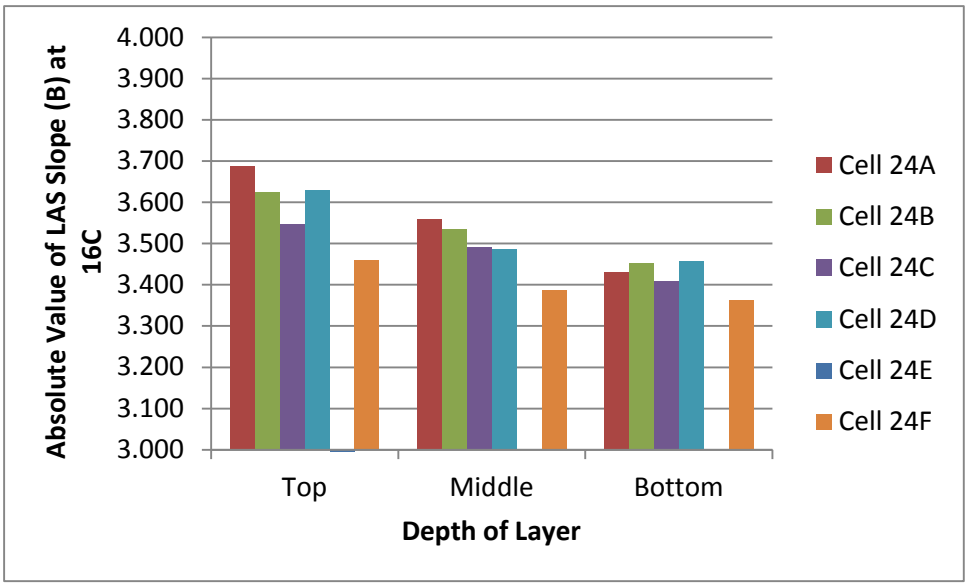

Figure 4.12(c) Absolute Value of LAS Slope (B) as a Function of Subsection and Layer – 2012

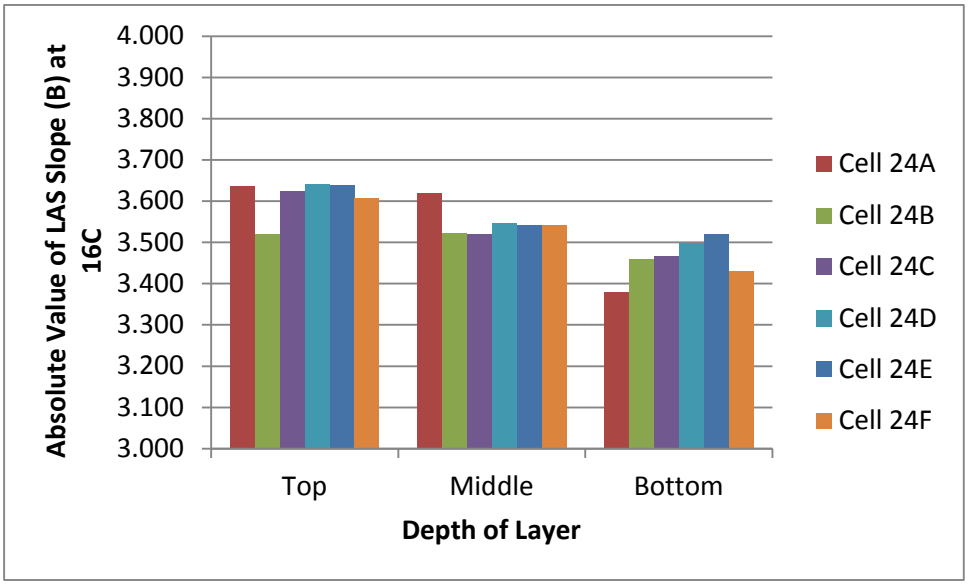

Figure 4.12(d) Absolute Value of LAS Slope (B) as a Function of Subsection and Layer – 2013

Figure 4.12 - Absolute Value of LAS Slope (B) as a Function of Subsection and Layer, 2010 - 2013

Similar to the mastercurve data, the LAS slope in Figures 4.12(a)-4.12(d) is generally higher for the Top layers than the Middle and Bottom layers for any given subsection and year. Also, similar to the mastercurve parameters, the LAS slope is significantly higher for the Top layers of all subsections in 2011 than in subsequent years. This can be seen in Figures 4.13 and 4.14 which show how the value of the LAS slope changes with time for the Top and Bottom layers.

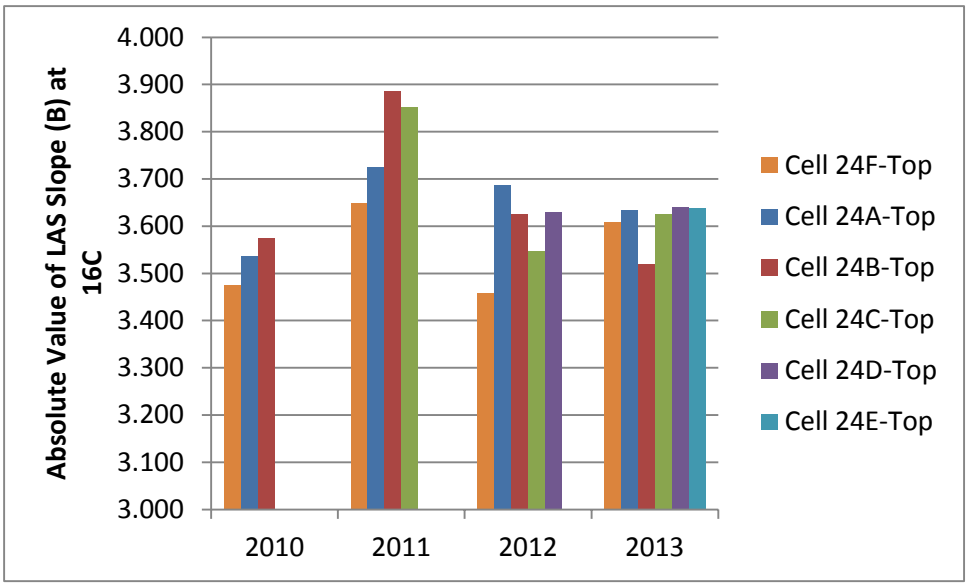

Figure 4.13 LAS Slope as a Function of Time – Top Layer

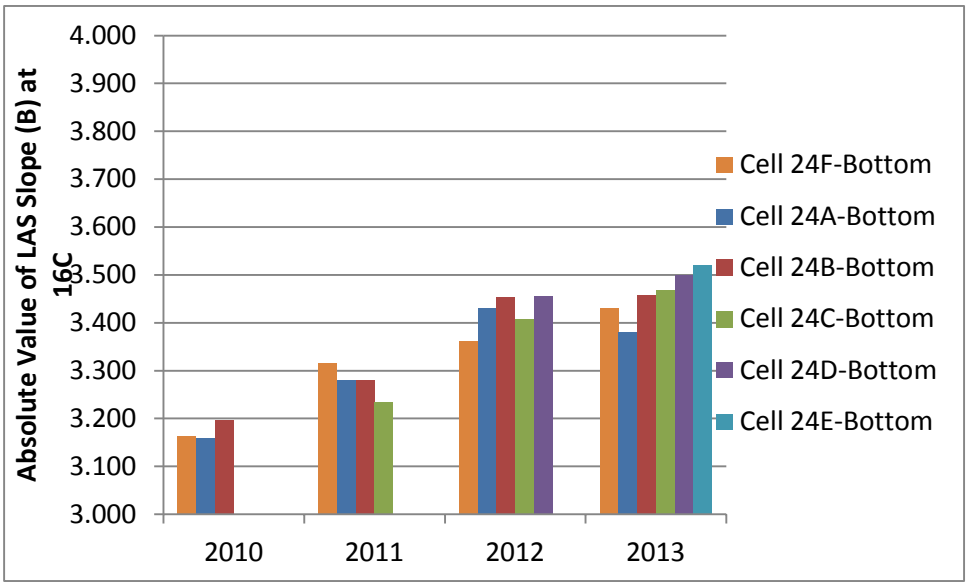

Figure 4.14 LAS Slope as a Function of Time – Bottom Layer

As in Figures 4.3 and 4.5, Cells 24A and 24B show a decrease in LAS Slope from 2012 to 2013 in Figure 4.13 while Cells 24C, 24D, and 24F show an increase. Differential aging before testing or possibly testing error could be responsible. In Figure 4.14, the LAS slope shows an increase with time for all layers, as expected.

If we consider just the data from 2013 shown in Figure 4.12(d), a couple of observations can be made:

- The Top layers of Cells 24A, 24C, 24D, and 24E have essentially the same values of LAS slope as Cell 24F. Since Cell 24A was sealed with a different emulsion (CSS-1 instead of CRS-2P) and at a different application rate than the other subsections it would not be unexpected that the behavior of Cell 24A could be different.
- If we discount Cell 24A from the interpretation of the data in Figure 4.12(d), it can be stated that after five years of service, the subsection that was sealed one year after construction had a lower LAS slope – and less apparent aging – in the Top layer (closest to the surface) than the sections sealed two or more years after construction. Although it is difficult to see because of the log scale, this observation can be corroborated by the data in Figures 4.1(d) and 4.2(d).

4.1.2 Mixture Testing Results

Indirect Tensile Creep testing was conducted on triplicate specimens at -20, -30, and -40°C. Data from the tests were used to generate creep compliance curve parameters. One specimen was sacrificed to determine Indirect Tensile Strength so that the critical cracking temperature could be determined. Data on indirect tensile testing is shown for each year from 2010-2013 in Tables 4.9-4.12.

Table 4.9 2010 MnROAD Mixture Test Results – Indirect Tensile

			Creep					
			Curve Coefficients			Compl.		
Cell	**Lane**	**Layer**	**D_0**	**D_1**	**m**	**-34°C, 7200 s**	**Strength (MPa)**	**Critical Cracking Temp, °C**
24A	Non-Travel	Top 25	2.25E-05	2.65E-06	0.256	7.69E-05	3.63	-36.0
		Bot 25	n/a	n/a	n/a	n/a	n/a	n/a
24B	Non-Travel	Top 25	2.36E-05	1.72E-06	0.294	8.14E-05	3.40	-34.0
		Bot 25	n/a	n/a	n/a	n/a	n/a	n/a
24F	Non-Travel	Top 25	2.46E-05	3.46E-06	0.253	9.71E-05	3.51	-37.5
		Bot 25	n/a	n/a	n/a	n/a	n/a	n/a

"n/a" means that test results are not available
"Top 25: refers to the topmost layer to a depth of 25 millimeters from the surface
"Bot 25" refers to the bottom layer that is 25 millimeters thick and starts 25 millimeters from the Top layer

Table 4.10 2011 MnROAD Mixture Test Results – Indirect Tensile

			Creep					
			Curve Coefficients			Compl.		
Cell	**Lane**	**Layer**	**D_0**	**D_1**	**m**	**-34°C, 7200 s**	**Strength (MPa)**	**Critical Cracking Temp, °C**
24A	Non-Travel	Top 25	1.74E-05	3.79E-06	0.221	6.88E-05	3.32	-31.9
		Bot 25	1.67E-05	3.63E-06	0.264	7.65E-05	3.70	-34.4
24B	Non-Travel	Top 25	2.18E-05	2.75E-06	0.280	8.83E-05	3.57	-36.2
		Bot 25	1.90E-05	2.72E-06	0.282	7.96E-05	3.12	-31.6
24C	Non-Travel	Top 25	1.70E-05	3.27E-06	0.263	7.82E-05	3.88	-33.5
		Bot 25	1.70E-05	3.67E-06	0.248	7.38E-05	3.96	-34.8
24F	Non-Travel	Top 25	1.49E-05	4.59E-06	0.225	7.35E-05	2.87	-30.9
		Bot 25	1.55E-05	3.46E-06	0.253	7.38E-05	2.94	-31.2

"n/a" means that test results are not available
"Top 25: refers to the topmost layer to a depth of 25 millimeters from the surface
"Bot 25" refers to the bottom layer that is 25 millimeters thick and starts 25 millimeters from the Top layer

Table 4.11 2012 MnROAD Mixture Test Results – Indirect Tensile

			Creep					
			Curve Coefficients			Compl.		
Cell	**Lane**	**Layer**	**D_0**	**D_1**	**m**	**-34°C, 7200 s**	**Strength (MPa)**	**Critical Cracking Temp, °C**
24A	Non-Travel	Top 25	2.30E-05	4.85E-06	0.246	9.46E-05	3.16	-35.7
		Bot 25	2.39E-05	3.55E-06	0.305	9.67E-05	3.35	-37.7
24B	Non-Travel	Top 25	2.15E-05	5.54E-06	0.255	9.97E-05	3.28	-37.4
		Bot 25	2.28E-05	4.44E-06	0.253	9.24E-05	2.79	-34.7
24C	Non-Travel	Top 25	2.19E-05	3.75E-06	0.268	8.46E-05	3.47	-37.1
		Bot 25	1.93E-05	2.73E-06	0.301	8.66E-05	4.01	-38.5
24D	Non-Travel	Top 25	1.73E-05	4.51E-06	0.233	7.92E-05	3.38	-34.2
		Bot 25	2.58E-05	3.05E-06	0.312	1.03E-04	3.46	-39.1
24F	Non-Travel	Top 25	2.38E-05	2.85E-06	0.313	1.06E-04	3.07	-37.3
		Bot 25	1.80E-05	4.42E-06	0.239	8.14E-05	3.24	-34.4

"n/a" means that test results are not available
"Top 25: refers to the topmost layer to a depth of 25 millimeters from the surface
"Bot 25" refers to the bottom layer that is 25 millimeters thick and starts 25 millimeters from the Top layer

Table 4.12 2013 MnROAD Mixture Test Results – Indirect Tensile

			Creep					
			Curve Coefficients			Compl.		
Cell	**Lane**	**Layer**	**D_0**	**D_1**	**m**	**-34°C, 7200 s**	**Strength (MPa)**	**Critical Cracking Temp, °C**
24A	Non-Travel	Top 25	1.64E-05	4.52E-06	0.235	7.55E-05	2.76	-30.3
		Bot 25	1.73E-05	3.63E-06	0.263	7.69E-05	3.45	-34.4
24B	Non-Travel	Top 25	1.86E-05	3.86E-06	0.280	9.43E-05	3.13	-35.2
		Bot 25	1.41E-05	5.04E-06	0.241	8.15E-05	4.26	-37.3
24C	Non-Travel	Top 25	1.60E-05	3.05E-06	0.265	7.73E-05	3.21	-33.3
		Bot 25	1.33E-05	4.47E-06	0.219	7.03E-05	3.79	-33.9
24D	Non-Travel	Top 25	1.60E-05	2.80E-06	0.254	6.78E-05	3.08	-30.9
		Bot 25	1.54E-05	3.22E-06	0.253	7.08E-05	4.24	-35.2
24E	Non-Travel	Top 25	1.77E-05	3.24E-06	0.274	7.72E-05	3.36	-34.0
		Bot 25	1.48E-05	3.19E-06	0.257	7.04E-05	3.55	-33.4
24F	Non-Travel	Top 25	1.45E-05	4.47E-06	0.233	7.41E-05	2.94	-32.0
		Bot 25	1.48E-05	4.59E-06	0.230	7.37E-05	3.42	-33.5

"n/a" means that test results are not available
"Top 25: refers to the topmost layer to a depth of 25 millimeters from the surface
"Bot 25" refers to the bottom layer that is 25 millimeters thick and starts 25 millimeters from the Top layer

The data in Tables 4.9-4.12 show an apparent trend in that the Indirect Tensile Strength at -30°C appears to decrease with time for the Top layers of any given subsection and year (Figure 4.15). This trend does not appear for the Bottom layers as shown in Figure 4.16.

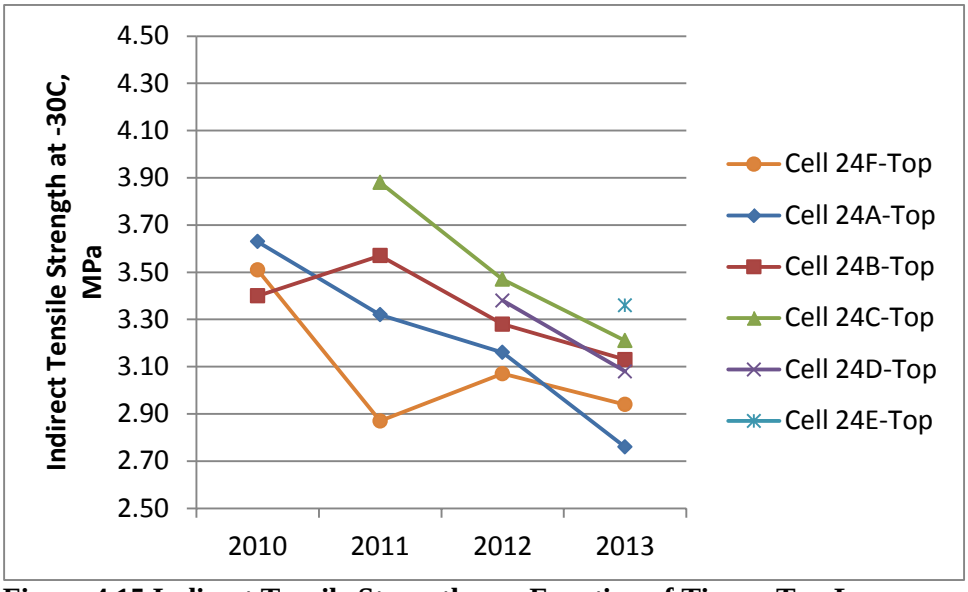

Figure 4.15 Indirect Tensile Strength as a Function of Time – Top Layer

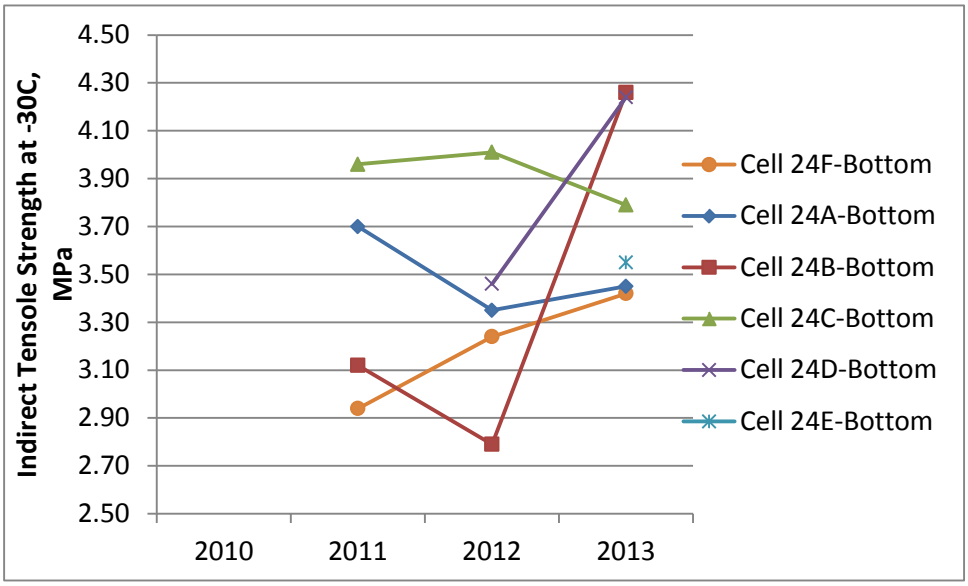

Figure 4.16 Indirect Tensile Strength as a Function of Time – Bottom Layer

The original Superpave models to estimate low temperature cracking performance incorporated several calculations into the Pavement Distress Model. As part of the Pavement Distress Model, the Crack Depth (Fracture) Model uses the Paris law for crack propagation to simulate the change in depth of a local crack subjected to a given cooling cycle [33]:

$$\Delta C = A(\Delta K)^n \qquad \text{[Eq. 8]}$$

where, ΔC is the change in crack depth due to cooling,
ΔK is the change in stress intensity factor due to cooling, and
A and n are coefficients related to other material properties.

Past experimental studies have indicated that the material property coefficients, A and n, can be related to the slope of the creep compliance curve and the tensile strength of the mix. The A coefficient can be estimated using the following relationship [33]:

$$\log A = 4.389 - 2.52*\log(k*S_t*n) \qquad \text{[Eq. 9]}$$

where,

S_t is the asphalt concrete tensile strength (psi);
k is a field calibration coefficient, determined to be 10,000; and
n is a material coefficient related to the slope of the creep compliance curve.

Since the term "$2.52*\log(k*S_t*n)$" will always be greater than 4.389 in Equation 9, then it can be seen that as the tensile strength decreases the A coefficient increases – meaning that the change in crack depth due to cooling will increase assuming all other factors stay the same. In other words, a decrease in tensile strength will lead to greater crack depth propagation.

The material coefficient n is a function of the creep compliance slope and can be estimated as follows [33]:

$$n = 0.8*[1 + (1/m)] \quad \text{[Eq. 10]}$$

A lower value of creep compliance slope, m, will cause the value of the "n" coefficient to increase. While this has the effect of decreasing the A coefficient some (meaning lower cracking propagation), it has the greater effect of increasing the exponent in Equation 8 which will increase cracking propagation.

Figure 4.17 and 4.18 illustrates the creep compliance slope, m, as a function of time for the Top layer.

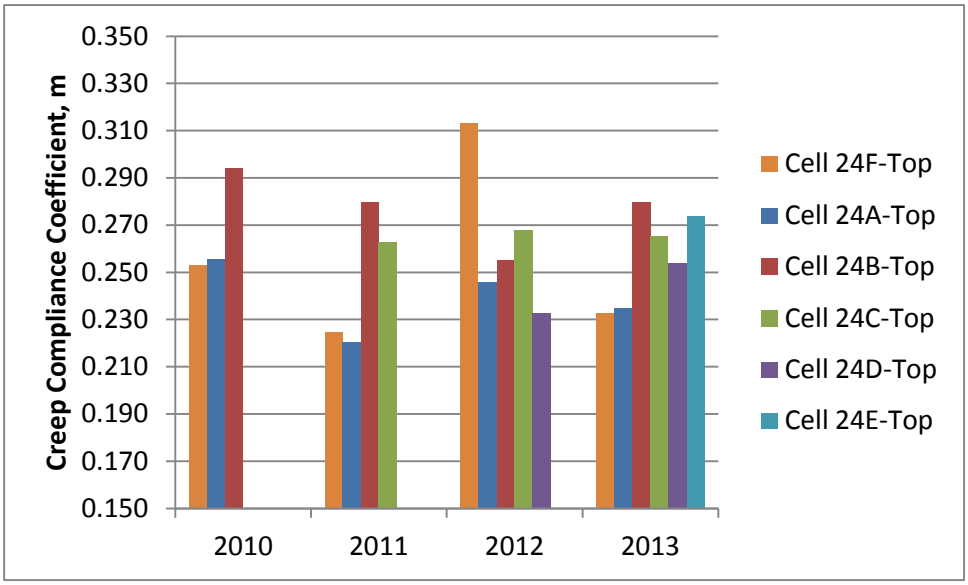

Figure 4.17 Creep Compliance Slope (m) as a Function of Time – Top Layer

Although there is some scatter in the data in Figure 4.17, the creep compliance slope generally is lowest for Cell 24F, with Cell 24A closely matching it, and generally highest for Cell 24B. The exception is in 2012 where the creep compliance slope of Cell 24F is significantly higher than any other subsection/year. If samples existed, it would have been good to verify the results as they appear to be in error given the nature of the remainder of the data. Once again, the concern with Cell 24A was that its behavior could be different since a different emulsion and application rate was used than was used for any other subsection.

The creep compliance slope, m, and indirect tensile strength have an impact on the critical cracking temperature determined using an analysis procedure by Christensen [34] which was based on work by Roque and Hiltunen during SHRP [35]. Critical cracking temperature for the Top layers of the subsections is shown as a function of time in Figure 4.18.

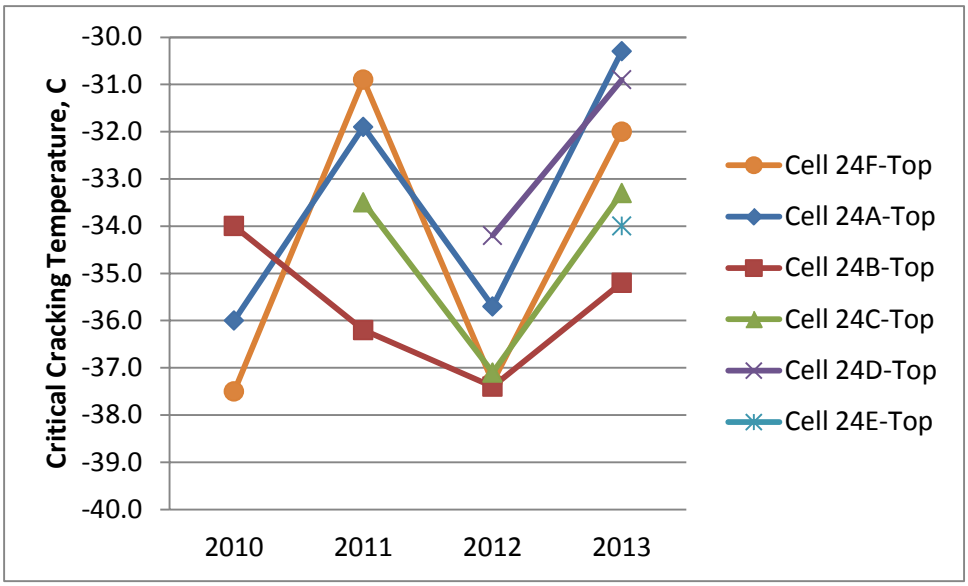

Figure 4.18 Critical Cracking Temperature as a Function of Time – Top Layer

As with the creep compliance data, it is difficult to see a trend on a year-by-year basis. What can be seen is that starting in 2011, Cell 24B has the lowest critical cracking temperature each year followed by Cell 24C. The low temperature for Cell 24F in 2012 is no doubt related to the relatively high creep compliance slope as seen in Figure 4.17.

After the three test specimens from each subsection/year/layer were tested using indirect tensile creep, the gage points were removed and the specimens were further processed to turn them into specimens suitable for testing following the Disk-Shaped Compact Tension, DC(T), test as described in ASTM D7313. For each subsection/year/layer, three specimens were tested at -24°C and the results averaged to determine fracture energy for the subsection/layer/year. The results of the DC(T) testing are shown in Table 4.13 and Figure 4.19.

Table 4.13 2010-13 MnROAD Mixture Test Results – DC(T)

			2010		2011		2012		2013	
			Fracture Energy		Fracture Energy		Fracture Energy		Fracture Energy	
Cell	**Lane**	**Layer**	**J/m^2**	**CV**	**J/m^2**	**CV**	**J/m^2**	**CV**	**J/m^2**	**CV**
24A	Non-Travel	Top 25	750.1	5%	502.1	31%	380.7	6%	480.0	26%
		Bot 25			661.0	7%	376.4	11%	429.1	13%
24B	Non-Travel	Top 25	874.3	n/a	424.4	5%	396.3	3%	565.7	19%
		Bot 25			468.0	12%	448.7	12%	413.2	11%
24C	Non-Travel	Top 25			526.6	13%	450.2	27%	482.4	19%
		Bot 25			454.6	29%	426.7	49%	495.4	24%
24D	Non-Travel	Top 25					342.3	14%	491.3	23%
		Bot 25					377.9	20%	490.4	9%
24E	Non-Travel	Top 25							497.9	6%
		Bot 25							566.8	27%
24F	Non-Travel	Top 25	619.9	n/a	480.6	20%	439.7	4%	367.2	13%
		Bot 25			426.2	8%	444.3	18%	527.6	9%

"n/a" means that test results are not available
"Top 25: refers to the topmost layer to a depth of 25 millimeters from the surface
"Bot 25" refers to the bottom layer that is 25 millimeters thick and starts 25 millimeters from the Top layer

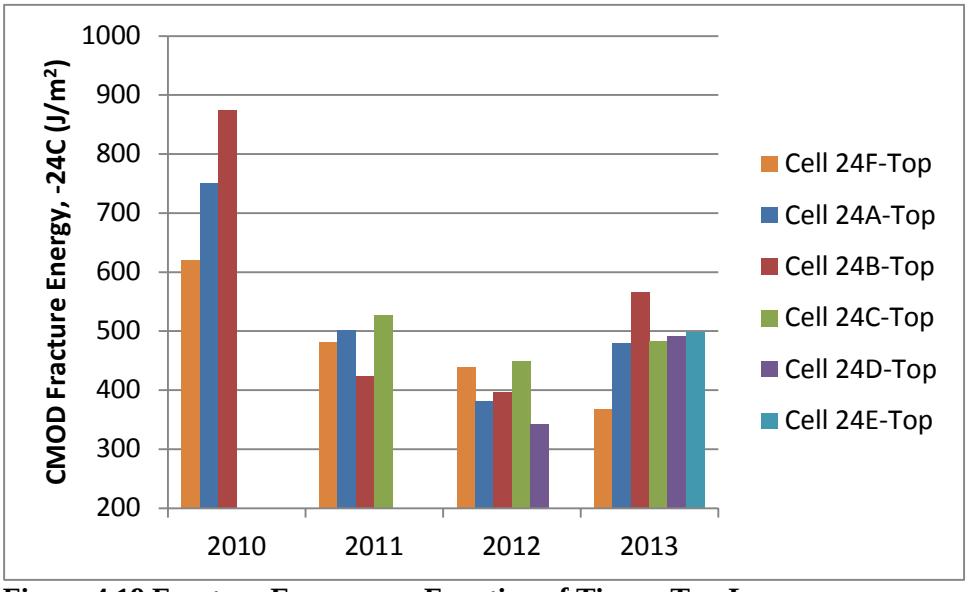

Figure 4.19 Fracture Energy as a Function of Time – Top Layer

The data in Table 4.13 and Figure 4.19 indicates a general decrease in fracture energy with time from 2010-2012. In 2013, the fracture energy values increase for every subsection except Cell 24F. Assuming a constant specimen density, as would likely be encountered in the Non-Travel lane, then fracture energy should be expected to decrease with time. The anomalous behavior for

most of the subsections in 2013 cannot be readily explained. Additional testing would be needed to validate the results.

If only Cell 24F is considered, it can be seen that the fracture energy decreases consistently with time. This is illustrated in Figure 4.20.

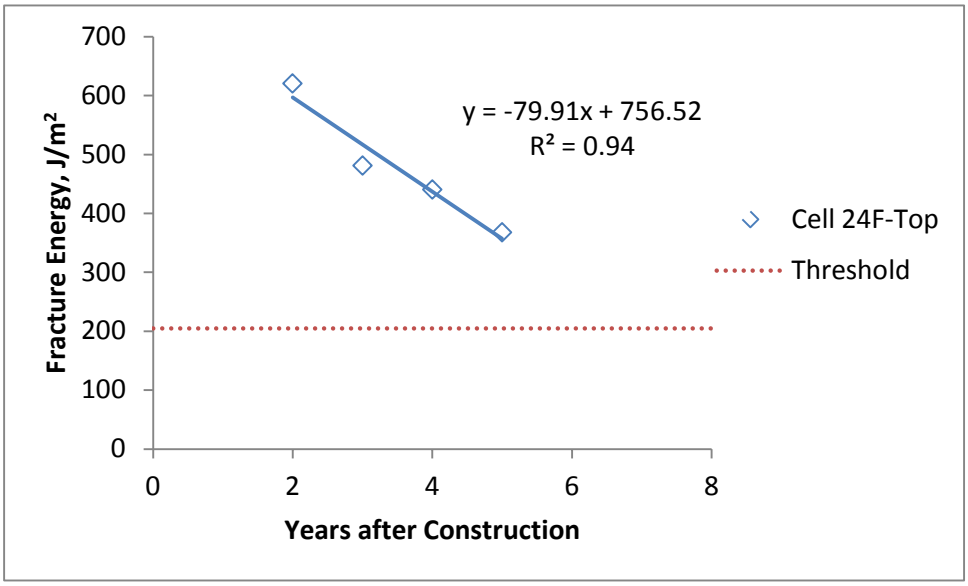

Figure 4.20 Fracture Energy as a Function of Time – Cell 24F Top Layer

If the progression of fracture energy with time is assumed to follow a linear path, as shown in Figure 4.20, then it can be expected that the fracture energy will cross the threshold value of 205 J/m^2 at seven years after construction (2015). This is near the upper end of the limit of time before users typically consider chip seals or other pavement preservation treatments.

The 205 J/m^2 threshold limit as shown in Figure 4.20 is derived from the 350 J/m^2 limit that was developed for specimens that are 50 millimeters thick [36]. Since the test specimens used in this study were only 25 millimeters thick, it was necessary to adjust the fracture energy threshold by a factor of 1.7 to account for the reduced specimen size[36].

4.1.3 Comparison of Binder and Mix Testing

It is difficult to directly compare binder to mixture test results since the layers are different dimensions. For instance, the Top layer for binder testing consists of material from the surface to a depth of 12.5 millimeters. The Middle layer for binder testing consists of material from a depth of 17.5 millimeters to 30 millimeters. The Bottom layer for binder testing consists of material from a depth of 35 millimeters to 47.5 millimeters. By contrast, the Top layer for mixture testing consists of material from the surface to a depth of 25 millimeters. The Bottom layer for mixture testing consists of material from a depth of 30 millimeters to 55 millimeters. Thus, the Top layer

for mixture testing really includes the Top layer for binder testing and most of the Middle layer for binder testing. The Bottom layer for mixture testing includes just the Bottom layer for binder testing, but also includes some material that is even deeper in the pavement. This is illustrated in Figure 4.21.

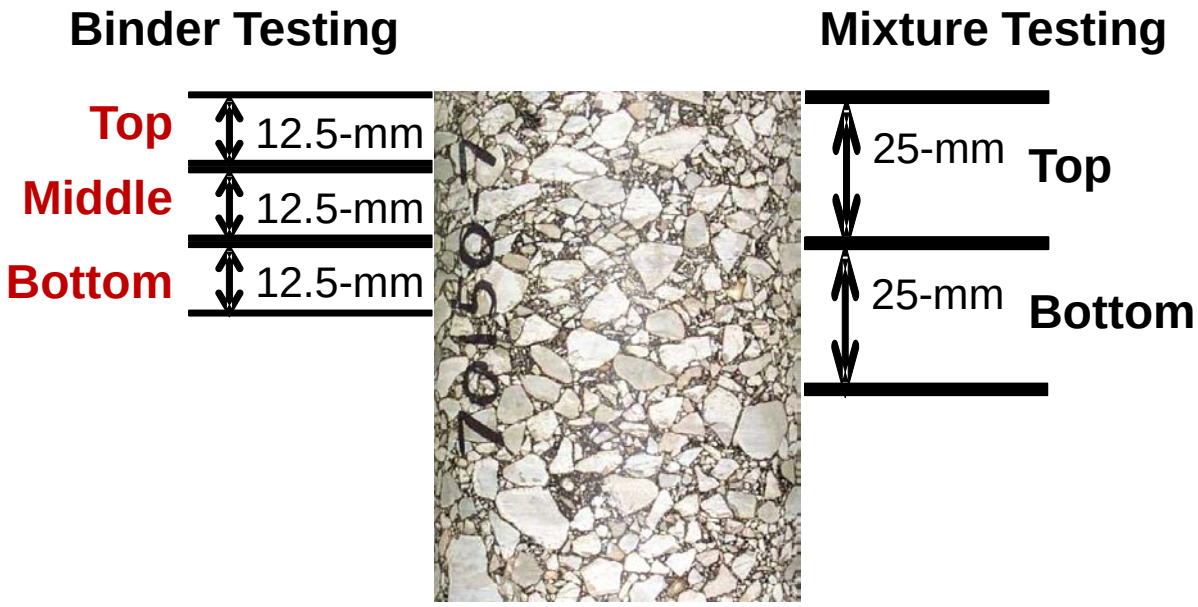

Figure 4.21 Layer Designations for Binder and Mixture Testing

Although the Top layers are not quite the same, it was still desired to compare the binder and mixture results to see if there was any trend relating the two. This data is illustrated in Figures 4.22 – 4.27 comparing DC(T) Fracture Energy, Indirect Tensile Strength, and Critical Cracking Temperature to the LAS Slope (B) and G-R Parameter.

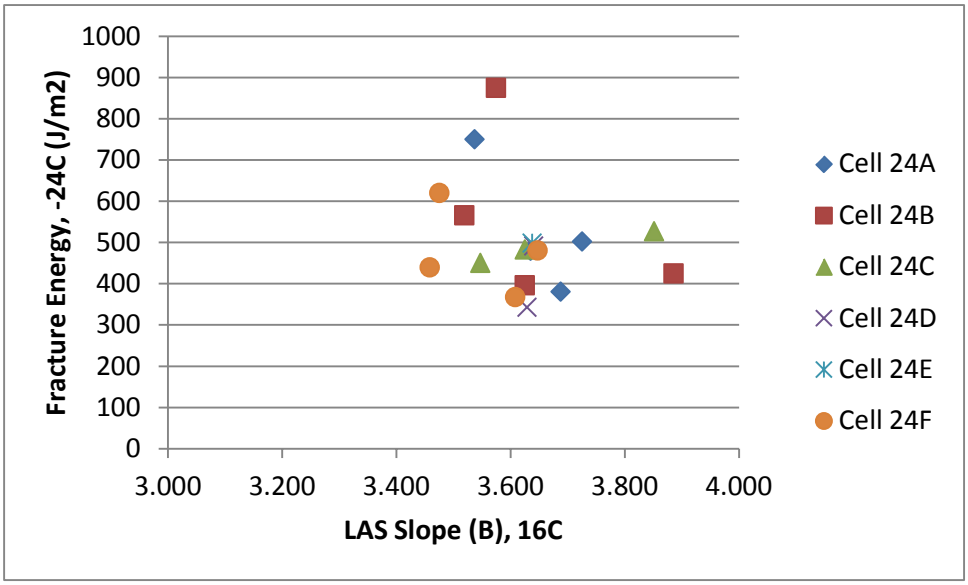

Figure 4.22 Comparison of DC(T) Fracture Energy at -24°C to LAS Slope (B) at 16°C

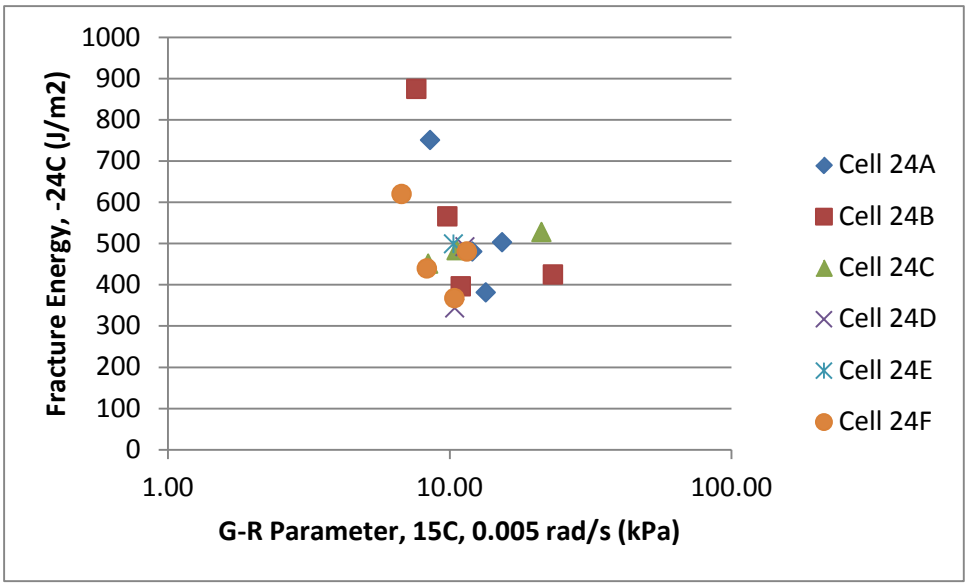

Figure 4.23 Comparison of DC(T) Fracture Energy at -24°C to G-R Parameter at 15°C, 0.005 rad/s

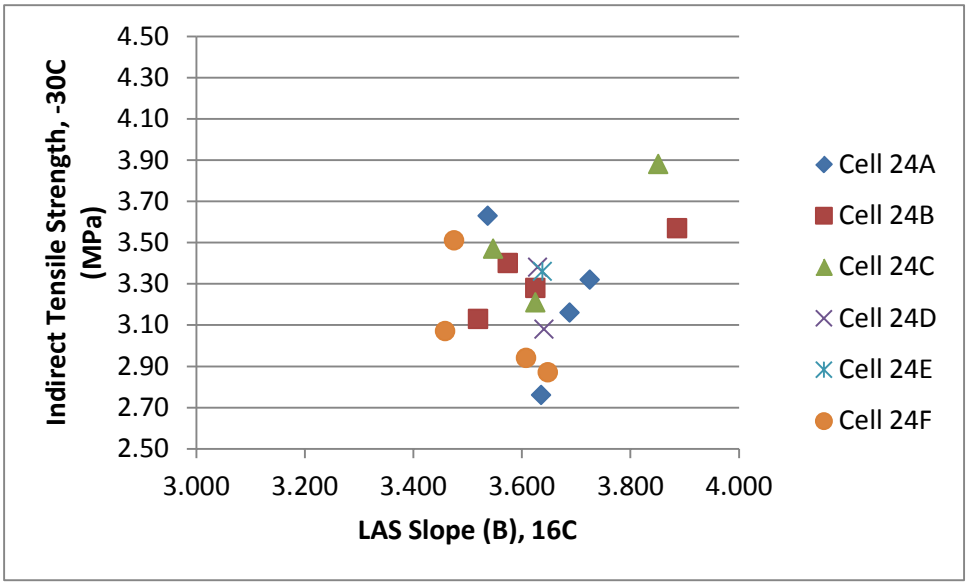

Figure 4.24 Comparison of Indirect Tensile Strength at -30°C to LAS Slope (B) at 16°C

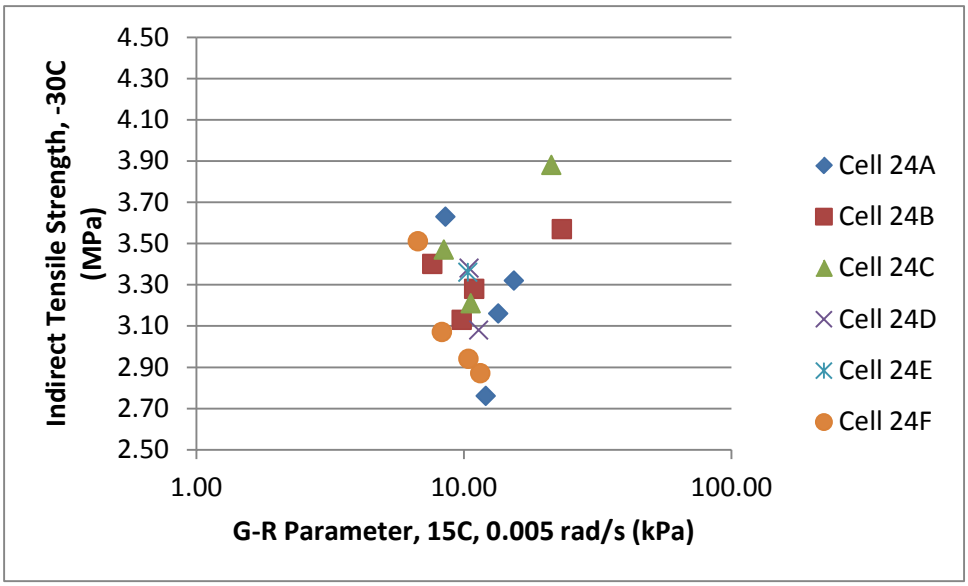

Figure 4.25 Comparison of Indirect Tensile Strength at -30°C to G-R Parameter at 15°C, 0.005 rad/s

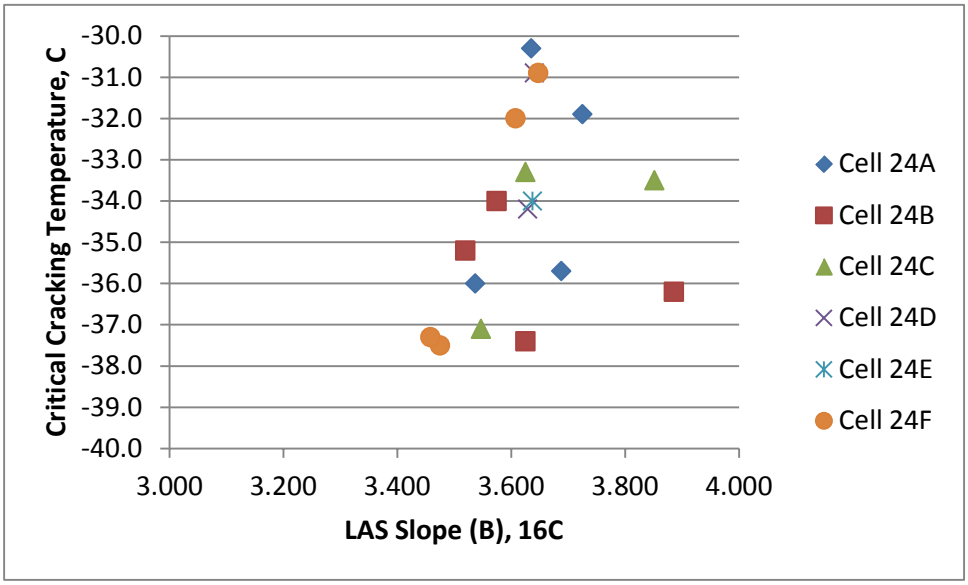

Figure 4.26 Comparison of Critical Cracking Temperature to LAS Slope (B) at 16°C

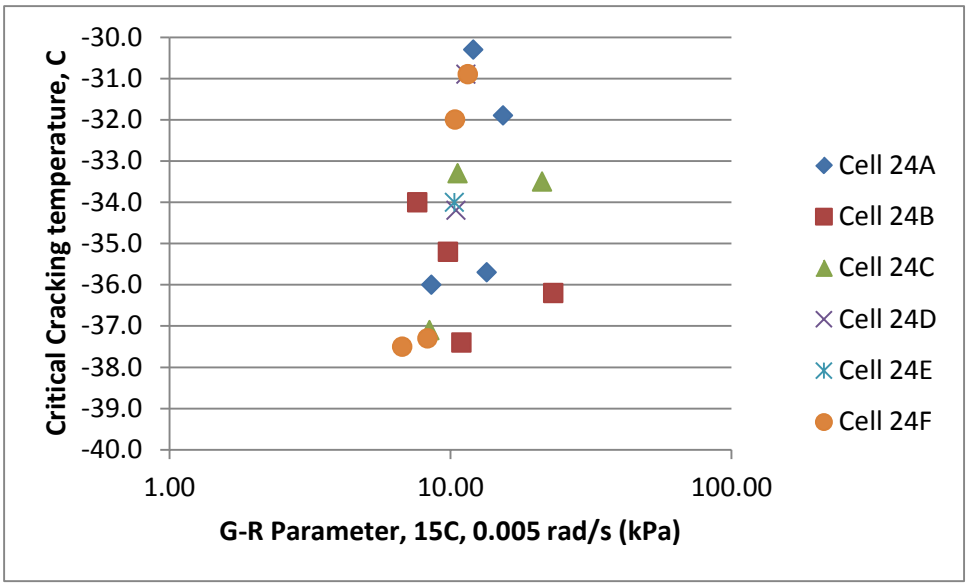

Figure 4.27 Comparison of Critical Cracking Temperature to G-R Parameter at 15°C, 0.005 rad/s

While there may be a trend for an individual subsection (like Cell 24F), on the whole there is little-to-no relationship apparent between the recovered asphalt binder properties believed to be related to aging and the cracking properties measured for the mixtures.

Even if the apparent anomalous 2011 binder test data (as shown by the dashed circle in Figure 4.28) is removed or shifted to the left, there doesn't appear to be a strong relationship between the binder and mix properties.

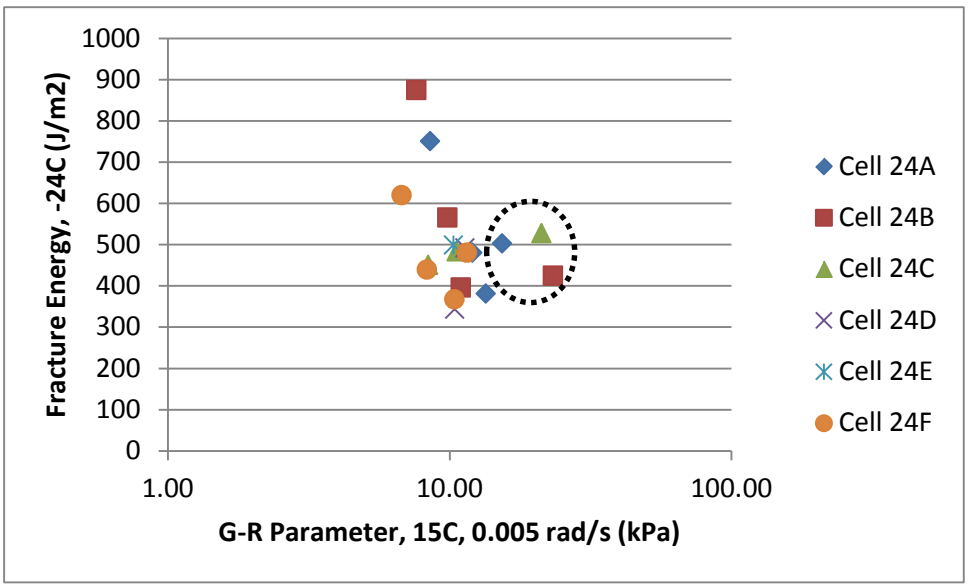

Figure 4.28 Comparison of DC(T) Fracture Energy at -24°C to G-R Parameter at 15°C, 0.005 rad/s with 2011 Binder Test Data Identified

Distress surveys were conducted on Cell 24 every six months starting in April 2010. As of the last coring in the Fall of 2013, no distresses had been identified in any of the subsections.

4.2 Minnesota TH-56

Highway 56 is a two-lane rural highway between I-90 and Leroy, Minnesota with a reported average daily traffic (ADT) at the time of construction in 1999 of 2000 vehicles. The roadway was built in two projects – one in 1995 (Mileposts 15-20) and one in 1999 (Mileposts 10-15). In 2000, at the end of the 1999 project and the beginning of the 1995 project a one-mile long seal coat (chip seal) test section was built. Each year, another one mile section was sealed. This is illustrated in Figure 4.29 for the 1999 project [25].

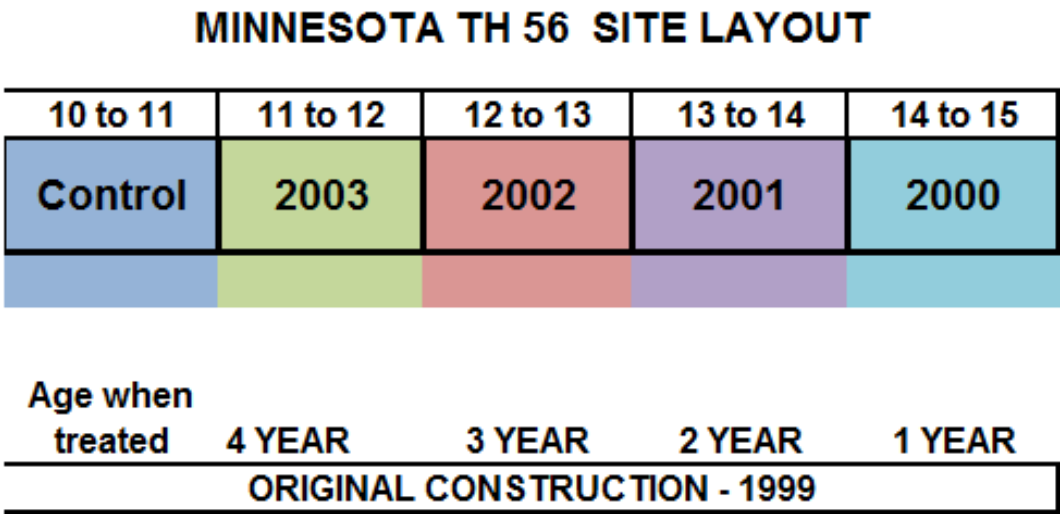

Figure 4.29 Test Section Layout for Minnesota TH 56

Test section details are shown in Table 4.14

Table 4.14 Test Section Sealing Details

Specimen Group ID	Control	T1	T2	T3	T4
Original Construction	1999	1999	1999	1999	1999
Chip Sealing Year	N/A	2000	2001	2002	2003
Age at Treatment Time, yr.	N/A	1	2	3	4
Emulsion Type	N/A	CRS-2P	CRS-2P	CRS-2P	CRS-2P
Aggregate Type	N/A	New Ulm Quartzite	Dresser Trap Rock	Dresser Trap Rock	Dresser Trap Rock
Binder Application Rate, gal/yd^2	N/A	0.32	0.34	0.38-0.42	0.40
Chip Application Rate, lb./yd^2	N/A	16	17-18	18-22	19

N/A= not applicable

After applying the chip seal coat, a fog seal was applied to the pavement surface with CSS-1h emulsion which was diluted at 1:1 ratio with water, and spread at an application rate of 0.11 gal/yd^2.

4.2.1 Sample Selection and Preparation

In 2011, cores were taken from the sections of the highway (Figure 4.30) with various chip sealing times and shipped to the Asphalt Institute laboratory for testing. Although cores were taken from both the 1999 and 1995 test sections, testing was confined to the sections that were originally constructed in 1999.

Figure 4.30 Coring of Minnesota TH 56 – 1999 Construction Test Sections

Initial preparation of all cores involved first removing the chip seal layer from the top of the cores. Care was taken to only remove the chip seal layer so that the properties of the underlying asphalt mixture could be examined to assess the effects of aging. Two cores for each test section

were then cut into three 12.5-millimeter layers as described for MnROAD Cell 24. Like layers were combined and the asphalt binder extracted and recovered for binder testing. Four additional cores were prepared for mixture testing by cutting into two 25-millimeter thick layers following the same procedure used for the MnROAD Cell 24 cores. One specimen was tested using the Indirect Tensile Strength test at -30°C. The remaining three specimens were tested first using Indirect Tensile Creep testing at -20, -30, and -40°C. After creep testing was completed, the gage points were removed and the specimens prepared for further testing. The specimens were then tested using the DC(T) test at -24°C.

4.2.2 Binder Testing

Test results from the temperature-frequency sweep tests on each test section and layer were used to generate a mastercurve at 15°C. Results are shown in Table 4.15. The data in Table 4.15 is also illustrated graphically in Figures 4.31 and 4.32 showing the G′/(η′/G′) parameter and the G-R parameter – both calculated at 15°C and 0.005 rad/s – as a function of depth in the pavement layer for each test section.

Table 4.15 Recovered Asphalt Binder from Minnesota TH 56 Cores: Mastercurve-Derived Parameters

			15°C, 0.005 rad/s				15°C, 10 rad/s	
Yr.	**Seal Yr.**	**Layer**	**Calculated G′/(η′/G′) MPa/s**	**G-R Parameter, kPa**	**R**	**δ, degrees**	**G*, kPa**	**δ, degrees**
1999	Control	Top	5.882E-04	117.63	2.149	59.9	20,740	34.1
		Mid	4.656E-04	93.11	2.064	61.6	19,120	32.4
		Bot	4.044E-04	80.89	2.088	61.8	18,949	35.0
1999	2000	Top	9.013E-05	18.03	1.960	67.6	11,740	40.9
		Mid	3.025E-05	6.05	1.801	72.2	8,429	43.3
		Bot	2.500E-05	5.00	1.839	72.2	8,003	46.1
1999	2001	Top	4.703E-05	9.41	1.900	70.0	9,854	43.7
		Mid	2.097E-05	4.19	1.835	72.6	7,169	45.1
		Bot	2.628E-05	5.26	1.864	71.8	7,986	46.0
1999	2002	Top	8.266E-05	16.53	1.954	67.9	11,446	41.5
		Mid	4.675E-05	9.35	1.842	70.7	9,974	42.0
		Bot	6.199E-05	12.40	1.906	69.2	10,960	42.4
1999	2003	Top	1.198E-04	23.95	1.986	66.6	12,802	39.9
		Mid	7.736E-05	15.47	1.939	68.3	11,249	41.5
		Bot	1.192E-04	23.84	1.979	66.7	13,084	40.1

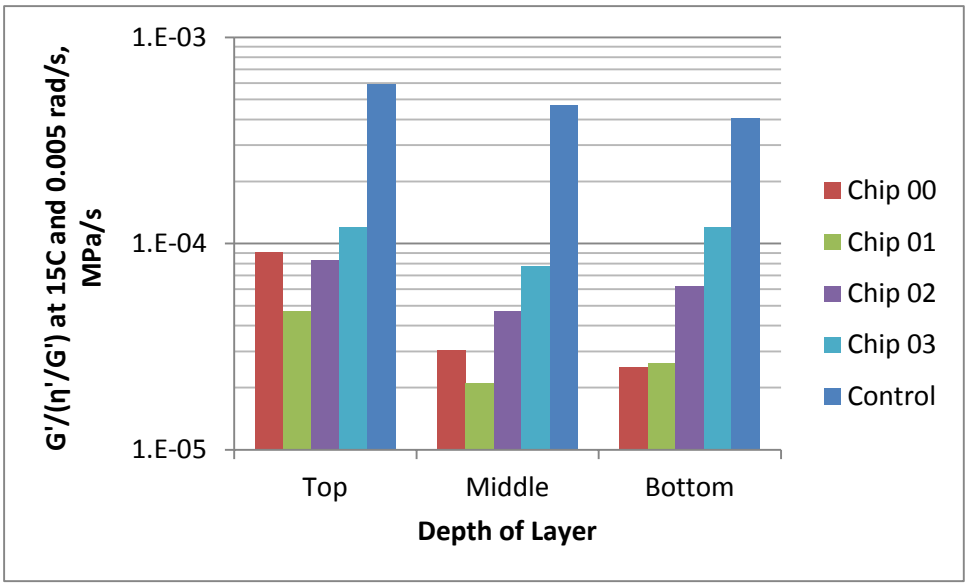

Figure 4.31 G′/(η′/G′) Parameter as a Function of Test Section and Layer – Minnesota TH 56

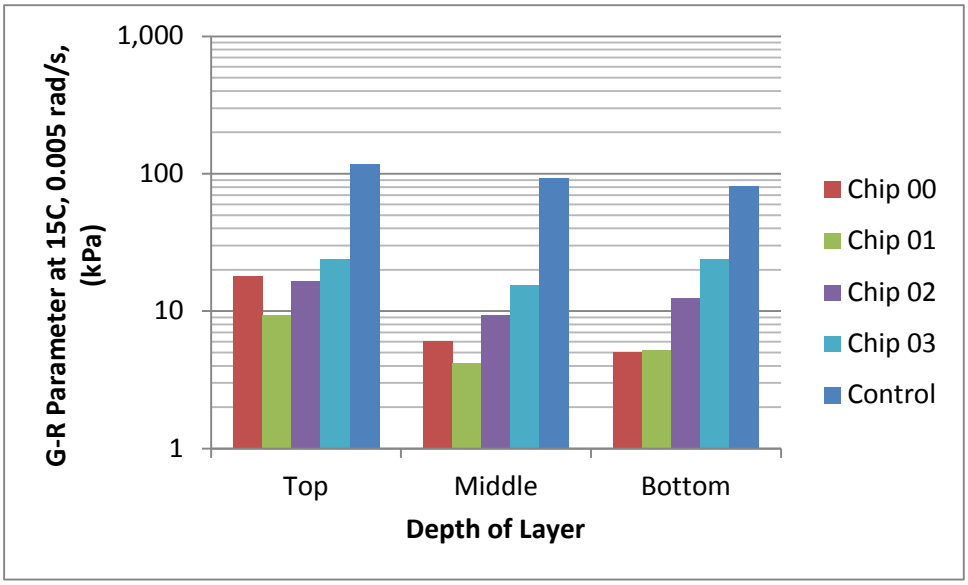

Figure 4.32 G-R Parameter as a Function of Test Section and Layer – Minnesota TH 56

In Table 4.15 and Figures 4.31 and 4.32, it can be seen that the derived parameters from the asphalt binder mastercurves generally show a rational response with depth. Near the surface (the "Top" layers), the asphalt binder shows an increase in stiffness and a decrease in phase angle, indicating a loss of relaxation properties as the binder ages. Further down in the pavement, the asphalt binder exhibits less aging as exhibited by lower stiffness and higher phase angle. Both the G′/(η′/G′) parameter and the G-R parameter – calculated at 15°C and 0.005 rad/s – capture the effects of increased stiffness and decreased phase angle seen with aging. This matches expectations and follows the same tendencies seen in the recovered asphalt binder from MnROAD Cell 24. Notable exceptions are the Bottom layer of the 2003 Chip Seal section,

which is essentially the same as the top layer, and the Bottom layer of the 2002 Chip Seal section, which is slightly higher than the Middle layer.

It appears from the data that the asphalt binder properties generally exhibit rational behavior as the time from construction to sealing increases. The G′/(η′/G′) and G-R parameters generally increase as time from construction to sealing increases – indicating an increase in aging. The Top layer of the 2000 Chip Seal is higher than the Top layer of the 2001 Chip Seal and similar to the 2002 Chip Seal. This could be a function of a number of variables including testing error. Regardless, the benefits of sealing at any of the times is apparent when compared to the Control (unsealed) section. The G′/(η′/G′) and G-R parameters of the Control section are nearly 4-5 times greater than the next highest value and as much as 10-12 times greater than the lowest values.

If the assumption can be made that the Bottom layer of the 2000 Chip Seal Section represents the t=0 condition, then a graph can be developed to examine the change in parameter with time from construction to sealing. This is shown for the G′/(η′/G′) and G-R parameters in Figures 4.33 and 4.34.

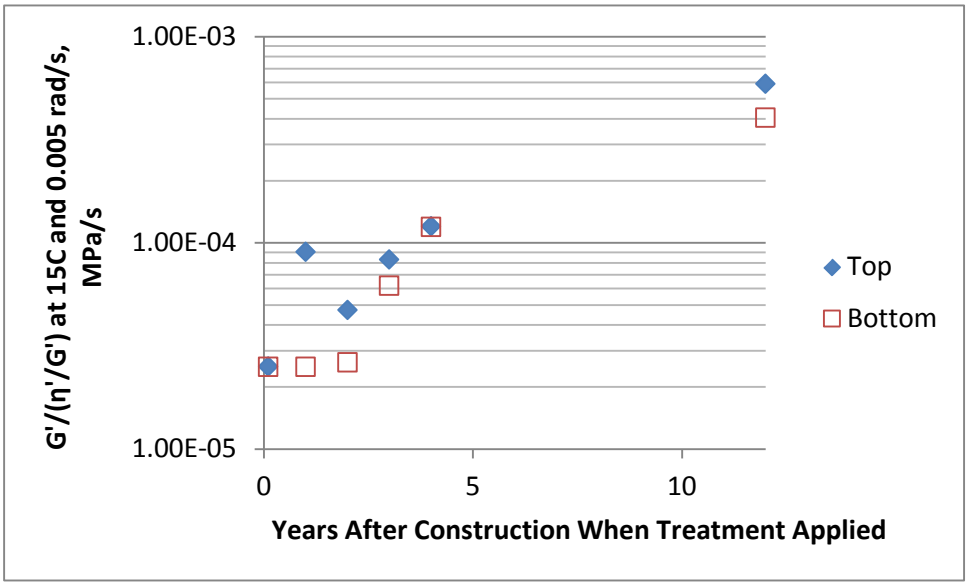

Figure 4.33 G′/(η′/G′) Parameter as a Function of Time When Sealing Occurred

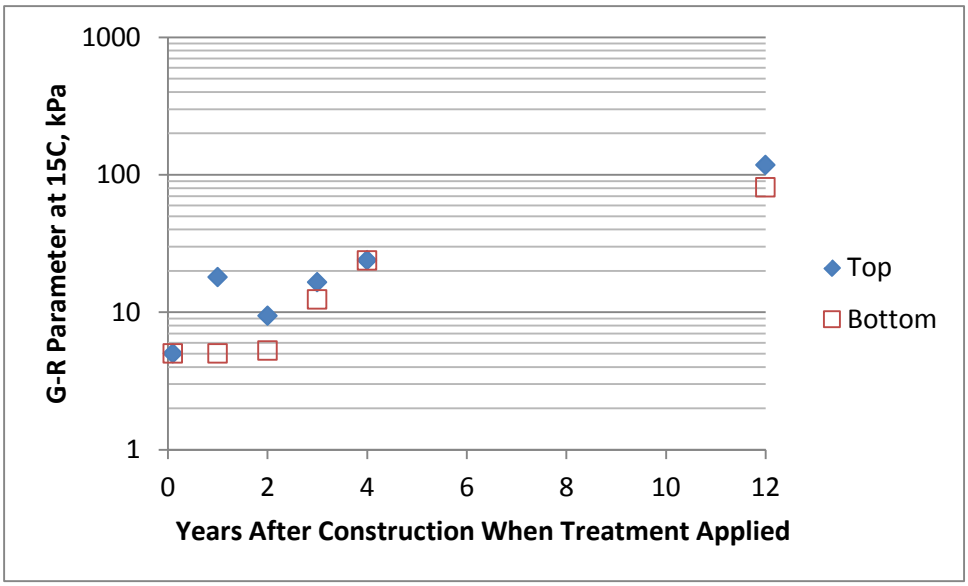

Figure 4.34 G-R Parameter as a Function of Time When Sealing Occurred

As can be seen in Figures 4.33 and 4.34, the progression of the binder parameter with aging is apparent and follows a generally linear trend on a semi-logarithmic graph. In reality, the assumption that the asphalt binder properties of the Bottom layer of the 2000 Chip Seal section represents the initial condition is probably not accurate as at least one year of aging had occurred prior to sealing and since then some aging had occurred at the lower depth of the pavement structure. If anything, the actual binder properties after construction (t=0) should be even lower than is represented in Figures 4.33 and 4.34. Nevertheless, the assumed data serves to illustrate the effect of sealing time on asphalt binder aging.

Figure 4.35 shows the data from the Top layers of each of the sections in a Black Space diagram. As before, for reference, curves are shown where the G-R parameter is equal to 180 and 600 kPa at 15°C and 0.005 rad/s. As with the data in Figures 4.31-4.34 there is a clear separation between the sections that were sealed within four years of the time of construction and the Control (unsealed) section.

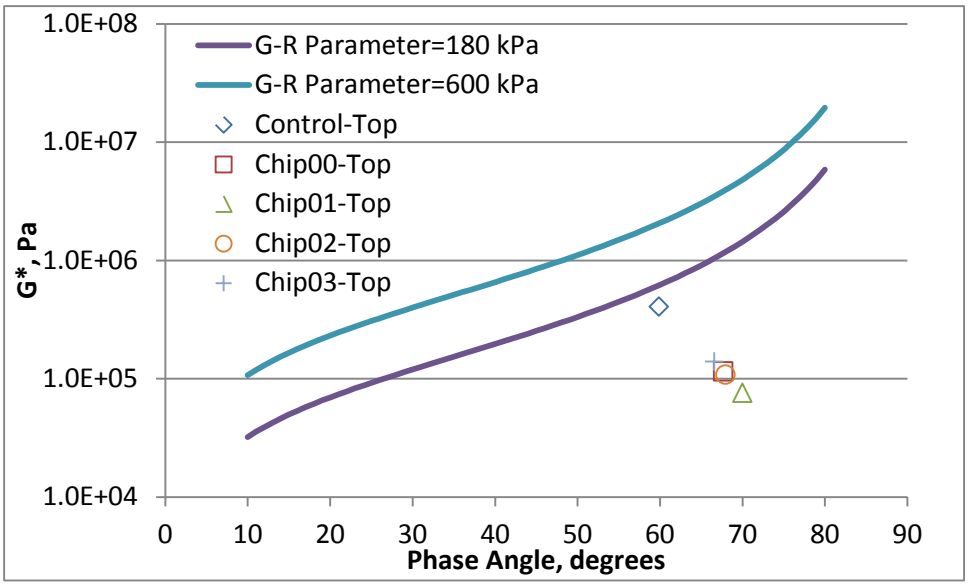

Figure 4.35 Black Space Representation of Top Layers of TH 56 Sections

In addition to the temperature-frequency sweep testing, the Linear Amplitude Sweep (LAS) test was conducted on the recovered asphalt binders at 16°C – the expected intermediate temperature grade for a PG 58-34 climate. Results from the LAS testing at 16°C on each test section and layer are shown in Table 4.16 and illustrated in Figures 4.36 and 4.37.

Table 4.16 Recovered Asphalt Binder from Minnesota TH 56 Cores: LAS at 16°C

			LAS Parameter		N_f	
Yr.	**Seal Yr.**	**Layer**	**A**	**B**	**γ = 2%**	**γ = 5%**
1999	Control	Top	2.191E+06	-4.780	79,733	999
		Mid	1.220E+06	-4.664	48,101	670
		Bot	4.271E+05	-4.571	17,967	273
1999	2000	Top	3.045E+05	-3.784	22,106	690
		Mid	5.107E+05	-3.437	47,157	2,022
		Bot	4.293E+05	-3.342	42,345	1,981
1999	2001	Top	1.603E+05	-3.605	13,175	484
		Mid	6.564E+05	-3.342	64,745	3,030
		Bot	4.902E+05	-3.390	46,751	2,092
1999	2002	Top	2.740E+05	-3.787	19,854	618
		Mid	3.910E+05	-3.632	31,541	1,131
		Bot	2.289E+05	-3.694	17,692	600
1999	2003	Top	3.534E+05	-4.001	22,076	565
		Mid	2.972E+05	-3.796	21,387	660
		Bot	3.673E+05	-3.954	23,699	633

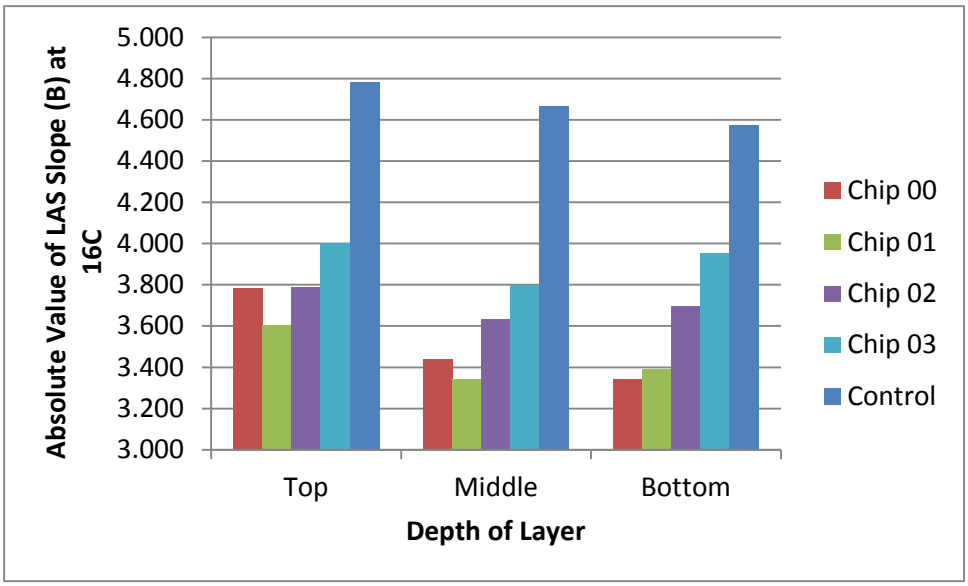

Figure 4.36 Absolute Value (B) of LAS Slope for MN TH 56 Sections

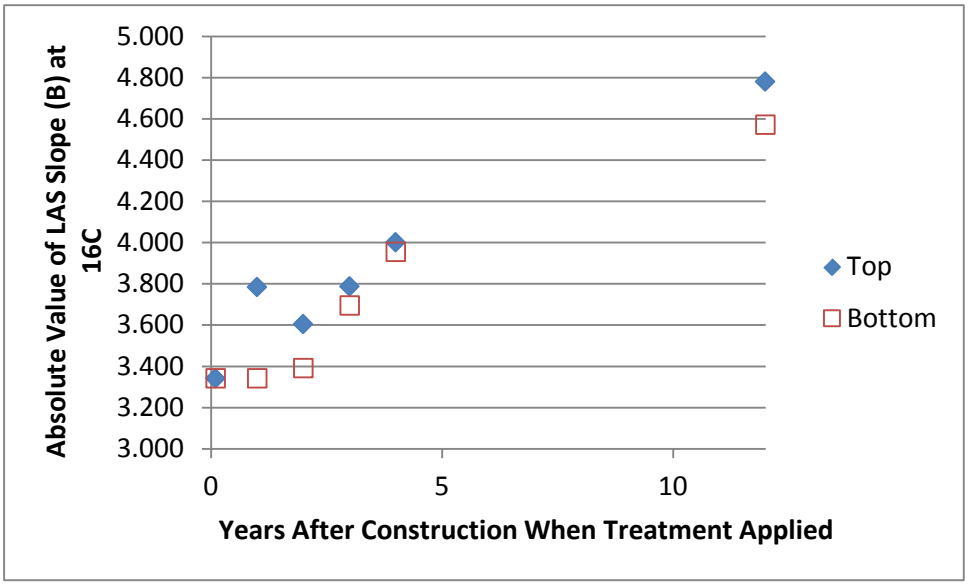

Figure 4.37 Absolute Value of LAS Slope (B) as a Function of Time When Sealing Occurred

As with the mastercurve data, the LAS slope in Figure 4.36 is generally higher for the Top layers than the Middle and Bottom layers for any Section. Also, similar to the mastercurve parameters, the LAS slope is significantly higher for the Control (unsealed) section than any of the sealed sections. The LAS slope was also generally higher for the MN TH 56 cores (3.34 to 4.78) than the MnROAD Cell 24 cores (3.16 to 3.89). This matches expectations, even if it is assumed that the asphalt binder properties from the original materials used during construction were somewhat different. MnROAD Cell 24 was constructed in 2008; MN TH 56 was constructed nine years earlier (1999).

As with the results from LAS testing of the MnROAD Cell 24 sections, the calculated number of cycles to failure (N_f) did not behave in a manner that reflected the change in aging of the asphalt binder. Oftentimes the N_f value at a given strain level was higher for the most aged asphalt binders.

4.2.3 Mixture Testing

Indirect Tensile Creep testing was conducted on triplicate specimens at -20, -30, and -40°C. Data from the tests were used to generate creep compliance curve parameters. One specimen was sacrificed to determine Indirect Tensile Strength so that the critical cracking temperature could be determined. Data on indirect tensile testing is shown in Table 4.17

Table 4.17 MN TH 56 Mixture Test Results – Indirect Tensile

			Creep					
			Curve Coefficients			Compl.		
Yr.	**Seal Yr.**	**Layer**	**D_0**	**D_1**	**m**	**-34°C, 7200 s**	**Strength (MPa)**	**Critical Cracking Temp, °C**
1999	Control	Top 25	2.10E-05	8.35E-06	0.188	7.30E-05	2.79	-19.9
		Bot 25	1.66E-05	8.50E-06	0.178	7.29E-05	2.73	-21.1
1999	2000	Top 25	1.79E-05	4.19E-06	0.239	6.25E-05	3.36	-27.2
		Bot 25	1.91E-05	4.00E-06	0.235	6.80E-05	3.55	-30.5
1999	2001	Top 25	1.80E-05	2.67E-06	0.266	5.48E-05	3.09	-22.0
		Bot 25	1.56E-05	4.54E-06	0.219	6.06E-05	2.91	-26.7
1999	2002	Top 25	2.48E-05	5.42E-06	0.212	7.43E-05	2.71	-23.5
		Bot 25	2.44E-05	3.45E-06	0.243	7.56E-05	2.94	-29.6
1999	2003	Top 25	1.12E-05	1.35E-05	0.136	7.98E-05	2.65	-22.0
		Bot 25	1.14E-05	1.14E-05	0.143	6.29E-05	2.84	-18.1

"n/a" means that test results are not available
"Top 25: refers to the topmost layer to a depth of 25 millimeters from the surface
"Bot 25" refers to the bottom layer that is 25 millimeters thick and starts 25 millimeters from the Top layer

The data in Table 4.17 shows an apparent trend in that the Indirect Tensile Strength at -30°C appears to generally decrease as the time from construction to sealing increases. This is true for the first two years (2000 and 2001). After two years, the Indirect Tensile Strength at -30°C remains essentially the same. This is illustrated in Figure 4.38.

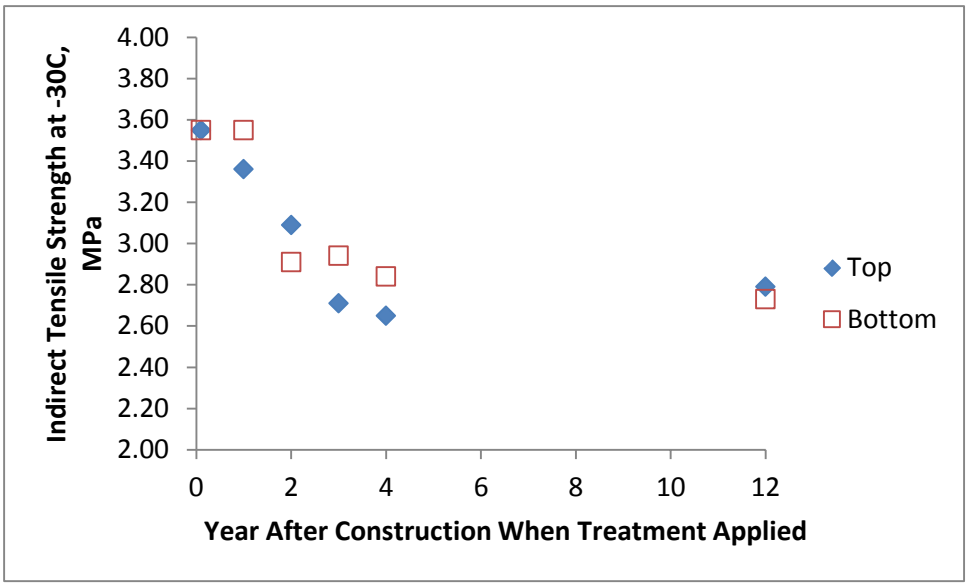

Figure 4.38 MN TH 56: Indirect Tensile Strength as a Function of Time from Construction to Sealing

The data in Table 4.17 shows no apparent trend for the creep compliance slope (m) as a function of time from construction to sealing. However, it is apparent that the creep compliance slope decreases significantly after the second year (2001) with values for 2002, 2003, and the Control sections being similarly low as illustrated in Figure 4.39.

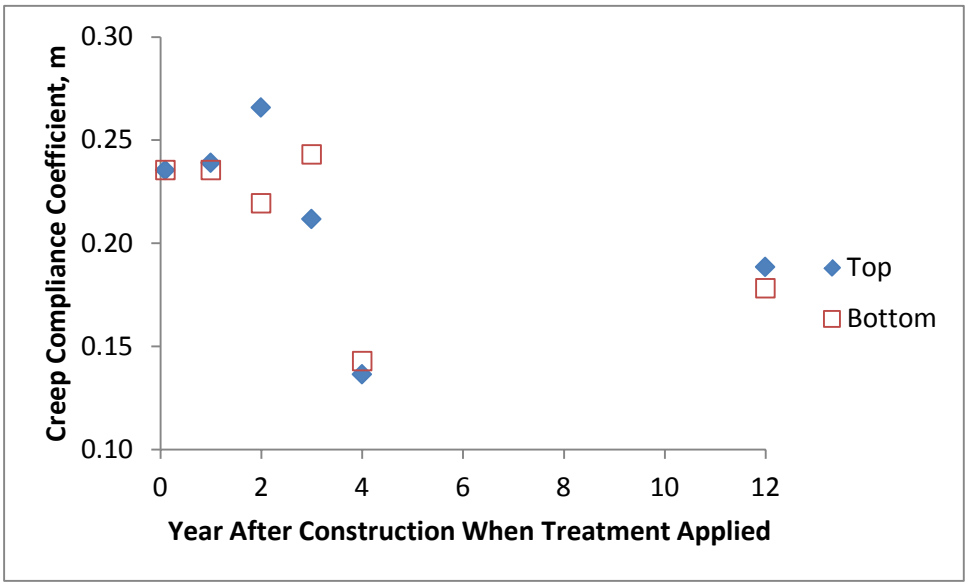

Figure 4.39 MN TH 56: Creep Compliance Slope (m) as a Function of Time from Construction to Sealing

As discussed earlier, the creep compliance slope (m) and indirect tensile strength have an impact on the critical cracking temperature determined using an analysis procedure by Christensen [35]

which was based on work by Roque and Hiltunen during SHRP [35]. Critical cracking temperature for the TH 56 sections is shown as a function of time in Figure 4.40.

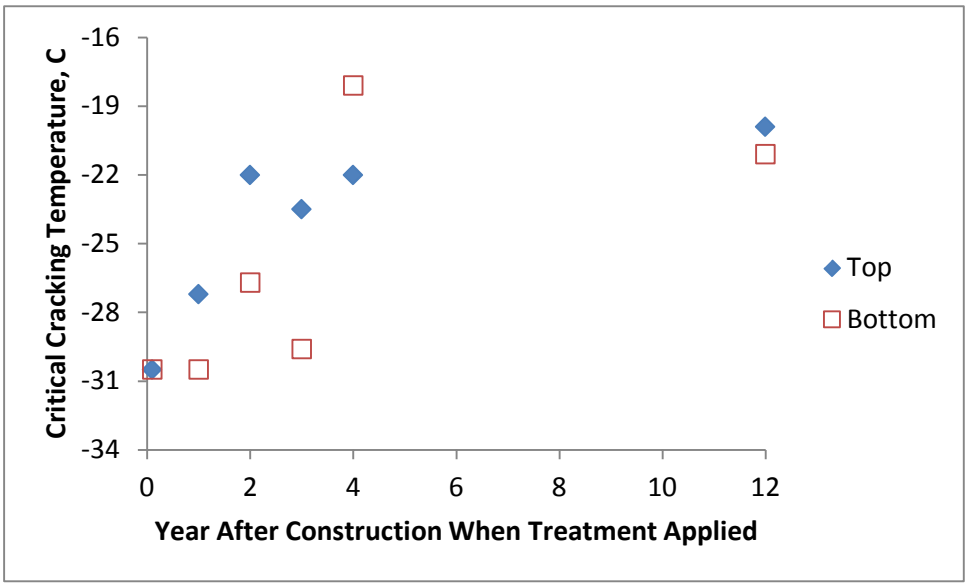

Figure 4.40 MN TH 56: Critical Cracking Temperature as a Function of Time from Construction to Sealing

Critical Cracking Temperature appears to follow a trend for the Top layers of the MN TH 56 cores of increasing temperature as the time increases from construction to sealing. From the time of initial sealing in 2000 to the Control (unsealed) section, the Critical Cracking Temperature changes by more than one full binder grade (7.3°C) indicating a greater propensity to experience low temperature cracking on the Control (unsealed) Section.

After the three test specimens from each section/layer were tested using indirect tensile creep, the gage points were removed and the specimens were further processed to turn them into specimens suitable for testing following the Disk-Shaped Compact Tension, DC(T), test as described in ASTM D7313. For each section/layer, three specimens were tested at -24°C and the results averaged to determine fracture energy for the section/layer. The results of the DC(T) testing are shown in Table 4.18 and Figure 4.41.

Table 4.18 MN TH 56 Mixture Test Results – DC(T)

Yr.	Seal Yr.	Layer	Fracture Energy J/m^2	CV
1999	Control	Top 25	151.2	11%
		Bot 25	179.9	6%
1999	2000	Top 25	277.4	20%
		Bot 25	308.4	n/a
1999	2001	Top 25	208.0	3%
		Bot 25	275.2	25%
1999	2002	Top 25	160.1	8%
		Bot 25	182.8	10%
1999	2003	Top 25	160.7	n/a
		Bot 25	207.6	7%

"n/a" means that test results are not available
"Top 25: refers to the topmost layer to a depth of 25 millimeters from the surface
"Bot 25" refers to the bottom layer that is 25 millimeters thick and starts 25 millimeters from the Top layer

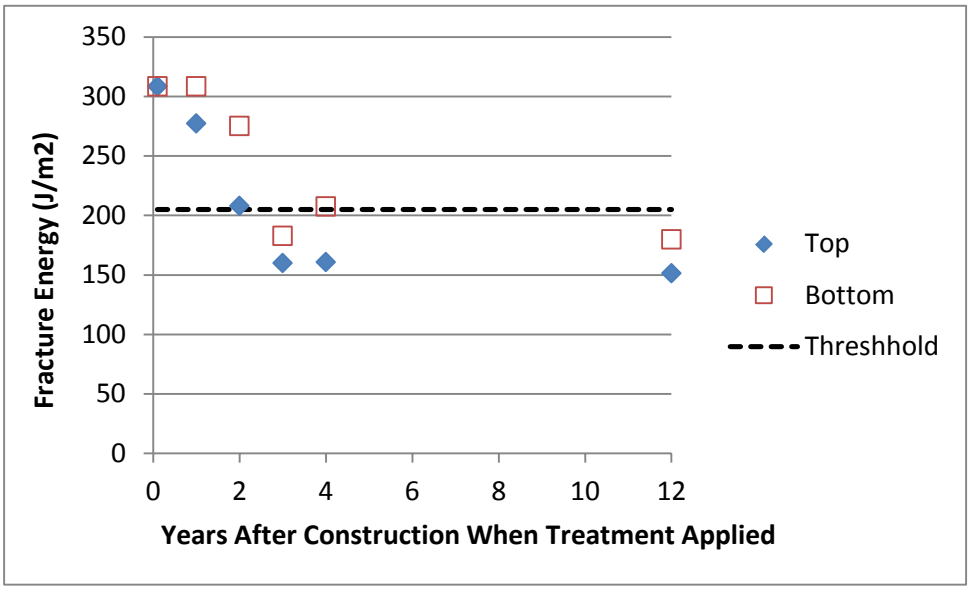

Figure 4.41 MN TH 56: Fracture Energy as a Function of Time from Construction to Sealing

Similar to the Indirect Tensile Strength data, the DC(T) data in Table 4.18 and Figure 4.41 indicates a general decrease in fracture energy for the first two years (2000 and 2001). After the second year of sealing, the fracture energy for the Top layers was essentially the same.

After twelve years in service (1999-2011), the fracture energy of the Control Section and the 2002 Chip Seal and 2003 Chip Seal sections were below the recommended threshold value indicating higher cracking potential. Had cores been taken at an earlier time in the pavement's

life – like in 2007 after eight years – the fracture energy values would be expected to be higher, but of a similar pattern as shown in Figure 4.41.

4.2.4 Comparison of Binder and Mix Testing

With the caveat previously stated that the Top layers used in the mixture tests were not quite the same as the Top layers used in the binder tests, it was still desired to compare the binder and mixture results to see if there was any trend relating the two. This data is illustrated in Figures 4.42 – 4.47 comparing DC(T) Fracture Energy, Indirect Tensile Strength, and Critical Cracking Temperature to the LAS Slope (B) and G-R Parameter.

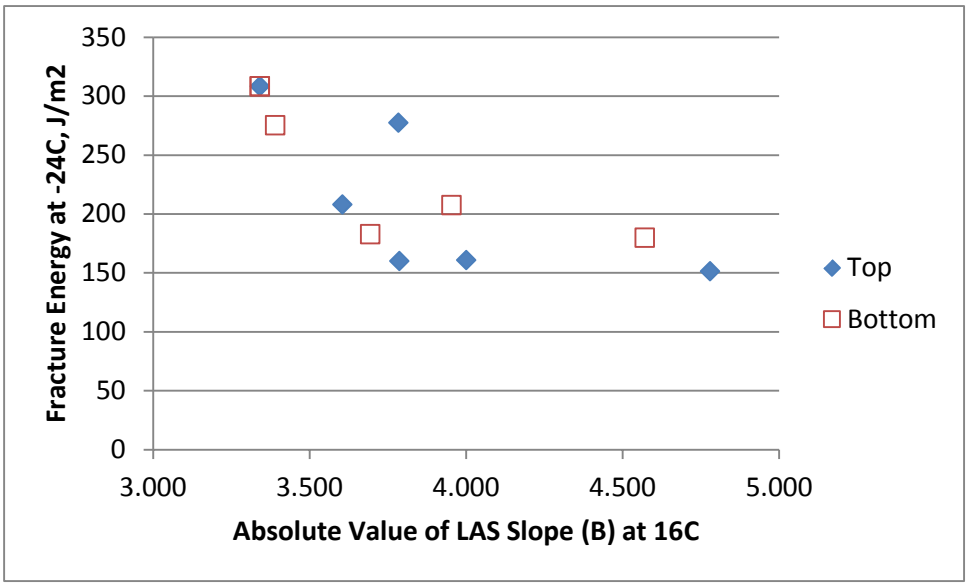

Figure 4.42 Comparison of DC(T) Fracture Energy at -24°C to LAS Slope (B) at 16°C

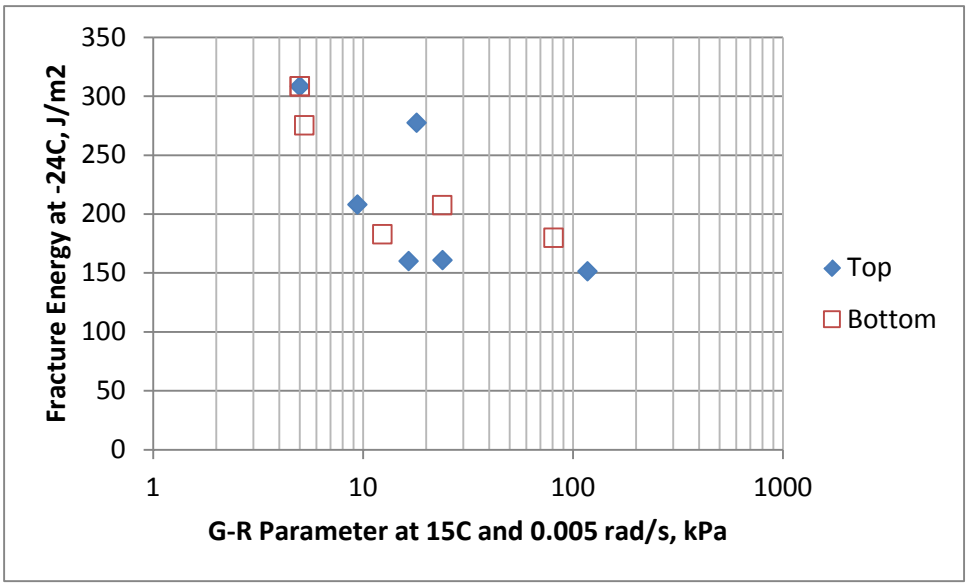

Figure 4.43 Comparison of DC(T) Fracture Energy at -24°C to G-R Parameter at 15°C, 0.005 rad/s

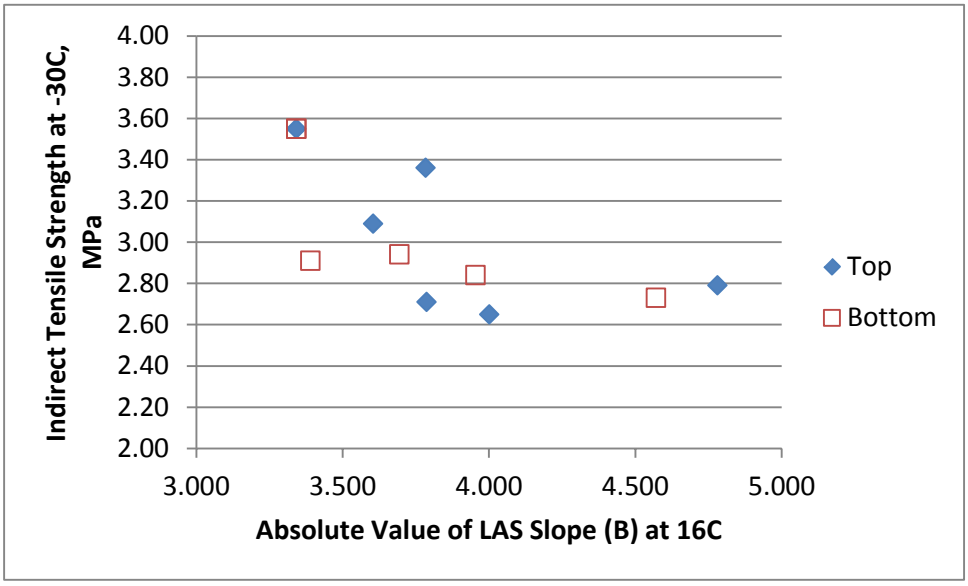

Figure 4.44 Comparison of Indirect Tensile Strength at -30°C to LAS Slope (B) at 16°C

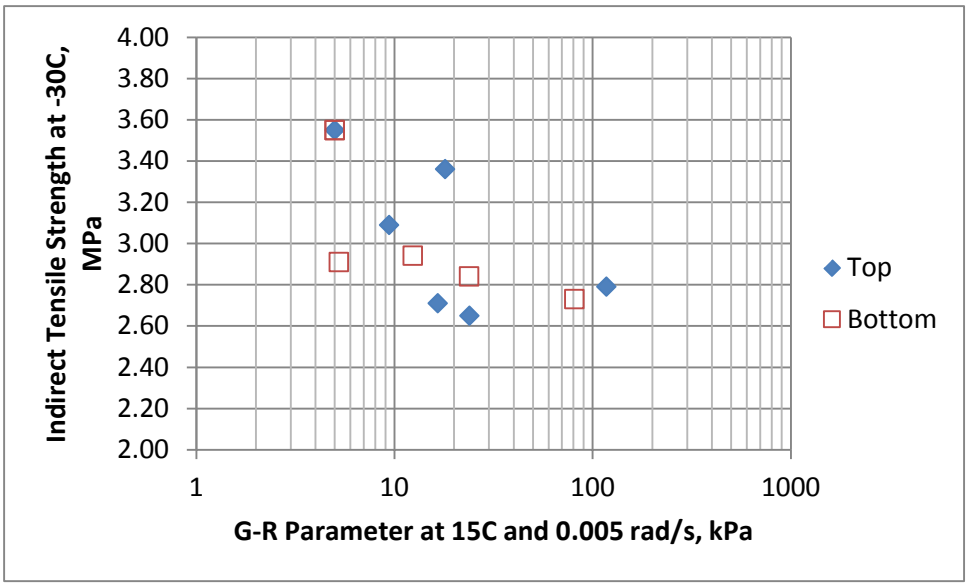

Figure 4.45 Comparison of Indirect Tensile Strength at -30°C to G-R Parameter at 15°C, 0.005 rad/s

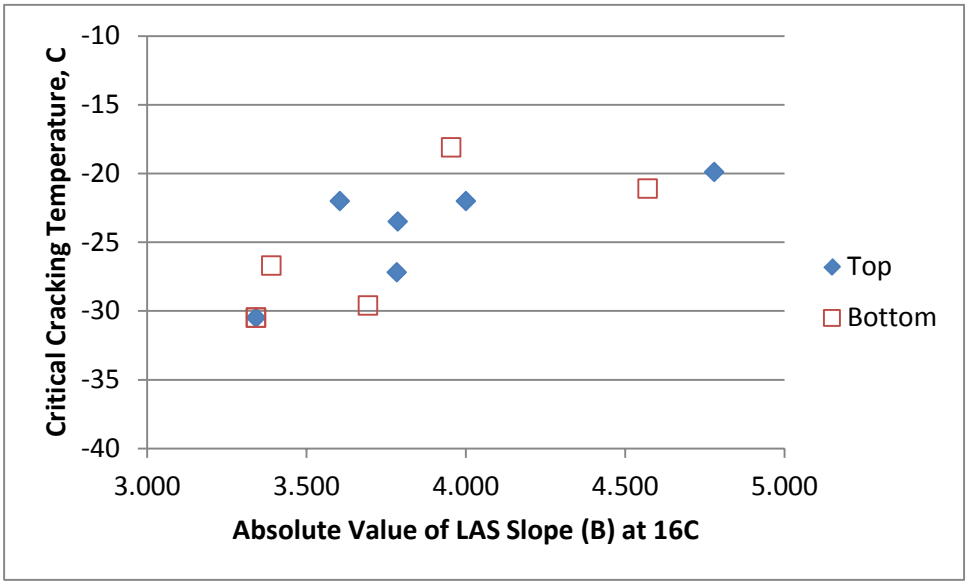

Figure 4.46 Comparison of Critical Cracking Temperature to LAS Slope (B) at 16°C

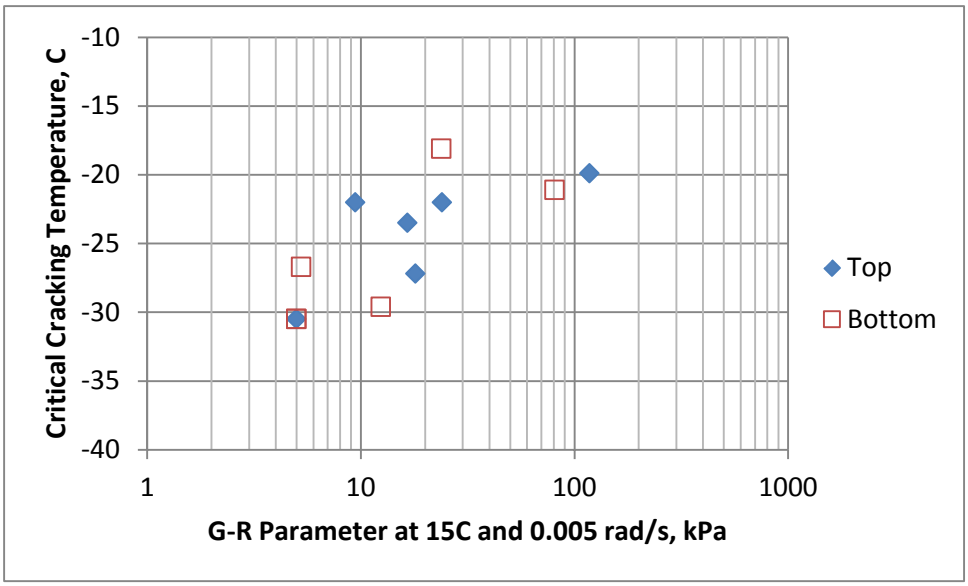

Figure 4.47 Comparison of Critical Cracking Temperature to G-R Parameter at 15°C, 0.005 rad/s

The data in Figures 4.42-4.47 illustrate a general relationship between binder properties and mixture properties for the MN TH 56 cores. As the binder parameter of interest (LAS Slope or G-R Parameter) gets larger, indicating more aging, the mixture properties related to cracking get worse – Indirect Tensile Strength decreases, Fracture Energy decreases, and Critical Cracking temperature increases. This relationship is rational but differs from the findings from MnROAD Cell 24 which showed little general relationship between binder and mixture properties. It is possible that the difference is related to the age of the two test sections studied (five years or less for MnROAD Cell 24 and twelve years for MN TH 56).

Measured distress data for TH 56 and ride information (as supplied by MnDOT) are shown in the Appendix.

Chapter 5 - Economic Considerations

As stated in the Introduction, the purpose of an effective pavement preservation program is to apply surface treatments at the right time to delay or prevent deterioration of the pavement due to either load-related or environmentally-induced damage. Environmentally-induced damage is considered to principally be related to the properties of the asphalt binder since no other component in an asphalt mixture is as affected by oxidative aging. The purpose of seals (fog or chip) is to reduce the supply of oxygen to the underlying mixture, thus delaying the onset of brittle behavior and surface cracking.

The cumulative impact of systematic, successive preservation treatments should be to postpone costly rehabilitation and reconstruction. On a life-cycle cost basis, this cumulative series of pavement preservation treatments is substantially less expensive than extensive reconstruction major rehabilitation strategies.

The purpose of this research was to attempt to quantify when treatments should be applied to minimize the effects of environmental aging on pavement life and minimize cost. To this end, the research focused principally on a designed experiment at the MnROAD Low Volume Road to study aging, but also examined an earlier aging/chip-seal experiment on TH 56 in southern Minnesota.

Of the two test sections studied, the TH 56 test section provided the clearest indication that asphalt binder properties could be used to quantify aging. Unfortunately, some of the recommended limits to serve as indications of the onset of cracking could not be validated by the experiment. Regardless, the TH 56 data suggests that waiting longer than 1-2 years to seal a pavement could result in fracture properties that would ultimately be the same as if the pavement were not sealed at all. It is important to note that this statement is not meant to imply that there is no benefit gained from applying a seal after two years. The data simply suggests that after twelve years of service, the chip seals applied after 1-2 years with no further treatment exhibited considerably reducing aging/cracking properties compared to the control section and the sections sealed after 3-4 years (as indicated by some mixture parameters).

In NCHRP Report 523, it is noted in the “Conclusions” that:

> “The process of identifying and tracking appropriate measures of performance is a key component of the optimal timing analysis. An appropriate measure is one that reflects the benefit of using the treatment; preferably it relates to the identified program objectives (e.g., if customer satisfaction is a preventive maintenance program objective, then pavement roughness could be used as a performance measure). In monitoring treatment performance, it is also important to recognize that a treatment can “last” much longer than it provides a benefit. Ultimately treatment performance (or true treatment “life”) is determined by the time at which the treated pavement’s performance reverts to the do-nothing condition, or when it reaches a defined threshold.” [37]

Applying the findings from NCHRP Report 523 to this research, it can be seen that all the chip seals on TH 56 have lasted past the useful life of 4-7 years normally projected for a chip seal [37], but at least in the case of the 2002 and 2003 seals, have reverted to the "do-nothing" condition represented by the Control section.

It was noted during construction of the TH 56 test sections that emulsion use increased by an average of 6-7% per year to accommodate the increased application rate needed to account for current pavement conditions. If the labor and equipment rates stay the same and the change in aggregate application rate is assumed to have a negligible cost, then by discounting inflation it can be expected that the cost to apply a chip seal on the TH 56 sections will increase by 6-7% per year due solely to the increased emulsion application rate. This is close to the value that the U.S. Office of Management and Budget (OMB) requires (seven percent real discount rate) for U.S. Federal agencies to use to evaluate public investments. For life-cycle cost analysis the OMB allows Federal agencies to use lower rates. Real discount rates of 2.5 percent (ten years) and 3.2 percent (thirty years) were reported by the OMB in 2003 [38]. For preventive maintenance treatments intended to evaluate life-cycle cost, the argument could be made to use a real discount rate of 3% in an economic analysis.

With the benefits gained in the long-term reduction of oxidative aging and environmental cracking it can be concluded that an early seal, within the first two years, was effective in mitigating aging-related damage on the TH 56 sections. By reducing the supply of oxygen initially to minimize aging, a second seal could then be applied at a more traditional timing (i.e., 4-7 years after the initial seal) with the expectation of a continued extension of service life.

Chapter 6 - Conclusions and Recommendations

The overall objective of this study was to determine the proper timing of preventive maintenance treatments in order to optimize life cycle costs and pavement performance. Specifically, the project was focused on better understanding and quantifying the environmental aging mechanism and how it can be reduced through pavement preservation.

Based on testing and analysis conducted on two test sections – MnROAD Cell 24 and Minnesota TH 56 – the following summary and conclusions can be made:

1. In the MnROAD Cell 24 and TH 56 test sections, aging of the asphalt pavement, as measured using several asphalt binder properties, was shown to be significantly higher near the surface (within the top 12.5 millimeters) than further down in the pavement structure. Near the surface, the asphalt binder shows an increase in stiffness and a decrease in phase angle, indicating a loss of relaxation properties as the binder ages. Further down in the pavement, the asphalt binder exhibits less aging as exhibited by lower stiffness and higher phase angle. All of the binder parameters that were studied – including the $G'/(\eta'/G')$ and G-R parameters calculated at 15°C and 0.005 rad/s, the slope (B) of the modulus-frequency curve from the Linear Amplitude Sweep (LAS) test, and the difference between the critical temperatures where the Stiffness from the BBR is equal to 300 MPa and the m-value from the BBR is equal to 0.300 – capture the effects of increased stiffness and decreased phase angle seen with aging as a function of depth from the surface.
2. The aging that was expected to occur as the time is extended from construction to sealing was not readily seen in the asphalt binder properties of the Cell 24 subsections. Contrary to expectations and initial data analysis all of the subsections, including the Control, exhibited no discernible trend indicating that time from construction to sealing had a significant effect on asphalt binder properties. With only five years of service from construction to the last coring, more aging may be needed to see any significant effects.
3. The aging that was expected to occur with time was observed by a change in the asphalt binder properties of the Bottom layers of the Cell 24 subsections. The Top layers of the Cell 24 subsections indicated some change in asphalt binder properties from the samples taken in 2010 to the samples taken in 2013, but with scatter in the data in the intervening years making it difficult to see a general trend.
4. None of the subsections had values for the $G'/(\eta'/G')$ and G-R parameters that were close to the limiting values suggested by other research as thresholds for cracking. This is not surprising given the relatively young age of the pavement (five years at the time of the last coring) and lack of cracking noted on any of the test sections from distress surveys.
5. Mixture testing of samples from the Cell 24 subsections generally did not show any significant trends of aging as the time from construction to sealing increased with the exception of the indirect tensile strength of the Top layers. In general, the cores from subsections sealed in 2009 and later had higher indirect tensile strength values than the Control subsection and the subsection sealed in 2008 (using a CSS-1 emulsion instead of a CRS-2P emulsion).

6. Mixture testing of samples from the Cell 24 subsections generally did not show any significant trends of aging as time increased with the exception of the indirect tensile strength of the Top layers. The indirect tensile strength values of all subsections decreased as time increased. The reduction in indirect tensile strength, combined with constant creep compliance slope, will lead to an increase in Critical Cracking Temperature (i.e., a warmer temperature). This trend was not easily seen as the creep compliance slope was not a constant value as time increased.
7. While some differences could be noted between the Top and Bottom layers for each Cell 24 subsection, the results were not conclusive. In most cases, the Bottom layers had higher indirect tensile strength and lower Critical Cracking Temperature than the Top layers within each subsection and coring year. This response indicates that less aging has occurred in the Bottom layers compared to the Top layers.
8. While there may be a trend for an individual subsection for a specific comparison (Cell 24F), on the whole there was little-to-no relationship apparent between the recovered asphalt binder properties believed to be related to aging and the cracking properties measured for the mixtures on MnROAD Cell 24.
9. Cores from the Minnesota TH 56 test section did indicate a much clearer picture of aging as represented by the various asphalt binder parameters. The Top layers of all the test sections had higher values of asphalt binder parameters believed to be related to aging than their corresponding layers further from the surface. The time between construction and sealing also had an effect on the asphalt binder parameters believed to be related to aging with the earliest chip seal section exhibiting the lowest values (indicating the least aging) and the Control (unsealed) section exhibiting the highest values (indicating the most aging).
10. Mixture tests on cores from the TH 56 test section generally confirmed the results of the binder testing with decreased indirect tensile strength and increased Critical Cracking Temperature as time from construction to sealing increases.
11. The fracture energy of the TH 56 specimens determined using the DC(T) test decreased for the first two years after construction and then reached a plateau, below the threshold value suggested for cracking, where the fracture energy of the cores from the 2002 and 2003 Chip Seal sections was the same as the Control (unsealed) section after 12 years of service.
12. The analysis of the fracture energy of the cores from TH 56 indicates that waiting more than two years after construction to place a chip seal could result in fracture properties that would ultimately be the same as if the pavement were not sealed at all. This is not to suggest that other benefits could not be realized by a later chip seal, but rather that the aging that impacts the fracture properties can be mitigated by sealing earlier.

Recommendations that can be made based on the results of this study are as follows:

1. The asphalt binder is the one component in an asphalt mixture specimen that is strongly affected by oxidative aging. Asphalt binder tests also are generally more reproducible and require less sample size than mixture tests. Consequently, it is recommended that asphalt binder tests be conducted on recovered material to assess the effects of oxidative aging. Of the asphalt binder tests used in this research, it is recommended that a rheological

parameter – such as the G′/(η′/G′) and G-R parameters at 15°C and 0.005 rad/s – be used to quantify aging. These parameters require more testing and analysis time than the LAS or Single-Point DSR tests, but provide more information that could be used in assessing other rheological parameters (such as Black Space plots). The BBR ΔT_c parameter has the advantage of being independent of the temperature at which the test is conducted, but requires more material and testing time (at least two test temperatures needed) to generate a result. The amount of material required becomes an important consideration when using recovered binder from a pavement sample to determine physical properties.

2. The threshold values identified by the Texas A&M research for the G′/(η′/G′) parameter at 15°C and 0.005 rad/s require more validation work. Only the asphalt binder from the TH 56 Control section was anywhere close to the threshold value. According to a site survey, this section did exhibit some various forms of cracking.
3. The asphalt binder parameters recommended for use are derived from rheological measurements – meaning small strain and linear viscoelastic properties such as complex shear modulus (G*) and phase angle (δ). Fracture properties might be needed to get a complete characterization of the effect of aging on binder properties and cracking. Further work should examine binder fracture tests. In the interim, despite the higher variability inherent in mixture testing, fracture properties can be determined using the Disk-Shaped Compact Tension test, DC(T), conducted at a temperature that is 10 degrees warmer than the low temperature PG grade for the project location. Since aging is dependent on the depth in the pavement structure, DC(T) testing should be conducted on the thinnest practical specimens representing the portion of the asphalt pavement closest to the surface. Based on the testing in this research, it is recommended that DC(T) specimens be 25-millimeters thick. It is recognized that thinner DC(T) specimens will have a different fracture energy than 50-millimeter thick DC(T) specimens. Some adjustment will be needed in comparing values from 25-millimeter and 50-millimeter thick specimens.
4. Because the asphalt pavement had only been in service for five years at the time of the last coring, it is recommended that the MnROAD Cell 24 test sections be left in place and sampling/testing continue. Testing could be conducted by the Minnesota Department of Transportation following guidelines developed by this research. It should not be necessary to sample every year as was done for this study; every 2-3 years should be sufficient to observe any continued effects of aging. Because pavement preservation involves applying treatments before distresses are apparent, it would be interesting to apply a second treatment to each section after it had been in service for seven years. This would allow Cell 24A, which was sealed in October 2008 to be sealed again in 2015. Subsequent subsections would be sealed in successive years. The Control subsection, Cell 24F, would remain unsealed. If desired, the experiment could be ended after twelve years.
5. In future aging studies involving chip seals, it is recommended that the actual chip seal be placed instead of simply using the asphalt emulsion application rate without any chips – essentially a fog seal. The presence of the aggregate chips would likely help to reduce UV aging which could have an effect on the aging properties of the pavement. UV aging is an important consideration for roofing materials.

References

1. "Intermodal Surface Transportation Efficiency Act of 1991," United States Congress, H.R. 2950, Public Law No: 102-240 (1991)
2. *Pavement Preservation: A Road Map for the Future: Ideas, strategies, and techniques for pavement preservation*, United States Department of Transportation, Federal Highway Administration, 1998 (Accessed July 2014), https://www.fhwa.dot.gov/infrastructure/asstmgmt/roadmap.pdf
3. *Transportation System Preservation Research, Development and Implementation Roadmap*, Joint Publication of Federal Highway Administration (FHWA), American Association of State Highway and Transportation Officials (AASHTO), and the Foundation for Pavement Preservation (FP^2), 2008 (Accessed July 2014), https://www.pavementpreservation.org/fhwa-resources/tsp-research-roadmap
4. C.J. Glover, R.R. Davison, C. H. Domke, Y. Ruan, P. Juristyarini, D.B. Knorr, and S. H. Jung, *Development of a New Method for Assessing Asphalt Binder Durability with Field Evaluation*, Federal Highway Administration and Texas Department of Transportation, College Station, TX (2005)
5. D.I. Hanson, P.B. Blankenship, G.N. King, and R.M. Anderson, *Techniques for Prevention and Remediation of Non-Load-Related Distresses on HMA Airport Pavements – Phase II*, Draft Final Report, Airfield Asphalt Pavement Technology Program, Phoenix, AZ (July 2010)
6. R.M. Anderson, G.N. King, D.I. Hanson, and P.B. Blankenship, King, "Evaluation of the Relationship Between Asphalt Binder Properties and Non-Load Related Cracking," *Asphalt Paving Technology, Journal of the Association of Asphalt Paving Technologists,* Volume 80, Lancaster, PA (2011), 615-649.
7. G.N. King, R.M. Anderson, D. Hanson, and P. Blankenship, "Using Black Space Diagrams to Predict Age-Induced Cracking," *7th RILEM International Conference on Cracking in Pavements: mechanisms, modeling, testing, detection, prevention and case histories*, (2012), 453-463.
8. D.A. Anderson, D.W. Christensen, and H.U. Bahia, "Physical Properties of Asphalt Cement and the Development of Performance-Related Specifications", *Asphalt Paving Technology, Journal of the Association of Asphalt Paving Technologists,* Volume 60, Eden Prairie, MN (1991), 437-532.
9. R.E. Reese and J.L. Goodrich, "California Desert Test Road - A Step Closer to Performance Based Specifications", *Asphalt Paving Technology, Journal of the Association of Asphalt Paving Technologists,* Volume 62, Chelsea MI (1993), 247-313.
10. G.M. Rowe, Prepared Discussion on "Evaluation of the Relationship Between Asphalt Binder Properties and Non-Load Related Cracking," *Asphalt Paving Technology, Journal of the Association of Asphalt Paving Technologists,* Volume 80, Lancaster, PA (2011), 649-662.
11. P.S. Kandhal, "Low-Temperature Ductility in Relation to Pavement Performance," *ASTM STP 628: Low-Temperature Properties of Bituminous Materials and Compacted Bituminous Paving Mixtures*, C.R. Marek (Ed.), American Society for Testing and Materials, Philadelphia, PA (1977)
12. R.A. Velasquez, M. Marasteanu, J.F. Labuz, and M. Turos, "Evaluation of Bending Beam Rheometer for Characterization of Asphalt Mixtures," *Asphalt Paving Technology,*

Journal of the Association of Asphalt Paving Technologists, Volume 79, Chelsea, MI (2010), 295-324.
13. E.V. Dave, B. Behnia, S. Ahmed, W.G. Buttlar, and H. Reis, Henrique, "Low Temperature Fracture Evaluation of Asphalt Mixtures Using Mechanical Testing and Acoustic Emissions Techniques," *Asphalt Paving Technology, Journal of the Association of Asphalt Paving Technologists*, Volume 80, Lancaster, PA (2011), 193-226.
14. G.R. Kemp and N.H. Predoehl, "A Comparison of Field and Laboratory Environments on Asphalt Durability," *Asphalt Paving Technology, Journal of the Association of Asphalt Paving Technologists*, Volume 50, Ann Arbor, MI (1981), 492-537.
15. "Pavement Preservation Definitions," FHWA memorandum, David Geiger, 2005 (Accessed July 2014), http://www.fhwa.dot.gov/pavement/preservation/091205.cfm
16. "Pavement Preservation: Toolbox Resources," FHWA IF-02-010, 2001 (Accessed July 2014), http://www.fhwa.dot.gov/construction/fs02010.cfm
17. LTPP InfoPave (Accessed July 2014), http://www.infopave.com
18. LTPP International Data Analysis Contest (Accessed July 2014), https://tsp2pavement.pavementpreservation.org/2014/03/04/ltpp-international-data-analysis-contest/
19. "MAP-21: Moving Ahead for Progress in the 21st Century," P.L 112-141, Bill funding surface transportation programs for FY2012-2014 (Accessed July 2014), https://www.fhwa.dot.gov/map21/
20. "Design of Pavement Experiment for the LTPP Program," (Accessed July 2014), https://www.fbo.gov/index?s=opportunity&mode=form&id=1633e2812757b731441f5b46d16ccf27&tab=core&_cview=0
21. G.N. King and H. King, *Spray Applied Polymer Surface Seals*, Final Report, FHWA Cooperative Agreement DTFH61-01-X-00004, Wichita, KS (2007)
22. G.N. King and H. King, "Spray-Applied Surface Seal: Fog and Rejuvenator Seals," *TRB 87th Annual Meeting Compendium of Papers DVD*, Transportation Research Board, Washington, DC (2008)
23. G.N. King and H. King, "Spray Applied Emulsion Preventive and Maintenance Seals: FHWA Research Study," *Proceedings, 1st International Sprayed Sealing Conference, Adelaide, South Australia*, Adelaide, Australia (2008)
24. A.C. Falchetto, M.O. Marasteanu, S. Balmurugan, and I. Negulescu, "Investigation of Asphalt Mixture Strength at Low Temperatures with the Bending Beam Rheometer," *Asphalt Paving Technology, Journal of the Association of Asphalt Paving Technologists*, Volume 83 (2014)
25. C. Cochran, *Aging/Optimization Study: Final Construction Report and Early Results*, Minnesota Department of Transportation St. Paul, MN (2005)
26. A. Johnson, T.R. Clyne, and B.J. Worel, *2008 MnROAD Phase II Construction Report*, Minnesota Department of Transportation, St. Paul, MN (2009)
27. M.W. Mirza and M.W. Witczak, "Development of a Global Aging System for Short and Long Term Aging of Asphalt Cements," *Asphalt Paving Technology, Journal of the Association of Asphalt Paving Technologists*, Volume 64, Chelsea, MI (1995), 393-430.
28. R.S. McDaniel, H. Soleymani, R.M. Anderson, P. Turner, and R. Peterson, *Recommended Use of Reclaimed Asphalt Pavement in the Superpave Mix Design Method*, NCHRP Web Document No. 30, National Cooperative Highway Research Program, Transportation Research Board, Washington, DC (2000)

29. D.A. Anderson, D.W. Christensen, H.U. Bahia, R. Dongre, M.G. Sharma, C.E. Antle, and J. Button, *Binder Characterization and Evaluation, Volume 3: Physical Characterization*, SHRP Report A-369, Strategic Highway Research Board, National Research Council, Washington, DC (1994)
30. C. Hintz, R. Velasquez, C. Johnson, and H.U. Bahia, "Modification and Validation of the Linear Amplitude Sweep Test for Binder Fatigue Specification," *Transportation Research Record 2207*, Transportation Research Board, Washington, DC (2011)
31. C. Hintz, R. Velasquez, Z. Li, and H.U. Bahia, "Effect of Oxidative Aging on Binder Fatigue Performance," *Asphalt Paving Technology, Journal of the Association of Asphalt Paving Technologists*, Volume 80, Lancaster, PA (2011), 527-548.
32. M. Kim, W.G. Buttlar, J. Baek, and I.L. Al-Qadi, "Field and Laboratory Evaluation of Fracture Resistance of Illinois Hot-Mix Asphalt Overlay Mixtures," *Transportation Research Record 2127*, Transportation Research Board, Washington, DC (2009)
33. R.W. May and R.B. McGennis, *Superpave Asphalt Mixture Analysis Text*, Asphalt Institute, Lexington, KY (1996)
34. D.W. Christensen, "Analysis of Creep Data From Indirect Tension Test on Asphalt Concrete," *Asphalt Paving Technology, Journal of the Association of Asphalt Paving Technologists*, Volume 67, Chelsea, MI (1998), 458-492.
35. R. Roque, D.R. Hiltunen, and W.G. Buttlar, "Thermal Cracking Performance and Design of Mixtures Using Superpave," *Asphalt Paving Technology, Journal of the Association of Asphalt Paving Technologists*, Volume 64, Chelsea, MI (1995), 718-735.
36. M.P. Wagoner and W.G. Buttlar, "Influence of Specimen Size on Fracture Energy of Asphalt Concrete," *Asphalt Paving Technology, Journal of the Association of Asphalt Paving Technologists*, Volume 76, Chelsea, MI (2007), 391-426.
37. D.G. Peshkin, T.E. Hoerner, and K.A. Zimmerman, *Optimal Timing of Pavement Preventive Maintenance Treatment Applications*, NCHRP Report 523, National Cooperative Highway Research Program, Transportation Research Board, Washington, DC (2004)
38. "Transportation Performance Management: Economic Analysis Primer," U.S. Department of Transportation, Federal Highway Administration, 2013 (Accessed July 2014), http://www.fhwa.dot.gov/infrastructure/asstmgmt/primer03.cfm

Appendix A: Minnesota TH56 Performance Data

MINNESOTA TH 56 CRACK SURVEY SUMMARY (from MnDOT)

Milepost	Original	Yr Chip Seal	Test segment	Longitudinal Cracking			Transverse Cracking			Thermal Cracking*		
	Const Date	Placed		Low	Medium	High	Low	Medium	High	Low	Medium	High
10 to 11	1999	Control	10.1	705			265			18		
	1999	Control	10.2	639			421			14		
	1999	Control	10.4	239	310	160	481			18		
	1999	Control	10.6	150			194			15		
11 to 12	1999	2003	11.2	20			8			5		
	1999	2003	11.4	16			186			14		
	1999	2003	11.5	40			83			6		
	1999	2003	11.7	98	46		149			13		
12 to 13	1999	2002	12.1	22	10		124			10		
	1999	2002	12.6				61			11		
	1999	2002	12.8				115			8		
	1999	2002	12.9				75			9		
13 to 14	1999	2001	13.2				83			7		
	1999	2001	13.4	270			186			8		
	1999	2001	13.8	15			76			17		
	1999	2001	13.9				120			16		
14 to 15	1999	2000	14.3	321	30		393			11		
	1999	2000	14.4	254			570			14		
	1999	2000	14.6	248			324			11		
	1999	2000	14.9	800	160		*			16		
15 to 16	1995	2000	15.1	200		180	280				3	15
	1995	2000	15.2	240		150	185				4	13
	1995	2000	15.5	70		15	299	33		4	6	7
	1995	2000	15.8				144	86			8	8
16 to 17	1995	2001	16.2	10			110	10		2	4	5
	1995	2001	16.3	40	115		153			2	3	9
	1995	2001	16.4				217			2	6	8
	1995	2001	16.7	46			175			4	8	5
17 to 18	1995	2002	17.1	90	41	12	213			1	5	6
	1995	2002	17.2			58	194			4	5	6
	1995	2002	17.8				125			3	5	6
	1995	2002	17.9	34			227			1	8	6
18 to 19	1995	2003	18.2	60	60		149			1	2	8
	1995	2003	18.3				200				6	5
	1995	2003	18.4		20		152				3	4
	1995	2003	18.8				109				4	1
19 to 20	1995	Control	19.2	40	141		485			4	6	5
	1995	Control	19.5				592			4	4	7
	1995	Control	19.6				320	100		2	7	5
	1995	Control	19.8		320	40	400	91		2	3	8

* Thermal Cracking - Number and severity of thermal cracks per 0.1 mile

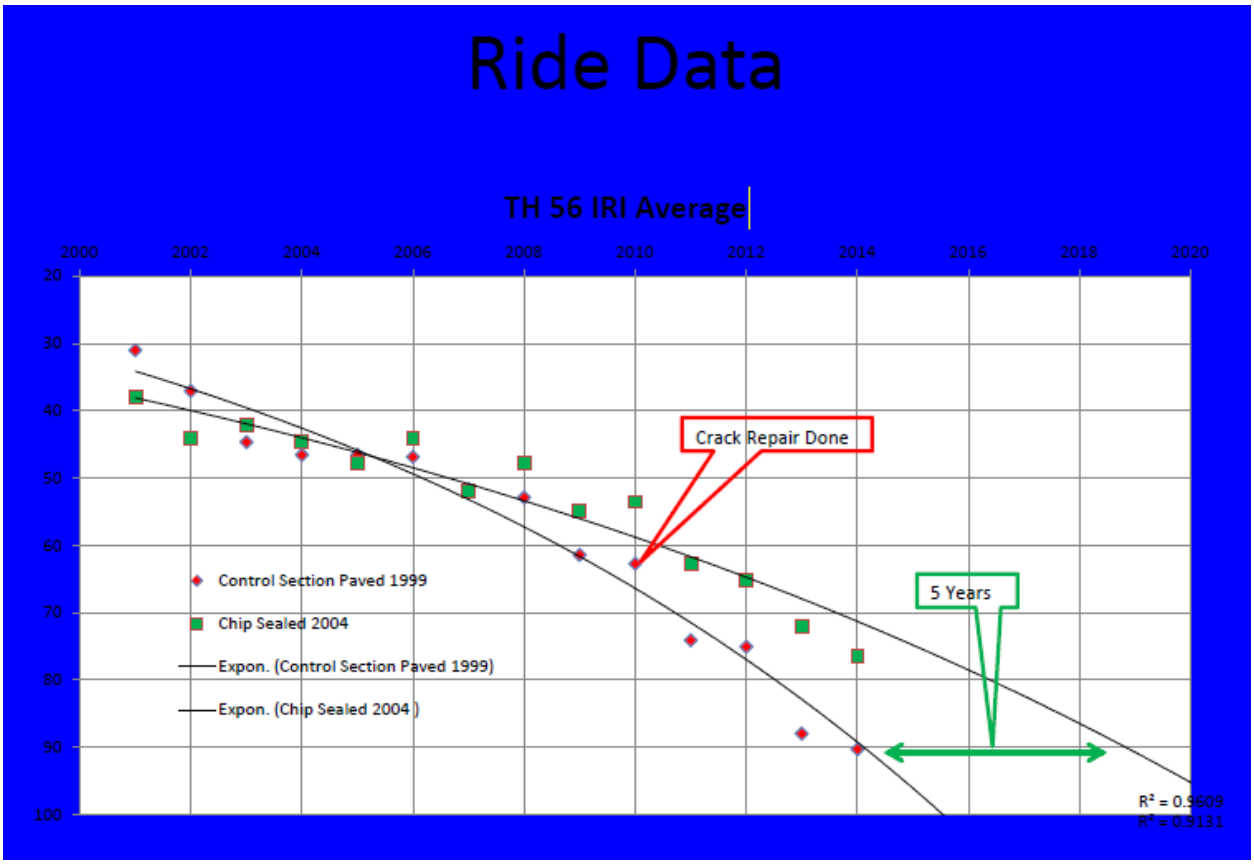
Ride Data
TH 56 IRI Average
2000
2002
2004
2006
2008
2010
2012
2014
2016
2018
2020
20
30
40
50
60
70
80
90
100
Crack Repair Done
5 Years
Control Section Paved 1999
Chip Sealed 2004
Expon. (Control Section Paved 1999)
Expon. (Chip Sealed 2004)
R² = 0.9609
R² = 0.9131